INVESTIGATIONS ON DOPED $(NH_4)_2ZnBr_4$

A THESIS
SUBMITTED TO THE
UNIVERSITY OF HYDERABAD
FOR THE DEGREE OF
DOCTOR OF PHILOSOPHY

BY
P. MADHUSUDANA RAO

SCHOOL OF PHYSICS
UNIVERSITY OF HYDERABAD
HYDERABAD, INDIA

OCTOBER, 1985

This is to state that I, P. MADHUSUDANA RAO have carried out the research embodied in the present thesis for the full period prescribed under Ph.D. Ordinances of the University under the supervision of Dr. K.V.Reddy.

I declare to the best of my knowledge that no part of this thesis was earlier submitted for the award of research degree of any University.

Date : 4th Nov 1985

P Madhusudana Rao
(P. MADHUSUDANA RAO)
Enrolment No.

K. V Reddy
(Signature of the Supervisor)

DEAN
School of Physics
University of Hyderabad
Hyderabad - 500 134

ACKNOWLEDGEMENTS

I wish to express my deep sense of gratitude to Dr. K.V.Reddy for his guidance and cooperation throughout the period of this work.

My thanks are due to Prof. Anil K. Bhatnagar and Prof. G.S. Agarwal for the facilities provided and their encouragement during the course of this investigation.

I would like to thank Prof. V. Hari Babu, Osmania University for allowing the use of the Microhardness unit and Thermoluminescence set up.

I wish to thank Dr. V.S.S. Sastry and Mr. K.Venu for the help rendered in doing the pulsed NMR work.

I would also like to thank my friends and colleagues Dr. YVS Ramakrishna, Dr.(Mrs) Y. Aruna, Dr. A.G.K.Moorthy, Dr. B. Bhanu Prasad, Dr. K. Sambasiva Rao, Mr.P.Ramakrishna and Mr. C.P. Rao (CIL) for their help and encouragement during the course of the work and Mr. P. Chandra Praknsh Reddy for the neat typing of this thesis.

Thanks are also due to the University Grants Commission for financial assistance during this period in the form of a fellowship.

P. Madhusudana Rao

(P. MADHUSUDANA RAO)

TO MY PARENTS.....

PREFACE

Incommensurate ferroelectrics with β-K_2SO_4 structure have been extensively investigated since 1977. The interest in this class of systems has so far centred around the phase transitions. These systems exhibit on cooling a series of phase transitions, generally covering paraelectric, incommensurate and ferroelectric phases. $(NH_4)_2ZnBr_4$ is the least investigated in this family of crystals. In fact, preliminary reports on physical properties of this system have appeared only recently. The thesis describes the investigations carried out on $(NH_4)_2ZnBr_4$ using photoluminescence, thermoluminescence, optical absorption, EPR, pulsed NMR and microhardness techniques. All these techniques have been applied to $(NH_4)_2ZnBr_4$ for the first time.

Chapter I provides the background information concerning the imperfections, phase transitions and the experimental techniques, relevant to the material presented in the subsequent chapters.

Chapter II contains brief description of experimental set ups, especially the apparatus for photoluminescence spectral and lifetime measurements developed as a part of the thesis work.

Chapter III presents the results of photoluminescence spectral and lifetime measurements, and optical absorption study of $(NH_4)_2ZnBr_4$. Excitation by 337.1 nm radiation from a nitrogen laser leads to two intense overlapping emission bands peaking at 630 and 660 nm at room temperature (RT). Cooling the crystal to 100 K produces a new emission band at 535 nm. X-irradiation at RT for 20 minutes or heat-treatment at 523 K for 1 hour or additional doping of Mn^{2+} ions causes a reduction in the intensity of the 630 and 660 nm bands. The X-irradiated crystal shows at 100 K the green emission, the orange emission being negligible. Luminescence decay measurements performed at 168, 271 and 303 K yielded varying profiles in accordance with varying contributions from the green and orange emissions at these temperatures. The lifetime values in the 1-3 milliseconds range are typical of Mn^{2+} ions in insulators. Optical absorption spectrum at RT of the

as-grown crystal shows absorption in the near UV region. X-irradiation produces a new absorption band at 460 nm, which could easily be bleached out by 460 nm light. Correlating various observations, Mn^{2+} ions in environments of cubic and lower symmetries, as well as in association with primary emission centres, are proposed to be responsible for the orange and green emissions. It is also proposed that F-like centres are produced in $(NH_4)_2ZnBr_4$ upon X-irradiation.

Chapter IV concerns with the thermoluminescence study of $(NH_4)_2ZnBr_4$. Two glow peaks at 356 and 407 K are observed when the crystals X-irradiated at RT are linearly heated. A detailed curve fitting of both the glow peaks has shown that first-order kinetics are applicable. Optical bleaching by 460 nm light after X-irradiation reduces the intensity of the 356 K peak. Though the TL emission spectrum could not be recorded, the glow appears to be orange in colour. The results are interpreted in conjuction with the information obtained from other studies. The glow peak at 356 K is attributed to de-trapping of electrons at Br^- vacancies, and the 407 K peak to de-trapping of electrons from impurities. The emission arises from Mn^{2+} ions presumably

when electrons liberated during the heating process recombine with holes in the vicinity of Mn^{2+} ions. Energy transfer to Mn^{2+} ions as activators from primary emission centres is well known.

Chapter V presents the results of investigations on $(NH_4)_2ZnBr_4$ using EPR and pulsed NMR techniques. The EPR spectrum at RT clearly shows that Mn^{2+} ions are present in three different environments. Careful temperature variation measurements revealed a phase transition occurring at ≈430 K. The measurements indicate that the crystalline phase immediately below 430 K is neither incommensurate nor ferroelectric. Two minima at 93 and 171 K, and a change of slope at ≈235 K are the salient features in the plot of the proton relaxation time versus temperature. The minimum at 171 K arises from the re-orientational motion of the NH_4^+ ion. It is suggested that the phase transition indicated by the change of slope at ≈235 K is neither displacive nor distortive type.

Chapter VI concerns with microhardness measurements on $(NH_4)_2ZnBr_4$. The effects of changes in the impurity and defect concentration brought out by different dopings,

and treatments like X-irradiation and thermal quenching on microhardness are systematically studied. It is established that Mn^{2+} ions in $(NH_4)_2ZnBr_4$ segregate near the dislocations during the growth process. Thermal quenching disperses Mn^{2+} ions away from dislocations and into isolated sites within the crystal matrix.

CONTENTS

CHAPTER I

INTRODUCTION

1. Native Defects
2. Impurities
3. Crystal Field Effects
4. Phase Transitions in Crystals
5. Compounds of Type A_2BX_4
6. Experimental Methods Used
   - 6.1 Electron paramagnetic resonance
   - 6.2 Pulsed nuclear magnetic resonance
   - 6.3 Optical absorption and photoluminescence
   - 6.4 Thermoluminescence
   - 6.5 Microhardness

References

Imperfect crystals have engaged the attention of physicists, chemists and metallurgists for many decades. Especially the properties of non-metallic, inorganic single crystals containing imperfection have been extensively studied. These systems are interesting because of the variety of native defects that could be formed, the possibility of studying the properties of chosen impurity ions and the role played by the imperfections in modifying the properties of the host crystal. Since each experimental technique provides information only about a specific aspect, the complete study of such crystals involves application of a variety of physical and chemical methods of investigation. However, a systematic study of the physical system is possible only when the detailed crystal structure is already known. Basic information concerning the unit cell and the detailed arrangement of atoms is obtained by the methods of X-ray crystallography. Only those aspects which are relevant to the present study are considered in the rest of this chapter.

1. Native Defects

A crystal lattice is never perfect. A variety of native defects could occur in an otherwise perfect lattice. At any temperature, the free energy of the crystal is a

minimum when a certain fraction of the ions leaves the lattice points in the bulk and forms a new layer on the surface. More and more cation and anion vacancies are expected to be produced in this manner, as the temperature rises. Such vacancies could be studied through modifications induced in the properties of the crystal as a whole. For example, ionic conductivity in the NaCl type alkali halides is mostly due to migration of cation vacancies. When the involved mechanisms are identified, measurements of ionic conductivity as a function of temperature provide precise values for the energies associated with respective mechanisms. Ionic crystals upon X- or γ-irradiation sometimes get coloured. The electrons liberated during the irradiation process get trapped at the anion vacancies and form what are called F-centres. The formation and properties of such centres have been extensively studied in alkali halides. Larger aggregates of simple F-centres like M-, N- and R- centres are also possible. Since F-centre involves a single electron, it could very conveniently be studied by EPR technique. Since the electron is loosely bound to the anion vacancy, it is highly delocalized. Interaction of the delocalized electron with ions as far away as 6th shell from the vacancy has been observed by ENDOR technique[1]. F-centre has a series of elec-

tronic states and hence it is possible to observe transitions between them. In the case of NaCl, KCl and KBr, the lowest energy absorption band falls in the visible region and hence these crystals acquire characteristic colour. The corresponding transition in the emission has also been observed at low temperatures. In ZnS or ZnSe (II-VI crystals), a complex consisting of a hole trapped on a sulphur (Selenium) ion adjacent to the Zn vacancy - Cl pair has been observed. Labelled 'A-centre', this has been studied in detail by EPR and photoluminescence techniques. The EPR study led to an unambiguous identification of the centre, where as the photoluminescence observations indicated that the F-centre acts as an acceptor. In addition to vacancies, certain other types of defects involving host lattice ions have been observed in alkali halides. The vacancy could be associated with an interstitial ion (Frenkel defect) and two halide ions can be bound together wherein a hole is trapped. The latter defect called V_k-centre has been identified and thoroughly studied by EPR and ENDOR techniques[2].

Extended defects like edge and screw dislocations occuring in crystalline solids play a major role in influencing the crystallization process and the mechanical properties. The dislocation theory of crystal growth is well

supported by experimental observations. For example, if the growth from solution is aided by a screw dislocation 'spiral staircase' growth results, leading to growth pyramids on the crystal surface and these have been observed. The mechanical properties of crystals like microhardness depend on the extend to which the dislocations are mobile. Defects like vacancies, impurities, vacancy-impurity dipoles, precipitates etc., effect the mechanical properties of crystals by their influence on the mobility of dislocations. Any treatment like quenching and annealing of the crystal, which alters the defect nature, concentration and distribution, is expected to influence the mechanicalpropertios.

2. Impurities

Real crystals contain foreign atoms as impurities which constitute simple point defects. Because of limitations in the purification of chemical substances, the crystals grown from salts inherently contain impurities. Only certain technologically important substances like Silicon are available in ultra-pure form and even these have impurities to the extent of 0.1 PPm. Usually the crystals are intentionally doped with specific impurities to modify the properties of host crystals. However, it

is not possible to dope any impurity into any host crystal, this being governed by solubility considerations. If the charge of the impurity ion is different from the charge of the host ion it replaces, then the charge compensation is usually achieved by the formation of vacancies in the host lattice and hence additional defects would be introduced. If two defects A and B have oppositecharges and the temperature is high enough such that at least one of them is mobile, associates of type AB may be formed, the A-B spacing being of the order of nearest - neighbour distance in the lattice. Impurities could also occupy interstitial sites in the lattice. Interstitial atoms are sometimes mobile at lower temperatures, and hence the associates in such cases would be formed more easily. More complex as. ociates involving more than two simple defects are also sometimes observed.

At relatively higher impurity concentrations, precipitation of impurities occurs. Precipitation is influenced by the conditions under which the crystals are grown and usually takes place along the dislocations and grain boundaries.

3. Crystal Field Effects

An ion with unfilled electron shells, like a transition metal or rare earth ion, when doped as an impurity into a crystalline solid, is perturbed by its neighbours in the lattice. This perturbation could be approximately taken into account by considering the electrostatic field set up by these neighbours, which are treated as point charges or extended charge distributions. The crystal field theory and ligand field theory involve the details of this process. The spectral or magnetic properties of the reference ion are usually calculated in terms of a number of unknown parameters which are proportional to the strength of the electrostatic field. The symmetry of the site of the reference ion controls the details of the calculation. Also, the number, degeneracy and symmetry types of energy levels of the reference ion depend solely on this symmetry. In the actual calculation, a Hamiltonian H for the reference ion is first formed including a term representing the electrostatic field. Like the solution of any problem in solid state physics formulated in quantum mechanical language, the solution of the above problem involves diagonalizing the Hamiltonian H. Group theoretical approach provides a simplified yet elegant

way of doing this. The basis for this approach is the existence of operators reflecting the symmetry properties of the physical system which leave the Hamiltonian of the system invariant. The resulting symmetry operations invariably form a group.

4. Phase Transitions in Crystals

Phase transitions are highly collective phenomena taking place simultaneously in the whole medium on a macroscopic scale. The interactions between the constituentsof the medium, which are the origin of collective behaviour, are typically short-ranged. Structural phase transitions (SPT_s) in solids involve mainly a cooperative change of atomic configuration at a critical applied temperature (T_c) and pressure. The phase transition phenomena near T_c are specified in terms of response functions. The existance of an order parameter η is a common feature of most phase transitions. η is non-zero below T_c and zero above it. Landau's theory predicts η to be proportional to $(T_c - T)^{1/2}$ near T_c. At $T = T_c$, $\eta(T)$ can be discontinuous, when the transition is said tobe of first order, otherwise it is of second order.

Among three dimensional systems, three distinct types of SPT_s could occur - displacive, order - disorder and

distortive. A displacive transition involves the displacement of atoms from their earlier positions leading to a rearrangement of the structure. An order - disorder phase transition is associated with the ordering of certain structure elements which are disordered before the transition. Such transitions are associated with the ordering of protons in hydrogen bonds (as in sulfates and cyanides) and the ordering of radicals because of hindered rotation (as in sodium nitrate). If Z' and Z represent the number of formula units in the upper and lower temperature phases, then for a ferrodistortive transition $Z = Z'$, where as for an antiferrodistortive transition $Z' = nZ$, where n is an even integer. Further sub division of structural phase transitions as based on the dielectric response of the system near T_c. An ortho-electric transition usually involves a displacement corresponding to a rotation of a sublattice configuration as in $SrTiO_3$ and there is no change in dielectric susceptibility near T_c. Ferroelectric transition involves the onset of a macroscopic polarization below T_c through a translational atomic displacement leading to a polar unit cell. A net polarization also exists in the case of an antiferrodistortive ferroelectric transitions such

as in Gd_2MoO_4, the systems exhibiting such a transition being known as "improper" ferroelectrics. Antiferroelectric structures could be represented as a set of two superimposed sublattices, the sublattice polarizations being induced by atomic translations as in the case of ferroelectrics. Strain, rotational and Jahn-Teller types of transitions, which are of displacive or distortive nature, also occur in three dimensional systems. Jahn-Teller transitions occur in crystals containing ions whose electronic ground state is orbitally degenerate. A cooperative distortion of the lattice is brought about by vibronic modes arising from the coupling of electronic excitations with the lattice vibrations of the frequency. In the past decade or so, certain crystalline solids showing a long range correlated deviation from three dimensional lattice periodicity have been found[3]. In these systems a local atomic property is modulated such that the wavelength of the modulation is not an integral multiple of the unit cell edge (i.e. $\neq$ n.a). In structurally incommensurate systems, the local property is an atomic position, whereasit is the electron charge density in charge density wave systems like layered transition metal dichalcogenides. Structurally incommensurate insulting crystals are characterized by a basic

lattice structure and a superimposed incommensurate lattice deformation and hence the translational symmetry is lost in such systems. Atomic arrangements in commensurate and incommensurate crystals are schematically shown in Fig.I.1. The translational symmetry is usually recovered by cooling down below a new critical temperature T_c, where a so-called "lock-in transition" takes place and the modulation becomes commensurate. The new unit cell parameters would be integral multiples of the high temperature form. Phase transitions to incommensurate phases could be described by a generalization of soft mode theory of structural phase transitions. In certain very specific low-dimensional systems, an interesting phase transition involving a change in the degree of delocalization of the electron density appears to take place[4].

Structural phase transitions could, of course, be observed by diffraction methods. A variety of non-diffraction methods could be effectively used to investigate SPT_s. EPR of transition metal ions used as probes has been extensively used to investigate the SPT_s in solids. Several as-pects of the EPR spectrum could be influenced by an SPT: the axial zero field splitting parameter D may deviate from linearity near T_c; the orientation of the principal axes of the spin Hamiltonian may change with T as T_c is

Fig. I.1

Atomic arrangement in commensurate (a) and incommensurate (b) crystals.

(a)

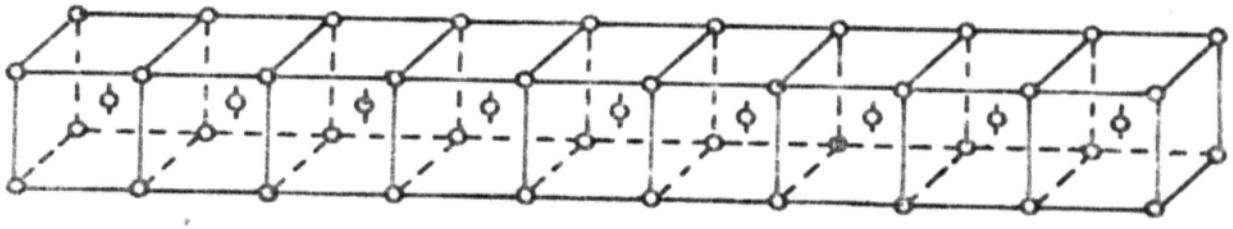

(b)

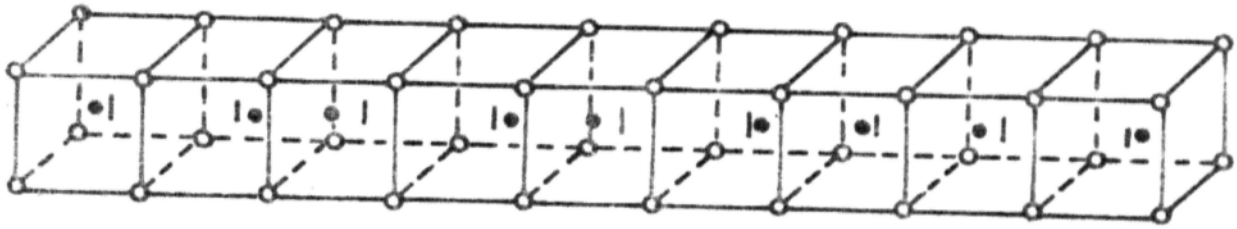

approached; fluctuations in some geometric parameter characterizing the local structure could influence the line widths; in a ferroelectric transition, a change in the dielectric constant that would occur at T_c will cause a change in the spectral intensity.

A nucleus is an excellent probe to investigate the changes due to an SPT occuring in the electric and magnetic interactions in the system at a microscopic level. Fluctuations in the electric field gradient, changes in the rates of motion of molecular groups, distrotions in the geometrical arrangement of atoms etc., are all brought about by an SPT, which have a corresponding effect on the spin-lattice relaxation time. In the case of crystals containing ions appropriate for NQR study, the structural changes modify the electric field gradient resulting in the modification of the NQR spectrum. In many crystals, a group of atoms, may be bonded together such that it could be treated as an independent unit, like $(ZnCl_4)^{2-}$ tetrahedra in Rb_2ZnCl_4. Vibrations of such a group involving various modes are observable in far infra-red. The intensity of frequency of the lines in the IR spectrum may change at the transition temperature or the lowering of the symmetry may cause splittings of the lines. In

many ionic crystals, the bandgap corresponds to wavelength in the UV or near UV region and hence the changes in the fundamental absorption edge as a function of temperature could be followed in an optical absorption experiment. A transition from cubic to tetragonal structure, for example, may cause a slight anisotropy of the absorption of light when the electric vector is rotated from the tetragonal axis to a direction normal to the axis. Similar observations can be made using photoluminescence. The ferroelectric phase transitions can easily be detected by measurement of dielectric constant. In the ferroelectric phase, dielectric hypothesis loops can be observed in strong electric fields. However, it is necessary to use a variety of experimental techniques to get the details of the ferroelectric phase. Measurements of specific heat and differential thermal analysis are also used to detect phase transitions in crystals.

5. Compounds of Type A_2BX_4

A_2BX_4 type compounds comprise a monovalent metal or NH_4^+ or an organic group (A), a divalent metal (B) and a halogen atom (X). An attractive feature of this class of compounds is the availability of a variety of structure types and the possibility of anion and cation

substitutions within related structure types. There are six important crystal structure categories among A_2BX_4 structures, the structure of β-K_2SO_4 being one of them. The basic structure of β-K_2SO_4 type of compounds is characterised by the space group $P_{ncm} - D_{2h}^{16}$ with $Z = 4$. In A_2BX_4 compounds, the BX_4 group can have a planar or a tetrahedral geometry. Ferroelectricity has been found only in tetrahedrally coordinated halide compounds having β-K_2SO_4 structure. In some of these systems an incommensurate phase appears between the high temperature Paraelectric phase and the ferroelectric phase. Additional phases might be expected to appear if A is an organic group, since additional coupling exists between the 'A' group and the BX_4 tetrahedra. Compared to the large number of A_2BX_4 compounds, the number of known ferroelectrics among them is very small.

Sudden interest in compounds of β-K_2SO_4 structure has arisen in 1977, when a well defined incommensurate phase was observed in K_2SeO_4.Rb_2ZnBr_4, Rb_2ZnCl_4, $(NH_4)_2ZnCl_4$ and $(N(CH_3)_4)_2$ $ZnCl_4$ aresome of the compounds in this category subjected to extencive investigations. The investigative techniques used include X-ray diffraction, neutron scattering, Raman scattering, IR, NMR, NQR, EPR and Differential thermal analysis.

6. Experimental Methods Used

6.1 Electron paramagnetic resonance (EPR)

EPR is a powerful technique for studying the paramagnetic impurities or defects in ionic crystals. Especially, ions belonging to the 3d group of the periodic table have been investigated extensively. In the crystal lattice the paramagnetic ion is exposed to the electrostatic field arising from the surrounding ions (ligands). The symmetry and the intensity of the field depend on the geometrical arrangement and the nature of the ligands, respectively. Some of the important interactions involved in the splitting of levels of the paramagnetic ions are the crystal field interaction, the interaction between the electron spin and nuclear spin of the ion, and the interaction between the electron spin and nuclear spin of the ligands which arises when the unpaired electrons are not entirely localized on the magnetic ion and their wave functions include orbitals belonging to the ligands. External magnetic field removes the spin degeneracy of the orbital states and the EPR study essentially consists of measuring transitions within the lowest lying Zeeman levels.

The EPR spectrum in general consists of several lines resulting from various interactions within the

paramagnetic ion and its interaction with the surroundings. The data obtained from the analysis of the EPR spectrum can be presented in a convenient form by using what is called the 'Spin Hamiltonian' which consists of terms representing various interactions. The Spin Hamiltonian formalism employs the concept of 'effective spin' of the ground state, S, which is obtained by equating the number of levels in the lowest group to (2S+1). When the ground state is an orbital singlet, the effective spin would be equal to the total spin of the ion. When referred to the principal axes (x,y,z) of the paramagnetic ion the general spin Hamiltonian including the ligand hyperfine term takes the form

$$
\begin{aligned}
\mathcal{H} = {} & g_x H_x S_x + g_y H_y S_y + g_z H_z S_z \\
& + D(S_z^2 - 1/3\ S(S+1)) + E(S_x^2 - S_y^2) \\
& + (2/6)(S_z^4 + S_x^4 + S_y^4 - 1/5\ S(S+1)\ (3S^2+3S-1)) \\
& + A_z I_z S_z + A_x I_x S_x + A_y I_y S_y \\
& + Q\ (I_z^2 - 1/3\ I(I+1)) + Q'\ (I_x^2 - I_y^2) \\
& + \sum_N A_{ij}\ S_i \cdot I_j^N
\end{aligned}
$$

The form of the spin Hamiltonian should reflect the local symmetry of the paramagnetic ion. If the symmetry is cubic, the following substitutions are to be made in the above Hamiltonian :

$$g_x = g_y = g_z = g$$

$$A_x = A_y = A_z = A$$

$$D = 0 \text{ and } E = 0$$

$$Q' = Q'' = 0$$

The substitutions relevant for axial symmetry are

$$g_z = g_{\parallel} \qquad g_x = g_y = g_{\perp}$$

$$A_z = A \qquad A_x = A_y = B$$

$$E = 0 \text{ and } \qquad Q = 0$$

An EPR study gives precise information about the strength and symmetry of the crystal field, about the paramagnetic ion, the nuclear spin of the ion, and in favourable cases the spins of ligands and thus enables a prediction of the local structure. The importance of EPR in the study of phase transitions has already been pointed out in section I.3.

A good account of the instrumentation and the experimental techniques involved in the EPR investigations is given in the books by Poole[5] and Alger[6].

6.2 Pulsed nuclear magnetic resonance (pulsed NMR)

In radio-frequency (rf) spectroscopy typical relaxation times amount to milliseconds or longer, and hence

the spins in the system have little time to relax. An excess population of spins might be built up in the excited state, thereby slowing down the rate at which energy is absorbed resulting in saturation. As the ratios of the probability of spontaneous emission to that of induced absorption is proportional to the cube of the frequency, saturation occurs more readily at lower frequencies. Because of these condierations, NMR relaxation times tend to be longer than their counterparts in EPR. Both CW and Pulse methods exist for investigating physical systems containing nuclear magnetic dipoles. However, pulse methods have several advantages over the CW NMR technique. In pulse methods, the signal is observed in the absence of rf field which has a perturbing influence on the spins. This enables application of high power rf pulses without saturation limitation, which contributes to enhancement of S/N. Also, since spin relaxation leads suitable for measuring relaxation times. The relaxation times of the spin can be determined from the response of the spin system to a chosen sequence of rf pulses. Fig.I.2 shows the typical response to the application of inverse recovery sequence (π-τ-$\pi/2$). Spectral information can be derived by Fourier transformation techniques.

Fig.I.2

Typical response of a physical system to the application of inverse recovery sequence ($\pi - \tau - \pi/2$).

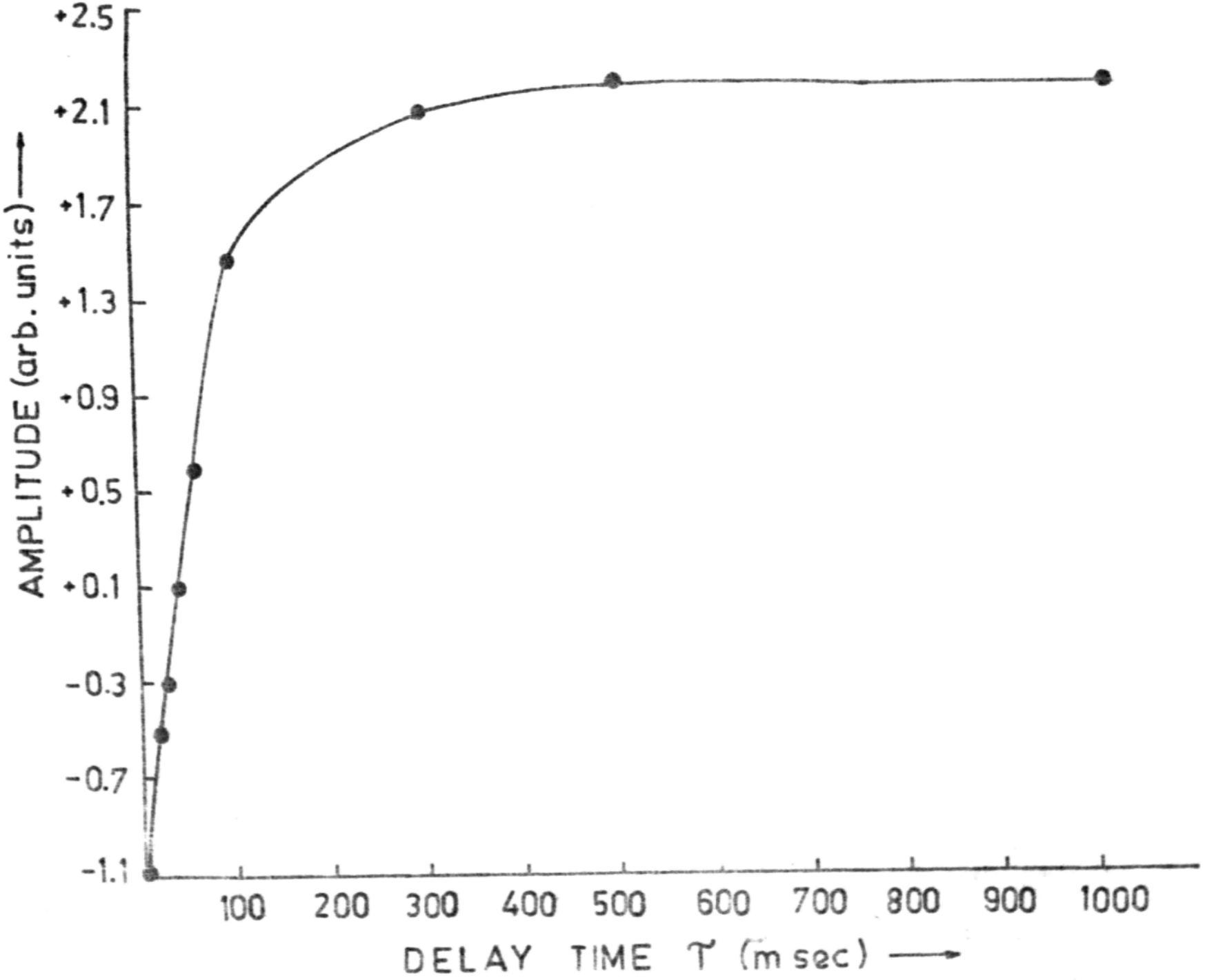
+2.5
+2.1
+1.7
+1.3
+0.9
+0.5
+0.1
-0.3
-0.7
-1.1
AMPLITUDE (arb. units) ⟶
100
200
300
400
500
600
700
800
900
1000
DELAY TIME τ (m sec) ⟶

In static magnetic field the resultant magnetic moment M aligns itself along the field. This alignment does not occur instantaneously, but over a time period several times longer than the spin-lattice relaxation time T_1. A natural frequency $\omega_0 = \gamma H_0$ exists at which the magnetization absorbs energy from the oscillatory field. The width $\Delta\omega$ of this resonant absorption is inversely proportional to the spin-spin relaxation time T_2. In the case of ionic crystals, nuclear relaxation is caused mainly by the presence of paramagnetic impurities in proportions sometimes as small as a few PPm. The saturating rf field H_1 induces spin flips at a rate $A \simeq \gamma_I H_1^2/\Delta H$, where H is the linewidth. Motional effects in solids can be conveniently studied by their influence on spin lattice relaxation. Such effects are mainly due to hindred motion, while they could also arise from spin rotation and translational diffusion.

The theoretical and experimental aspects of NMR are elegently described in the books by Abragam[7] and Farrar and Becker[8].

6.3 Optical absorption and photoluminescence

Optical absorption and photoluminescence techniques are extensively applied for studying impurities and other

lattice defects in ionic crystals. Together, these techniques provide complete information about the energy levels of the defects, and in favourable cases the polarization properties of absorption and emission spectra provide information about the defect symmetry in a direct way.

In the crystal lattice the impurity ions are exposed to the crystal field, resulting in the splitting of the free ion terms and optical transitions are observed between these crystal field-split states. These transitions are intra-ionic, but several other modes of absorption are possible in ionic crystals containing defects. Photoluminescence is excited by absorption of light in a wavelength range which may correspond to a transition between energy levels of the localized states of the defect responsible for the emission, or a transition between the states of a sensitizer in which case the excitation energy is later transferred to the luminiscent ion, or a transition between a localized state and the conduction band or a transition involving valence and conduction bands. Excitation spectrum, which is a plot of luminescence intensity at a particular λ versus the wavelength of the excitation, provides information concerning the absorption of excitation

light and hence supplements the results of the direct absorption measurements.

The minimum detectable defect concentration is generally much lower in luminescence than in absorption measurements, because of the absence of background signal.

The theoretical and experimental aspects of optical spectroscopy are treated in the books by Dicke[9] and Di Bartolo[10].

6.4 Thermoluminescence

Thermoluminescence (TL) is one of the most sensitive methods for studying structural and radiation-related defects in insulators. The process involves the presence of two basic types of centres called the 'trapping centre' (trap) and the 'luminescence centre'. Both the centres are made up of an imperfection (native defect or impurity ion) and its surroundings in the crystal. When free carriers are available in the crystal, for example during X-irradiation, they get trapped at the trapping centres. A carrier in a trap is in an excited state and the nature of the trapping centre is such that the carrier in the excited state cannot make a direct transition to the ground state. Upon thermal stimulation, the trapped

carriers are released into the conduction or valence band and eventually captured either by luminescence centres, or by recombination centres in close proximity to the luminescence centres. In the latter case, the energy released in the recombination process is transferred to the luminescence centres. The emission occurs when the excited luminescence centres make a radiative transition to the ground state. The TL process involving energy transfer to the luminescence centres is schematically shown in Fig. I.3.

The evaluation of trap parameters is the first objective of experimentation. The measurements usually start with X- or γ-irradiation of the crystal. The crystal is next heated slowly at a linear rate and the radiation emitted is recorded. The glow curves thus recorded are used to determine trap parameters such as energies, frequency factors, trap densities and transition probabilities. For traps of a single depth, the shape and peak temperature of the glow peak are independent of the initial occupancy of the traps, if first order kinetics are involved. Sometimes two or more glow peaks occur closely, resulting in a considrable overlap. A thermal cleaning technique is used in such cases to resolve the peaks. In this method, the crystal is first

Fig. I.3

Schematic diagram of simple model for processes including energy transfer occuring in thermo-luminescence.

heated at a chosen rate to a temperature just higher than the temperature of the lowest glow peak, and then rapidly cooled to RT. The procedure is repeated for subsequent glow peaks.

The identification of luminescence centres is often made by obtaining the spectral dependence of thermoluminescence. For this purpose, the crystal is maintained at a temperature slightly less than the temperature of each of the glow peaks, and the emission spectrum is recorded using a fast scan. Additional information required in the interpretation of TL results is usually obtained by parallel EPR, optical absorption and photoluminescence investigations.

6.5 Microhardness

Microhardness is one of the most sensitive among the mechanical properties of crystalline solids. It is usually measured by a static indentation method. The resistance of materials to indentation varies with their elastic properties. Since the ultimate structure of solids consist of compressible atoms held together by bonding forces, changes in the nature and extent of bonding as well as defects present in the lattice are expected to influence the elastic properties and hence

heated at a chosen rate to a temperature just higher than the temperature of the lowest glow peak, and then rapidly cooled to RT. The procedure is repeated for subsequent glow peaks.

The identification of luminescence centres is often made by obtaining the spectral dependence of thermoluminescence. For this purpose, the crystal is maintained at a temperature slightly less than the temperature of each of the glow peaks, and the emission spectrum is recorded using a fast scan. Additional information required in the interpretation of TL results is usually obtained by parallel EPR, optical absorption and photoluminescence investigations.

6.5 Microhardness

Microhardness is one of the most sensitive among the mechanical properties of crystalline solids. It is usually measured by a static indentation method. The resistance of materials to indentation varies with their elastic properties. Since the ultimate structure of solids consist of compressible atoms held together by bonding forces, changes in the nature and extent of bonding as well as defects present in the lattice are expected to influence the elastic properties and hence

the microhardness. In view of th se, it is most appropriate to consider microhardness as a measure of resistance to dislocation motion. This point of view has been well-accepted in the literature. Resistance to the motion of dislocations caused by the bonding forces alone is the intrinsic hardness of the crystal. The hardness of a high purity, good quality and well annealed crystal is sometimes called 'minimum hardness'. It is well known that various imperfections strongly influence the microhardness of single crystals.

The observations essentially consist of measuring the size of indentation marks formed on a suitably prepared surface of the sample under appropriate load. Various designs have been tried for the tool used to make indentations. For a diamond pyramid having square base and with the angle between the faces at the vertex as 136°, the microhardness H_μ is given by

$$H_\mu = \frac{1.854\ P}{d^2}$$

where P is the load used in grams and d is the length of the diagonal in microns.

Microhardness is a technique which isincreasingly applied now a days to investigate microinhomogenities in

the distribution of impurities in single crystals, the effect of dislocation density on the mechanical properties of crystals, the polarity of crystallographic planes of semiconducting compounds etc.

The book by Glazov and Vigdorovich[11] treats all aspects of microhardness in a detailed manner.

References

1. W.B. Fowler, " Physics of Color Centres ", Academic Press, New York (1968).

2. C.P. Slichter, " Principles of Magnetic Resonance ", Harper and Row, New York (1963).

3. R.Blinc, Physics Reports (Review section of physics Letters), 79, 331 (1981).

4. Z. Iqbal, R.R. Chance and R.H. Baughman, J.Chem.Phys.66,5520 (1977).

5. Jr., C.P. Poole, " Electron Spin Resonance - A Comprehensive Treatise on Experimental Techniques", Interscience Publishers, Inc., New York (1967).

6. R.S. Alger, " Electron Paramagnetic Resonance : Techniques and Applications ", John Wiley and Sons, Inc., New York (1968).

7. A. Abragam, "The Principles of Nuclear Magnetism", Oxford University Press (1961).

8. T.C. Farrar and E.D. Becker, " Pulse and Fourier Transform NMR", Academic Press, New York (1971).

9. G.H. Dieke, " Spectra and Energy levels of Rare Earth Ions in Crystals ", Interscience Publishers, Inc., New York (1968).

10. B. Di Bartolo, " Optical Interactions in Solids ", John Wiley and Sons, Inc., New York (1968).

11. V.M. Glazov and V.N.Vigdorovich, " Microhardness of metals and Semiconductors ", Consultants Bureau, New York (1971).

CHAPTER II

APPARATUS AND MEASUREMENTS

1. Photoluminescence

    1.1 Emission spectra

    1.2 Emission lifetimes

    1.3 Temperature variation

2. Optical Absorption

3. Thermoluminescence

    3.1 Glow curves

    3.2 Thermoluminescence spectral dependence

4. Electron Paramagnetic Resonance

5. Pulsed Nuclear Magnetic Resonance

6. Microhardness

1. Photoluminescence

1.1 Emission spectra

The experimental set up used for recording emission spectra is shown schematically in Fig. II.1. The CaL model NL 103 nitrogen laser used for excitation consists of plasma column, copper clad epoxy sheet, spark gap and gas line. The perspex plasma column encloses two aluminium electrodes of 55 cms effective length. A double side copper clad glass epoxy sheet is used as the energy storage element. The spark gap is pressurized to about 2 kg/cm^2 at an excitation voltage of 12.5 kV DC. The exact pressure and voltage required depend on the electrode spacing. The pulse repetetion can be controlled by triggering the spark gap with a trigger generator. The laser pulse generated has a width of 10 nano seconds with a peak power of about 200 kW and a pulse repetetion rate upto 50 Hz. The cross-section of the laser beam is a rectangle of dimensions 5 x 15 mm^2. The beam was focussed onto the crystal by a cylindrical lens (2" dia and 75 mm focal length). Fluorescence from the crystal was gathered in a perpendicular direction and focussed onto the entrance slit of a high resolution monochromator (JOBIN YVON model HRS 2). The excitation

Fig. II.1

Block diagram of the set up used for recording emission spectra.

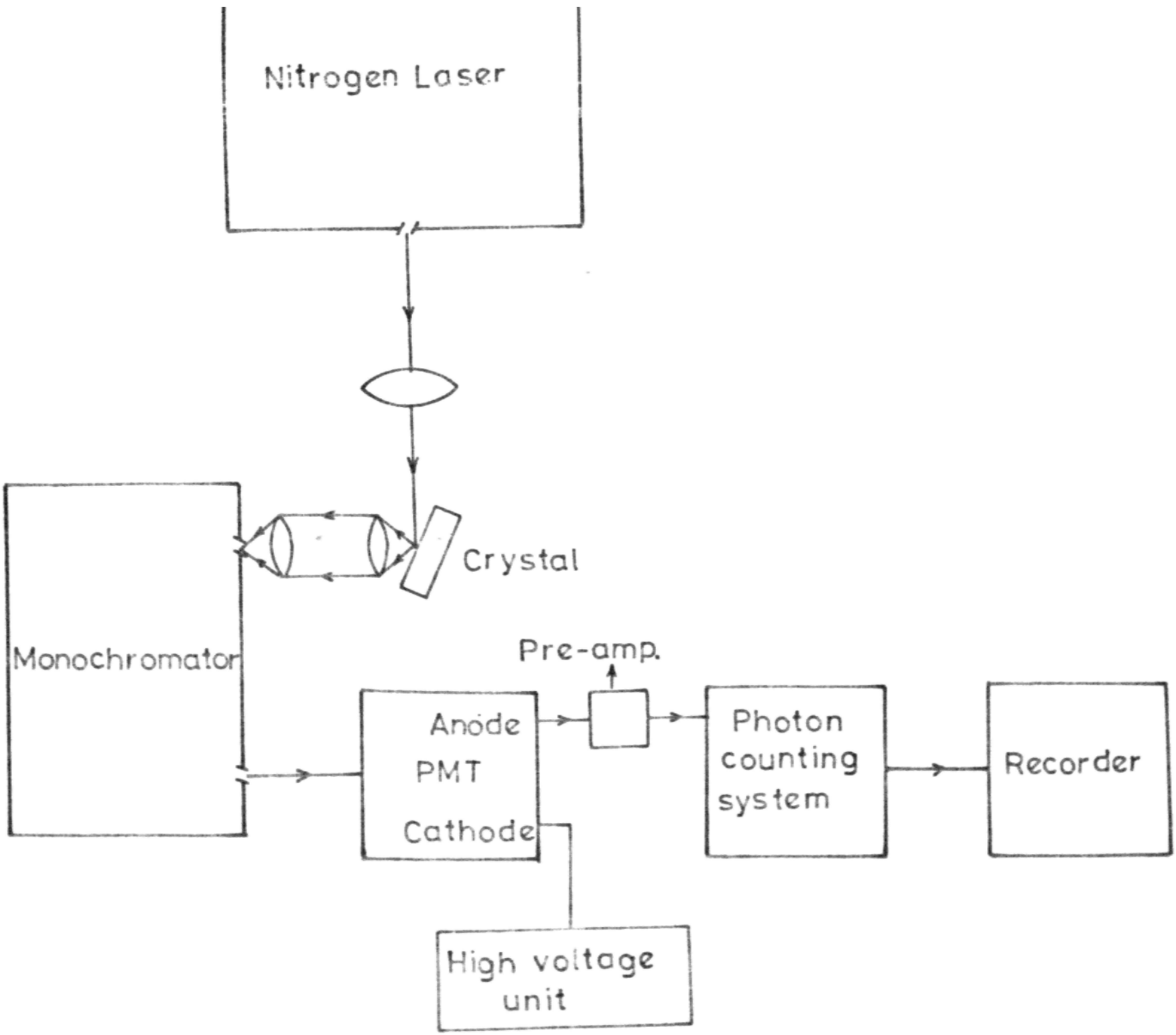
Nitrogen Laser
Crystal
Monochromator
Pre-amp.
Anode
PMT
Cathode
Photon counting system
Recorder
High voltage unit

laser beam at 337.1 nm was blocked by using Melles Griot type OG 335 DWO 13541 filter. After the wavelength selection, the light was detected by EMI 9558 QB Photomultiplier tube having S-20 response. The P.T is housed in a Products for Research Inc. housing model TE 104 RF which has a provision for thermoelectrically cooling the photocathode to 233 K. The signal processing was done using a photon counting system assembled from ORTEC component units. It consists of an ORTEC model 9301 fast pre-amplifier, 9302 amplifier - discriminator, 9315 photon counter and 9325 D-A converter. The rise time of the preamplifier is 1.5 nsec. Features of the 9302 include wideband high gain amplifier and an integral discriminator which is a leading edge type whose level can be adjusted over a range from 50 mV to 1 V. The ORTEC 9315 photon counter contains two DC 100 MHz counters (A and B), both of which may be independently gated from an external source. The ORTEC 9325 D-A converter converts any three selected consecutive digits from the output of a 9315 photon counter into an analog voltage. The analog output of the photon counting system is recorded by a Hewlett - Packard 7132 A Y-t recorder or HP model 7002 X-Y recorder.

1.2 Emission lifetimes

The experimental arrangement used for recording luminescence decay curvesis shown in Fig. II.2. Nitrogen laser is used as the excitation source for the decay measurements. The laser beam was split into two perpendicular components of equal intensity by using a beam splitter. One component was used in conjuction with a silicon PIN photodiode (EG&G model 5082-4207) for deriving trigger pulses for box-car integrator (Princeton Appl. Res. model 162) and oscilloscope (Tektronix model 475 A). The circuit used for this purpose is shown in Fig. II.3. The other component was used for optical excitation, the emission being detected by the PMT, the output of which was given to either the oscilloscope or box-car averager. Most of the experiments were done by point-by-point measurement. Decay curves were also recorded directly using a Y-t recorder. Optimisation of various parameters was done by viewing the decay curve on the oscilloscope.

Fig. II.2

Block diagram of the life-time measurement set up.

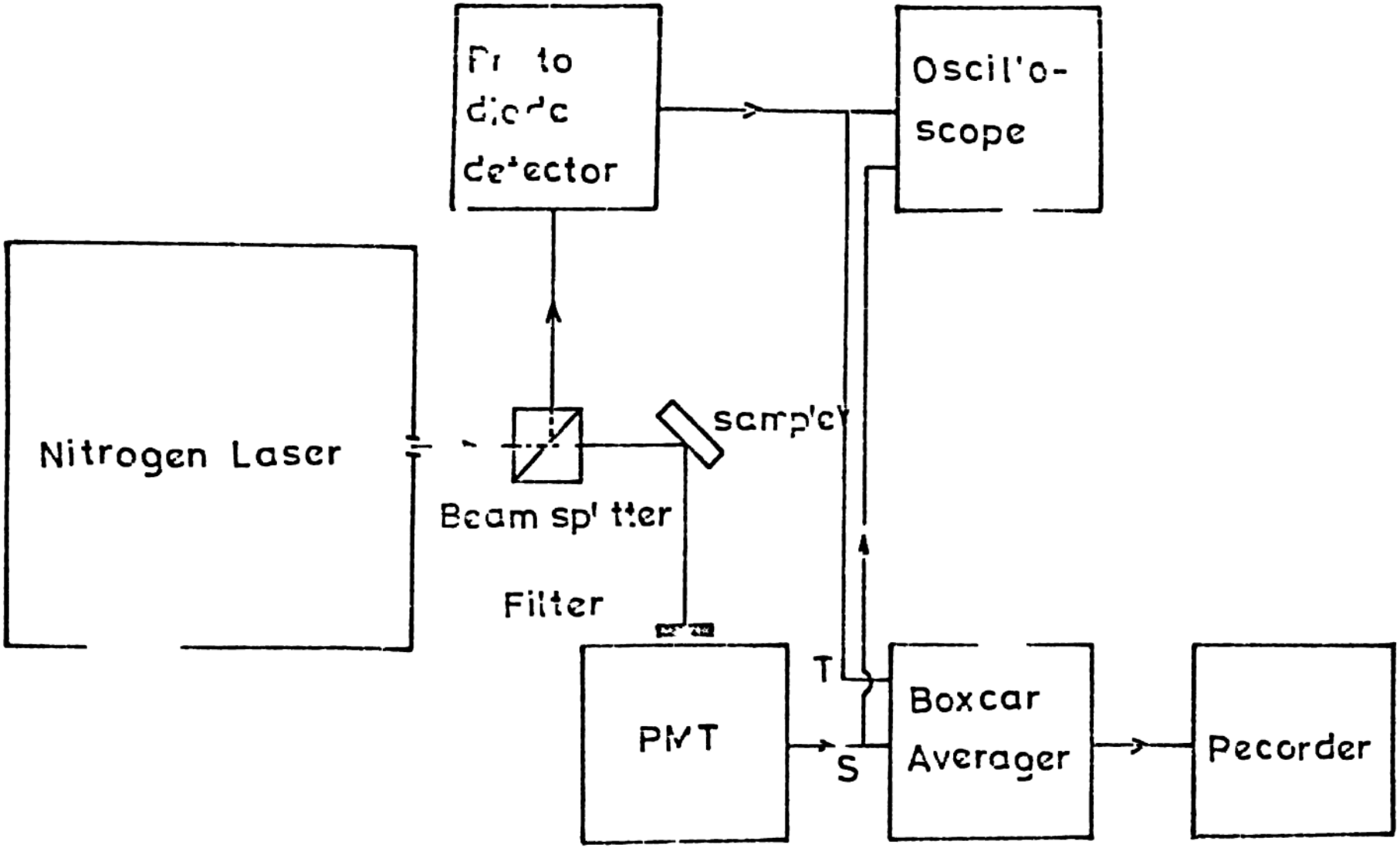
Photo diode detector
Oscil'o-scope
Nitrogen Laser
sample
Beam splitter
Filter
PMT
T
S
Boxcar Averager
Recorder

Fig. II.3

Photodiode detector

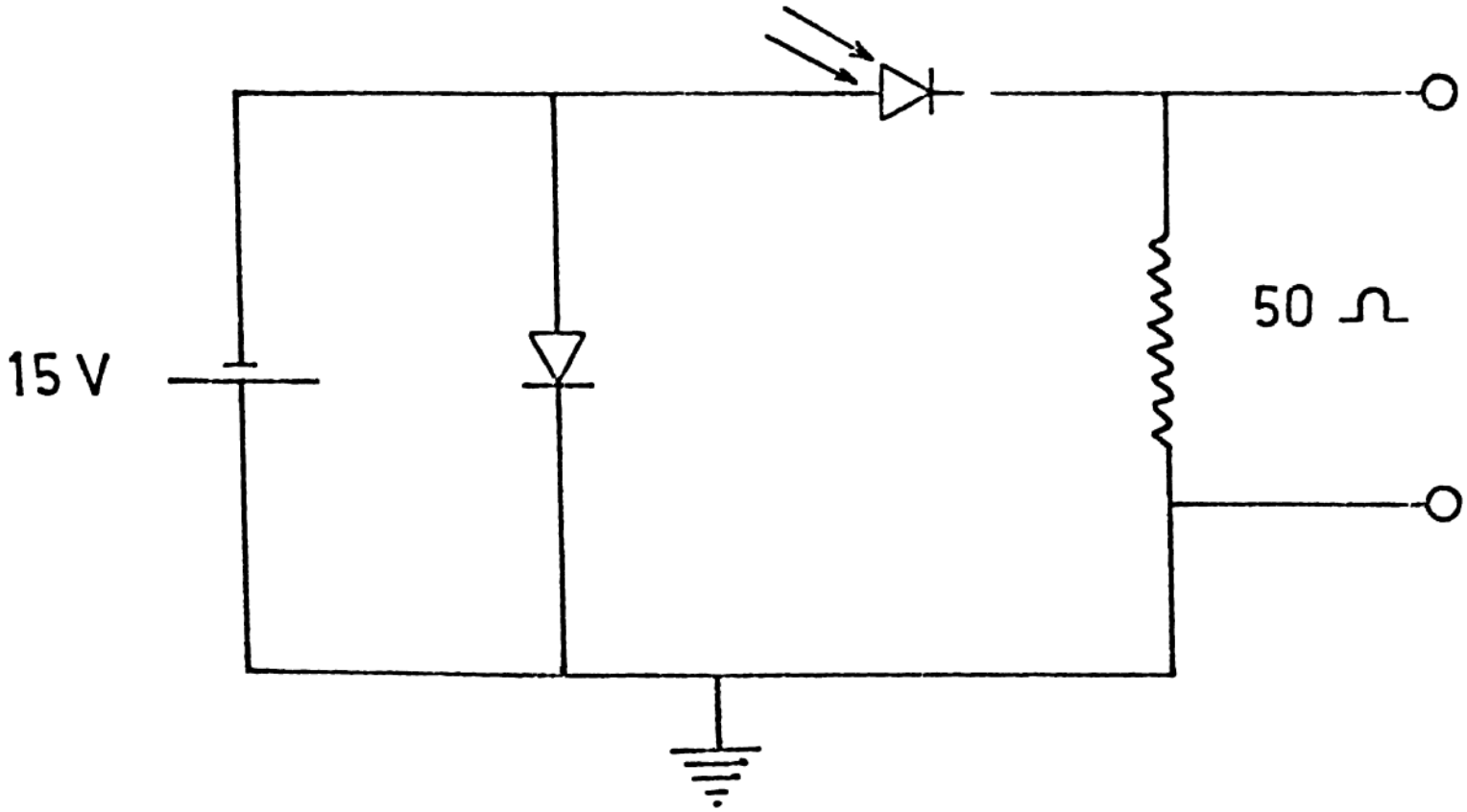
15 V
50 Ω

1.3 Temperature variation

The emission spectra were recorded at low temperatures with a cryostat. All the low temperature measurements were made using a home-made general purpose all stainless steel optical cryostat*. The cryostat is of cold finger type with two concentric gold-plated shields around the cold-finger. Measurements in the range 110-300 K were made by winding a heater on a portion of the cold-finger and using a home-made temperature controller. An iron-constantan thermocouple was used as the sensing element. The temperature was set using a 10 turn helipot, the estimated stability being $\pm$ 0.5°. The block diagram of the temperature controller is shown in Fig. II.4.

2. Optical Absorption

Shimatzu UV-200S spectrophotometer, operating in the wave length range of 200-700 nm, was used for optical absorption work. This is a double beam spectrophotometer having seperate sample and reference compartments. All the measurements were made only at

---

* generous gift from the University of Utrecht, Holland

Fig. II.4

Block diagram of the temperature controller.

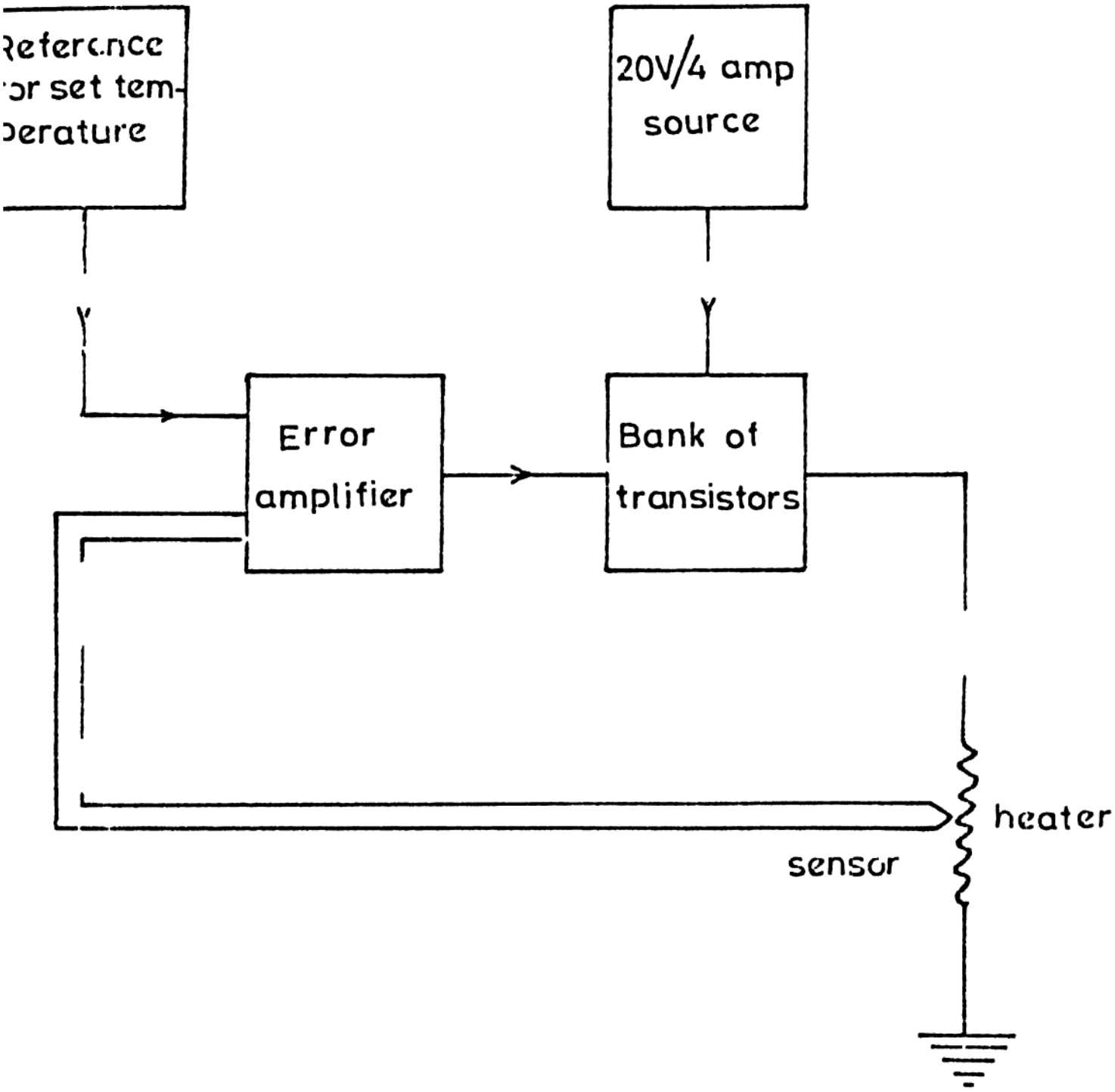
Reference
or set tem-
perature
20V/4 amp
source
Error
amplifier
Bank of
transistors
heater
sensor

room temperature. Samples of size 3 x 3 x 2 mm^3 were used in the present measurements. The equipment is fitted with a wavelength marking mechanism, whose calibration was assumed. The band positions were determined by recording the spectra on an expanded scale and using the wavelength markings on the chart. Spectra were recorded both before and after X-irradiation.

3. Thermoluminescence

3.1 Glow curves

Fig. II.5 shows the set up* used for recording thermoluminescence glow curves. It consists essentially of a programmed heating system and a sensitive detector assembly. A temperature programmer (Indotherm model 487) capable of linear heating in the range 273 - 1273 K and at rates 25° and 50° per minute, a strip and a 40 gauge chromel-alumel thermocouple comprise the heating system. The detector assembly consists of a photomultiplier (E.M.I 5256 B), a high voltage power supply, a preamplifier, a DC amplifier and a recorder (HP model 7002 X-Y recorder).

---

* Available in the solid state and Material Science labs, Physics Department, Osmania University, Hyderabad.

Fig. II.5

Block diagram of the set up used for recording thermoluminescence glow curves.

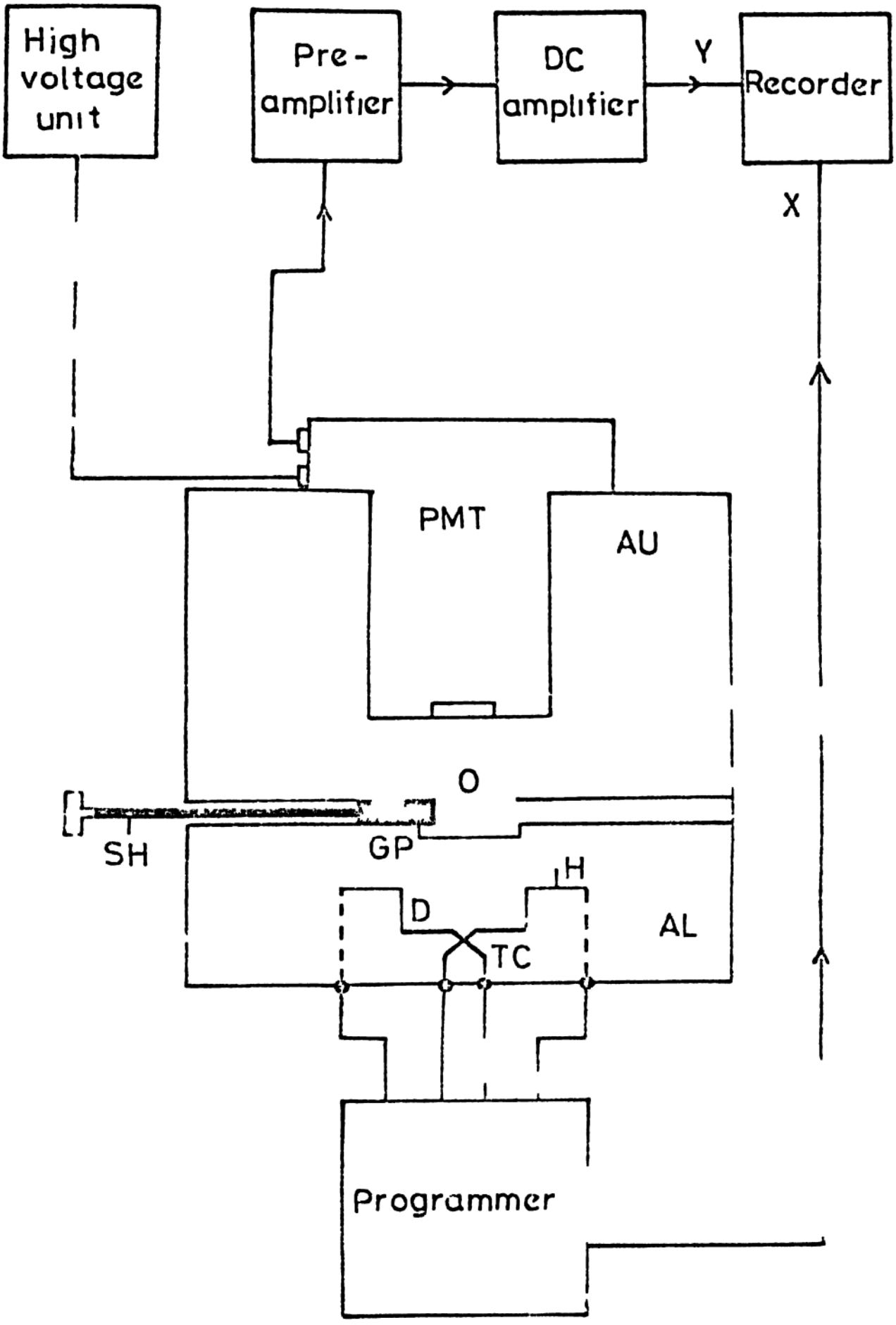
High voltage unit
Pre-amplifier
DC amplifier
Y
Recorder
X
PMT
AU
O
SH
GP
H
D
TC
AL
Programmer

The sample chamber is a light aluminium box with two compartments. The top of lower compartment has an opening (O) at the centre with a shutter arrangement (SH). The lower compartment (AL) consists of a kanthal strip heater (H) fitted exactly below the opening (O). The PMT is appropriately arranged within the upper chamber (AU). The opening is covered by a glass plate (GP) to protect the photocathode from thermal radiation. A small depression (D) in the middle of the kanthal strip ensured a fixed position for the sample throughout the measurement. Since the thermocouple is spot welded to the bottom of the depression, correct reading of the sample temperature was ensured. The temperature programmer used is specifically designed for thermoluminescence measurements. A line varying voltage reference obtained from an electronic ramp generator is compared with the thermocouple emf and the error signal is amplified by a chopper amplifier of high stability. The heater power is proportionately controlled by the amplified error. After the set temperature is reached, power to the heater is automatically switched-off.

divided into three distinct parts - transmitter, probe and receiver. The transmitter is a pulsed rf source which can deliver very short, high power (upto 3 KW) rf pulses. A single coil series resonant circuit forms the probe. With this probe, it is possible to tune the frequency of operation, over the range 2 to 30 MHz, using appropriate rf coils. The receiver part consists of a fast recovery pre-amplifier, a tuned amplifier, a phase sensitive detector and a low pass filter. A commercial box-car averager (Princeton Applied Research model 162) was used for making measurements on the transients. The temperature controller used for low temperature measurements has already been discussed under section 1.3.

6. Microhardness

Microhardness measurements were made using a Vicker's microhardness tester in conjunction with a MM2 Universal microscope. The indentations were made by applying a 60 gm load for 10 seconds. To study the effect of quenching, samples were maintained at various temperatures in the range RT to 773 K for 1 hour before dropping onto a thick copper plate.

CHAPTER III

PHOTOLUMINESCENCE AND OPTICAL ABSORPTION STUDY OF $(NH_4)_2ZnBr_4$

1. Summary of Results of Work Reported on Some Systems having β-K_2SO_4 Structure

A_2BX_4 compounds having β-K_2SO_4 structure, like Rb_2ZnCl_4, Rb_2ZnBr_4, $(NH_4)_2ZnCl_4$ and $(N(CH_3)_4)_2ZnCl_4$ have been extensively investigated in the past few years. The interest in such compounds has been the successive phase transitions and the ferroelectricity which they exhibit. Though many more compounds fall under this category, the present summary is limited to the four compounds mentioned above.

The incommensurate phase in a compound having β-K_2SO_4 structure was first discovered in K_2SeO_4 by Iizumi et al by inelastic neutron scattering. Earlier studies have shown that both Rb_2ZnCl_4 and Rb_2ZnBr_4 have phase sequences of normal - incommensurate - ferroelectric, similar to the sequence observed for K_2SeO_4. Rb_2ZnCl_4 has normal phase above 302 K (T_1), an incommensurate phase between 302 and 190 K and a ferroelectric phase below 190 K (T_c). The corresponding temperatures in Rb_2ZnBr_4 are 346 K and 187 K. Both these compounds exhibit incommensurate structures along the c-axis. Below T_c spontaneous polarization develops

along the a-axis with c^* equal to one-third of c^* of the highest temperature phase. From NQR measurements, Aleksandrova et al[2] concluded that the region where modulation is described by plane wave limit (broad solitons) spreads upto 210~220 K in Rb_2ZnCl_4. The soliton lattice appears below this limit. Neutron scattering[1] and Raman scattering[3] studies of K_2SeO_4 have revealed temperature dependent soft modes. Though similar effects were observed in Raman scattering study[4] of Rb_2ZnBr_4, the details are different. In the Raman scattering study of K_2SeO_4, a rapid increase in the scattering intensity of soft modes was observed as T_i is approached from below. Such an increase was not observed for Rb_2ZnBr_4. This observation indicates that the mechanism in Rb_2ZnBr_4 is not as typically displacive type as in the case of K_2SeO_4, but rather in-between displacive and order-disorder type. However, from the intensities of satellite reflections in X-ray diffraction pattern Gesi and Iizumi[5] concluded that the ferroelectricity in Rb_2ZnCl_4 is induced by the same mechanism as is found in K_2SeO_4. In the Raman spectrum of Rb_2ZnCl_4[6] , peaks were observed around 300 cm^{-1}, 140 cm^{-1} and below 100 cm^{-1}. The peaks

around 300 and 140 cm^{-1} have been asigned to internal modes of $ZnCl_4$ radicals. No peaks were observed above 400 cm^{-1}, which indicates that the ions in $ZnCl_4$ radical are loosely coupled. Wada et al[7] have observed two soft modes in K_2SeO_4 by Raman scattering measurements. The one observed below the incommensurate transition has been asigned to the amplitude mode and the order observed in the low temperature commensurate phase to the phase mode. In an extension of this work to Rb_2ZnCl_4[8], Wada et al observed the amplitude mode but could not detect the phase mode above 77 K, the lowest temperature of their measurements. Francke et al[9] extended this work to lower temperatures and detected a phase mode at 72 K. Spin-lattice relaxation measurements by Blinc et al[10] have demonstrated that in the incommensurate phase of Rb_2ZnCl_4 the spin-lattice relaxation rate is dominated by phasons. Recent studies have brought out more phases in both Rb_2ZnCl_4 and Rb_2ZnBr_4. From dielectric, thermal and X-ray diffraction measurements Matsunaga and Nakamura[11] concluded that four phases exist in Rb_2ZnCl_4 as follows :

I. $T > 406$ K normal, with $C = C_o$

II $319\ K < T < 406$ K paraelectric, with $C = 4C_o$

III $270\ K < T < 319$ K, antiferroelectric, with $C = 4C_o$

IV $T < 270$ K, ferroelectric, with $C = 3C_o$.

In the same system, Sato et al[12] have detected from dielectric constant measurements a weak-ferroelectric phase over a narrow temperature range from 268.5 K to 276 K. From X-ray diffraction study, Ueda et al[13] observed five phase transitions at 50,80, 108, 200 and 347 K in Rb_2ZnBr_4. A supercooling effect together with thermal hysteresis was observed at the incommensurate - commensurate transition temperature of 200 K. The super-cooling effect has been attributed to the surface pinning of the crystal. The lowest temperature transition at 50 K is found to depend on the heating rate, which is presumed to be due to surface pinning or the impurity pinning. NMR measurements by Blinc et al[14] have shown the existence of regions where the modulation wave is floating. The floating regions co-exist with other regions where the mode wave is static. Impurity phase pinning and

a roughening of the mode wave at higher temperatures are proposed to account for these effects. Aleksandrova et al[15] have observed second-order quadrupole shifts in the NMR spectra of ^{87}Rb in the incommensurate phase of Rb_2ZnCl_4 and Rb_2ZnBr_4.

Belobrova et al[16] found a phase transition in $(NH_4)_2ZnCl_4$ at T_c = 266 K by NQR technique. Below T_c, the crystal is ferroelectric with space group $P_{21}cn$ and with the trebling of the lattice parameter along the c-axis. The temperature dependence of the details in the NQR spectra around T_c has shown that the crystal has incommensurate phase above T_c.

Sawada et al[17] observed five successive phase transitions in $(N(CH_3)_4)_2ZnCl_4$ at 293, 279, 276.3, 181 and 161 K using DTA technique. Dielectric constant measurements indicated ferroelectricity along the a-axis in the range 276.3 and 279 K. The ferroelectric phase transition is presumed to be of incommensurate - commensurate type. Reorientations of CH_3 and $N(CH_3)_4^+$ were detected in PMR spectra even at 120 K[18]. The double minima observed in the temperature dependence of relaxation time (T_1) has been attributed to the

motion of CH_3 groups about their C_3 axes and the isotropic reorientations of the TMA ion. The observed values for the T_1 minima indicated the presence of two inequivalent tetramethyl groups of equal number.

Though the four compounds mentioned so far have been extensively investigated, the related compound $(NH_4)_2ZnBr_4$ has received very little attention. Infact, the first papers containing preliminary results have appeared only recently. Osaka et al[19] have studied the dielectric and thermal properties of $(NH_4)_2ZnBr_4$ and observed two phase transitions at 216.5 and 439 K. The phase transition at 216.5 K is a first order phase transition and associated with thermal hysteresis of about 11^o. They have suggested that $(NH_4)_2ZnBr_4$ has a superlattice structure at room temperature similar to that in $(NH_4)_2ZnCl_4$. Spontaneous polarization of 0.22 μ Coul/cm^2 was observed at 133 K. Moskalev et al[20] have studied $(NH_4)_2ZnBr_4$ by NQR technique, and observed a discontinuous change of NQR frequencies at 222.5 K with a temperature hysteresis of 10^o. A first order phase transition is indicated here. Another phase transition at $\sim$428 K and a weak anomaly at 365 K were found by DTA technique. Pyroelectric charge measurements indicated a value of

0.2μ Coul/cm^2 for the spontaneous polarization. NQR measurements seem to indicate that incommensurate phase is absent in $(NH_4)_2ZnBr_4$.

We have undertaken a comprehensive study of $(NH_4)_2ZnBr_4$ by a variety of physical techniques and the results obtained from photoluminescence and optical absorption measurements are presented in this chapter. Such measurements have not been reported so far on any A_2BX_4 type compound having β-K_2SO_4 structure.

2. Crystal Growth and Characterization

Single crystals of $(NH_4)_2ZnBr_4$ were grown by slow evaporation from aqueous solution of NH_4Br and $ZnBr_2$ taken in stoichiometric proportion. The LR grade Zinc Bromide produced by two different chemical firms, namely Thomas and Thomas (India) and Burgoyne (India) was used for crystal growth. Likewise, the Ammonium Bromide produced by Loba Chemie Industriat Co. (India) and Modern Chemical Corporation (India) was used. $CuBr_2$, $MnBr_2.4H_2O$, $CoBl_2.6H_2O$, $NiCl_2.6H_2O$, NaCl and $BiCl_3$ used as dopants were of Analar grade produced by BDH (England) or BDH (India). Double distilled water was used for preparing the solutions. Two different

evaporation procedures were employed. In one method the beaker containing the solution was covered with a perforated filter paper and left at ambient temperature for evaporation. Such evaporations at ambient temperature were carried out in Summer months as well as in winter months when the temperature over a 24 - hour period varied in the approximate range 26 to 43°C and 12 to 26°C respectively. In the second method the beaker was kept in an oven whose temperature was maintained constant and hence the evaporation occured at a constant temperature. On different runs the oven was maintained at 25, 30 or 35°C. Also, beakers of 100, 250 and 500 cc capacities were used at each of the temperatures mentioned above. In all at least 50 growth runs were made to obtain crystals for the present work. The time taken for the crystals to appear obviously depends on how close the prepared solution was to the state of supersaturation. However, the shortest time for many good single crystals to form simultaneously in the beaker was about 72 hours, when the evaporation occured at a constant temperature of 35°C. Evaporations involving the use of seeds were not tried because the crystals obtained were big enough

for all the investigations. Good single crystals were obtained from almost all the runs, the only differences being the duration of growth and the number of isolated single crystals formed. The crystals were allowed to grow upto a size of approximately 3 mm x 3 mm x 1.5 mm. The same growth habit was observed in all cases. The crystals are clear, have all the 6 faces precisely formed, and of good quality. A photograph of some of the crystals obtained is shown in Fig. III.1. Crystals were also grown from solution to which $CuBr_2$, $MnBr_2.4H_2O$, $CoCl_2.6H_2O$, $NiCl_2.6H_2O$, NaCl and $BiCl_3$ were added as dopants. For all the dopants, a range of concentrations viz. 0.1, 0.5, 1.0, 2.0 and 5 by weight, was used. No changes were observed in the growth habit or in any other features when dopants were added to the starting solutions. In fact, identical crystals were obtained whether or not any dopants were added, and whatever be the conditions of evaporation. The crystals have distinct cleavage plane perpendicular to the b-axis as observed in the case of $(NH_4)_2ZnCl_4$[21].

Various characterization procedures were employed to check the formation of $(NH_4)_2ZnF_4$ crystals.

Fig. III.1

Photograph of some of the crystals of $(NH_4)_2ZnBr_4$

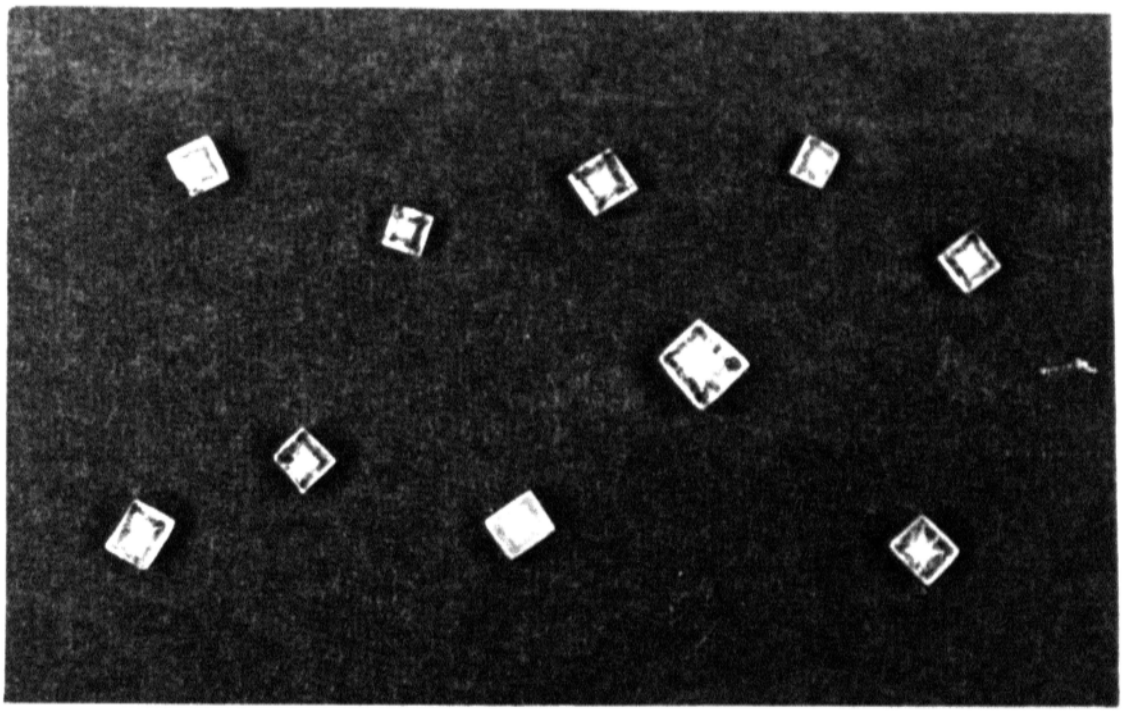

Qualitative chemical analyses were made to confirm the presence of Ammonium, Bromine and Zinc in the compound. Complete X-ray fluorescence analysis was carried out to estimate the relative numbers of Zn^{2+} and Br^{-} ions. This analysis also revealed the presence of Mn^{2+} ions in the lattice. The single crystals obtained were ground into fine powder and X-ray powder diffractogram was recorded. The diffractogram thus recorded is shown in Fig. III.2. The 'd' values deduced from the diffractograms together with those calculated from the lattice parameter data available in the literature for $(NH_4)_2ZnBr_4$[20], are given in Table III.1. The good agreement between the two sets of values establishes that the crystals obtained are those of $(NH_4)_2ZnBr_4$.

Fig. III.2

X-ray diffractogram of powdered $(NH_4)_2ZnBr_4$ crystals.

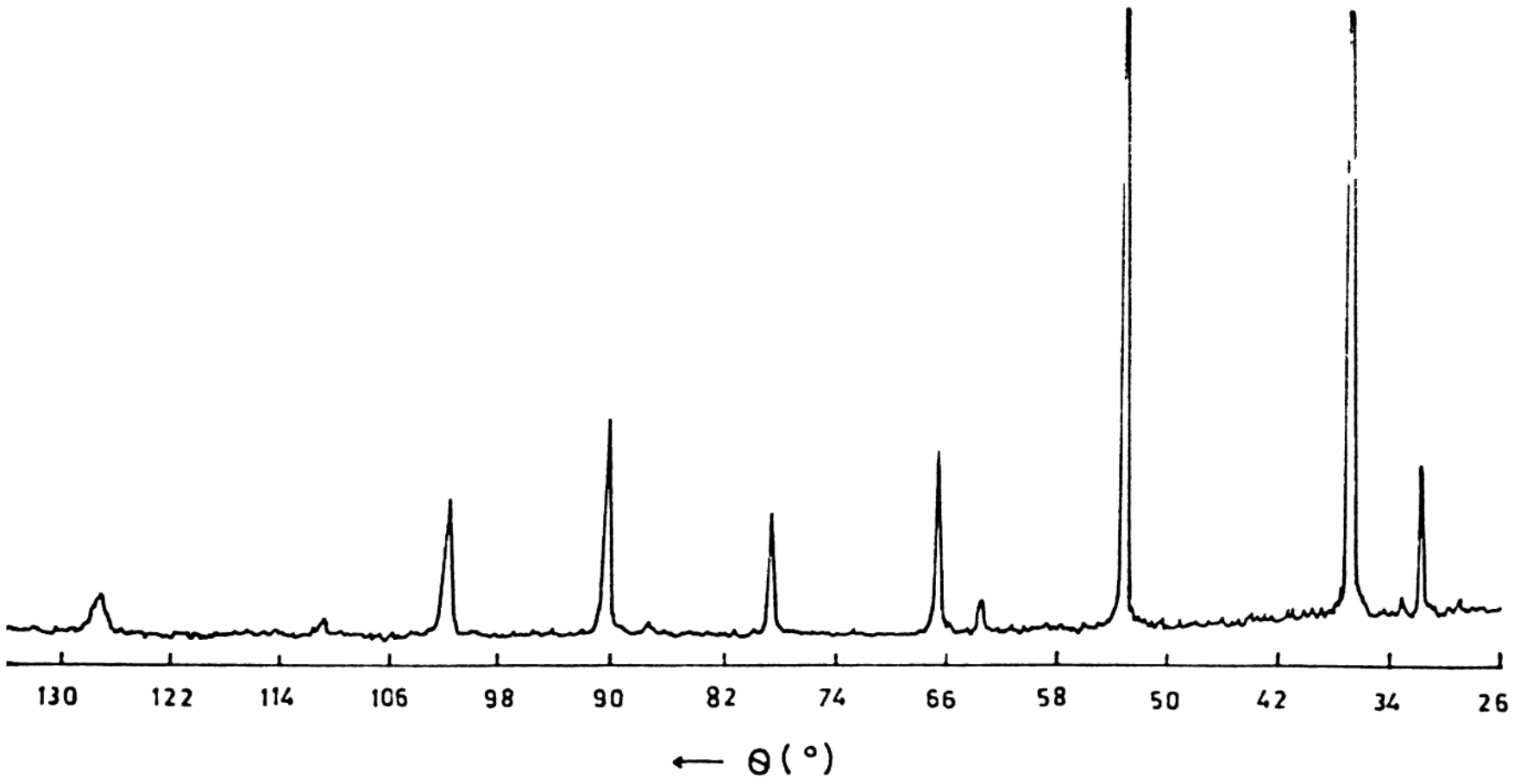
130
122
114
106
98
90
82
74
66
58
50
42
34
26
← θ(°)

Table III.1

'd' values of $(NH_4)_2 ZnBr_4$ lattice

d measured (Present work)	d calculated from the reported lattice parameters *
3.26	3.25
2.00	1.99
1.70	1.71
1.63	1.64
1.41	1.41
1.26	1.26
1.15	1.15
1.10	1.10
1.00	1.00

* A.A. Moskalov et al. Phys.Stat. Sol (a) 72, K 19 (1982)

3. Measurements

3.1 Photoluminescence spectral measurements at room temperature

The set up used for photoluminescence spectral measurements was established as a part of the present thesis work. For the photoluminescence measurements, a sample of size 3 x 3 x 1 mm^3 was fixed on to the cold finger of a stainless steel optical cryostat, with broad face making an angle of 45° w.r.t the direction of the laser beam. Since the beam from the nitrogen laser had a cross section of 15 x 5 mm^2 at the exit of the laser, a cylindrical lens was used to focus it onto the crystal. The width of the focussed spot was about 1 mm. The emitted light was viewed at an angle of 90° w.r.t the laser beam, and was focussed onto the slit of the monochromator using a two-lens combination. The emission spectrum was first monitored on the photon counter of the photon counting system by manual operation to fix the peak position. Sitting on the peak, the position of the laser spot on the sample and the orientation and position of the collecting lenses were adjusted to get the maximum reading on the digital display of the photon counter. The discriminator level was then adjusted to get a reasonable signal to noise

ratio. Finally, the gain of the amplifier and the PMT voltage were adjusted to get about 80% of the maximum deflection of the pen on the recorder, corresponding to the three digits on the photon counter chosen for digital to analog conversion. The emission spectrum was then recorded by using a suitable scan speed.

Fig. III.3 shows the photoluminescence (PL) spectrum at room temperature (RT) of a " Pure " (crystals grown from solution to which no dopants were intentionally added are referred to as " pure ") crystal of $(NH_4)_2ZnBr_4$. The spectrum contains an intense band at 630 nm and a shoulder around 660 nm. The same spectrum was observed for all the crystals grown by using various dopants in the starting solution, except $MnBr_4 \cdot 4H_2O$. Crystals grown from a solution to which 2% $MnBr_4 \cdot 4H_2O$ was added as dopant show a very much reduced emission which could not be recorded. To find out the effect of X-irradiation, the same sample which was used for recording the PL spectrum earlier, was exposed to X-rays for 20 minutes. The crystal acquires orange colour upon X-irradiation. The PL spectrum of the X-irradiated crystal contains the 630 and 660 nm bands as before, but with very much reduced intensity. Also, no new band is observed at R.T.

Fig. III.3

The Photoluminescence spectrum of "pure" $(NH_4)_2ZnBr_4$ at RT ; 337.1 nm excitation.

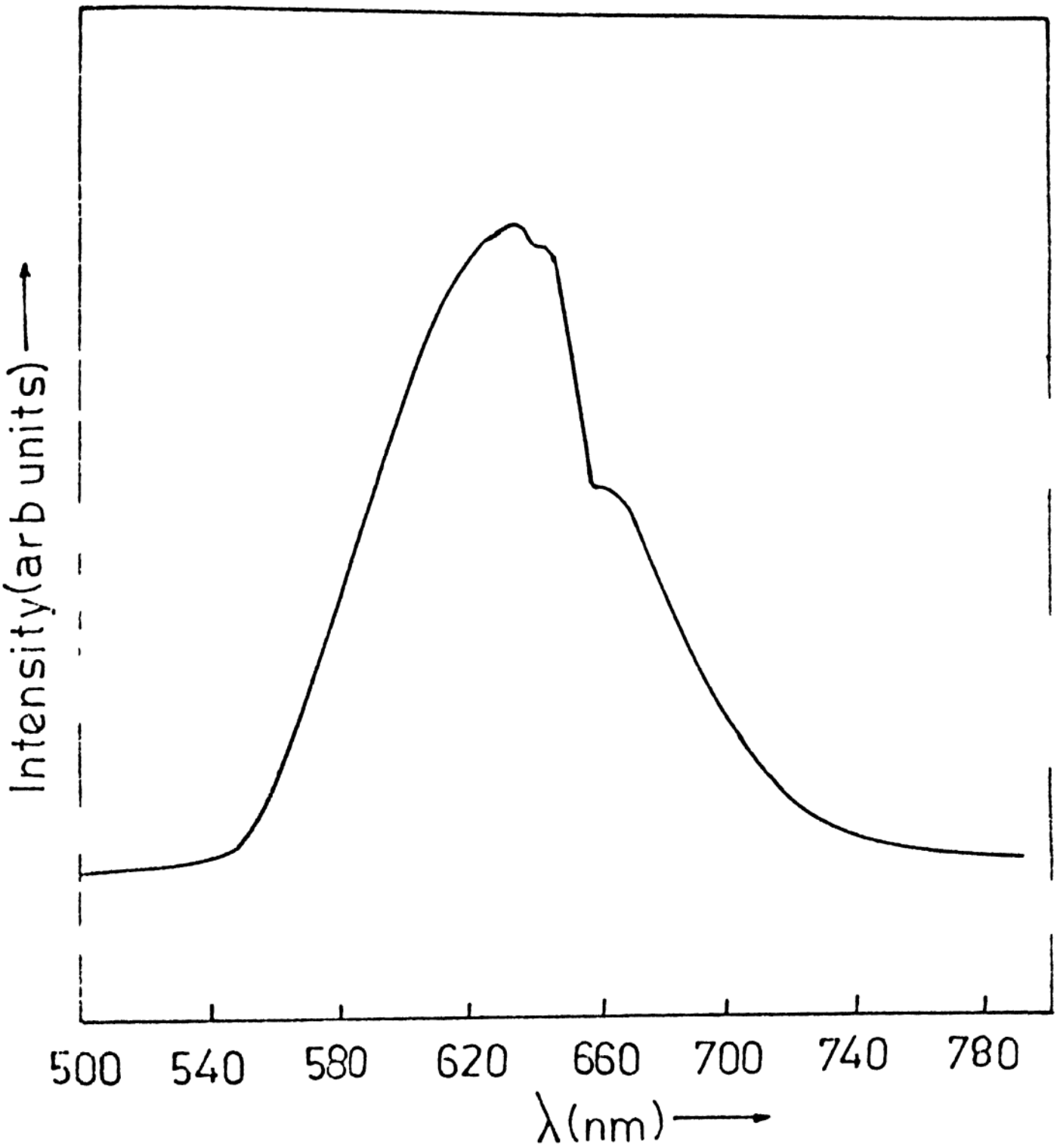
Intensity(arb units)
500
540
580
620
660
700
740
780
λ(nm)

The acquisition of orange colour by the crystal upon X-irradiation, shows the formation of colour centres. Since the native defects in a crystal lattice are influenced by thermal treatment, it was felt worthwhile to find out the effects of thermal quenching on the PL spectrum. Accordingly, an as-grown crystal was maintained at a temperature of 200°C for 1 hour and then rapidly quenched to R.T. This sample, when excited by the laser beam as before, showed feeble orange emission, where as the emission was intense before the thermal treatment.

3.2 Photoluminescence spectral measurements at 100 K.

Photoluminescence spectra were recorded at 100 K, by cooling the sample mounted on the cold finger which was in direct contact with liquid nitrogen. The temperature of the sample could be changed by controlling the power supplied to the heater wound on the cold finger. The PL spectrum of an as-grown sample at 100 K contains the 630 and 660 nm bands, but with very much reduced intensity as compared to the spectrum at RT. Also, the spectrum contains a new band peaking at 535 nm. Fig. III.4 shows the PL spectrum recorded at 100 K of a sample which was X-irradiated for 20 minutes. The green emission band peaking at 535 nm dominates the spectrum, the orange emission being negligible.

Fig. III.4

The photoluminescence spectrum of a "pure" $(NH_4)_2ZnBr_4$ crystal X-irradiated at RT for 20 minutes and recorded at 100 K.

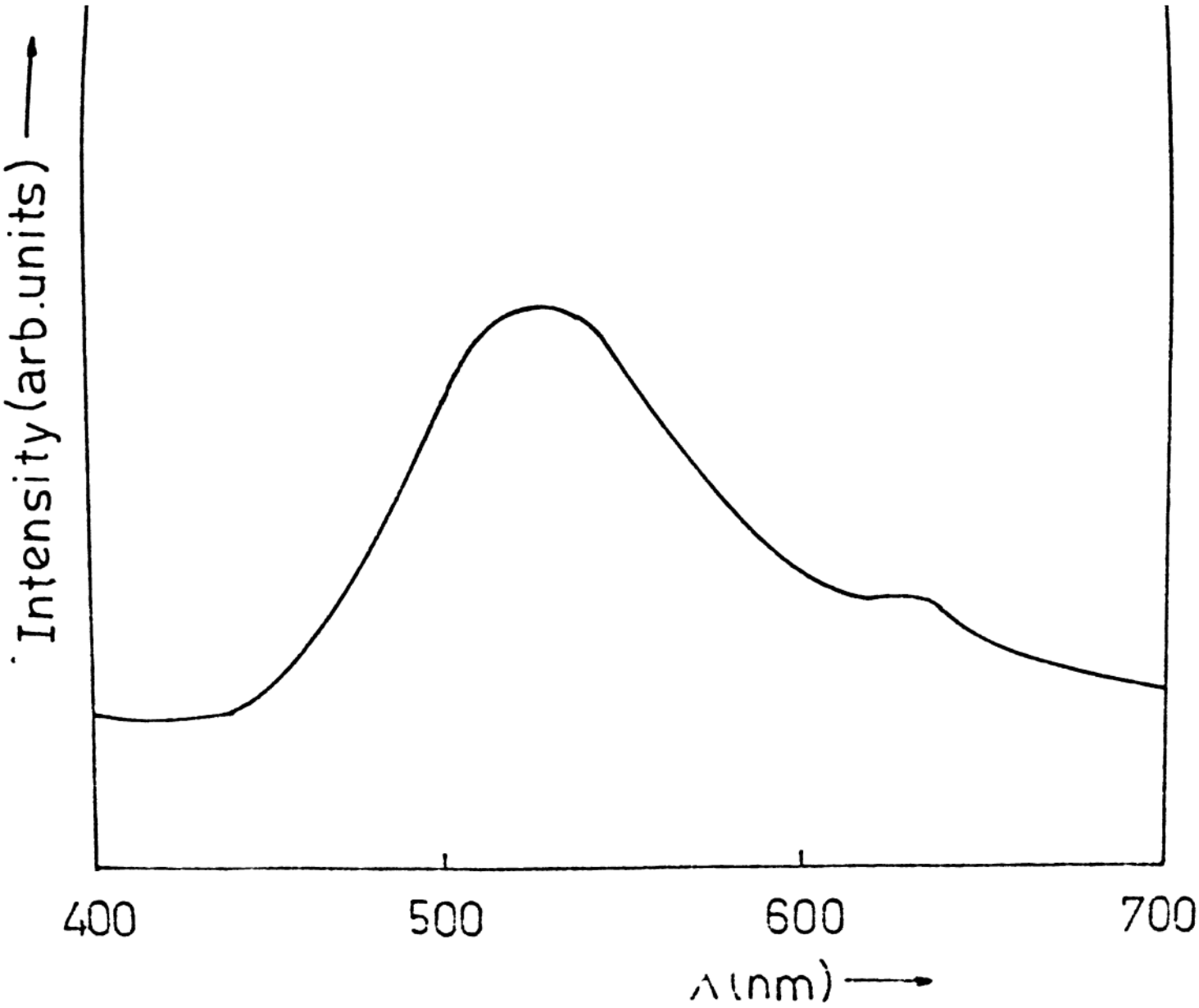
Intensity (arb.units)
400
500
600
700
λ (nm)

3.3 Measurement of luminescence lifetimes

The set up used for determining the luminescence lifetimes at various temperatures was established as a part of the present thesis work. It consists mainly of an arrangement for obtaining trigger pulses, a box-car integrator and a high frequency oscilloscope. The lifetimes associated with the emitting ions were deduced from the respective decay curves. The following procedure was employed for recording the decay curves. First an idea of the decay involved was obtained by observing the decay curve on the oscilloscope following excitation by the laser pulse. The pattern was then optimised by manipulating the appropriate settings. The trigger and the signal input were then given to the box-car integrator. An aperture range of 10 m.secs was found to be appropriate. In the manual operation, exponentially averaged D.C.signal at delay times corresponding to 5,6,7,8,10,15,20,30,40,50,60,80 and 90% of the aperture range was measured with the oscilloscope. In the scan mode, an aperture width of 5 nano seconds was chosen and the aperture range of 10 m.secs was scanned while recording the exponentially averaged D.C. signal level on a y-t recorder.

A typical decay curve obtained for a "pure" crystal at R.T. following pulsed excitation from the nitrogen laser is shown in Fig. III.5. The single exponential curve obtained was analysed using a standard fitting procedure with the help of a D.C.M. Computer. The analysis yielded a value of 1.5 m.secs for the lifetime. In a systematic run, decay curves of a "pure" crystal were recorded at the controlled sample temperatures of 303, 271 and 168 K. At 303 K the emission was orange, where as at 168 K it was mostly green. At the intermediate temperature of 271 K, both the emissions were present. Fig. III.6 shows the decay curves recorded at 303 K and 168 K. The value for life time deduced from the decay curve obtained at 168 K is 2.31 milliseconds.

3.4 Optical absorption measurements

Largest single crystals (about 4x4x1 mm^3) that were obtained in various growth runs were used for the optical absorption measurements. Thin rectangular copper strips just fitting the sample and reference compartments, and having an opening at the expected beam position were used as sample holders. The chosen single crystal was mounted on a thick black paper having a hole of about 3 mm dia such that the crystal covered the entire hole, and this

Fig. III.5

Luminescence decay observed for "pure" $(NH_4)_2ZnBr_4$ at RT, following excitation by a 10-nano second pulse from nitrogen laser.

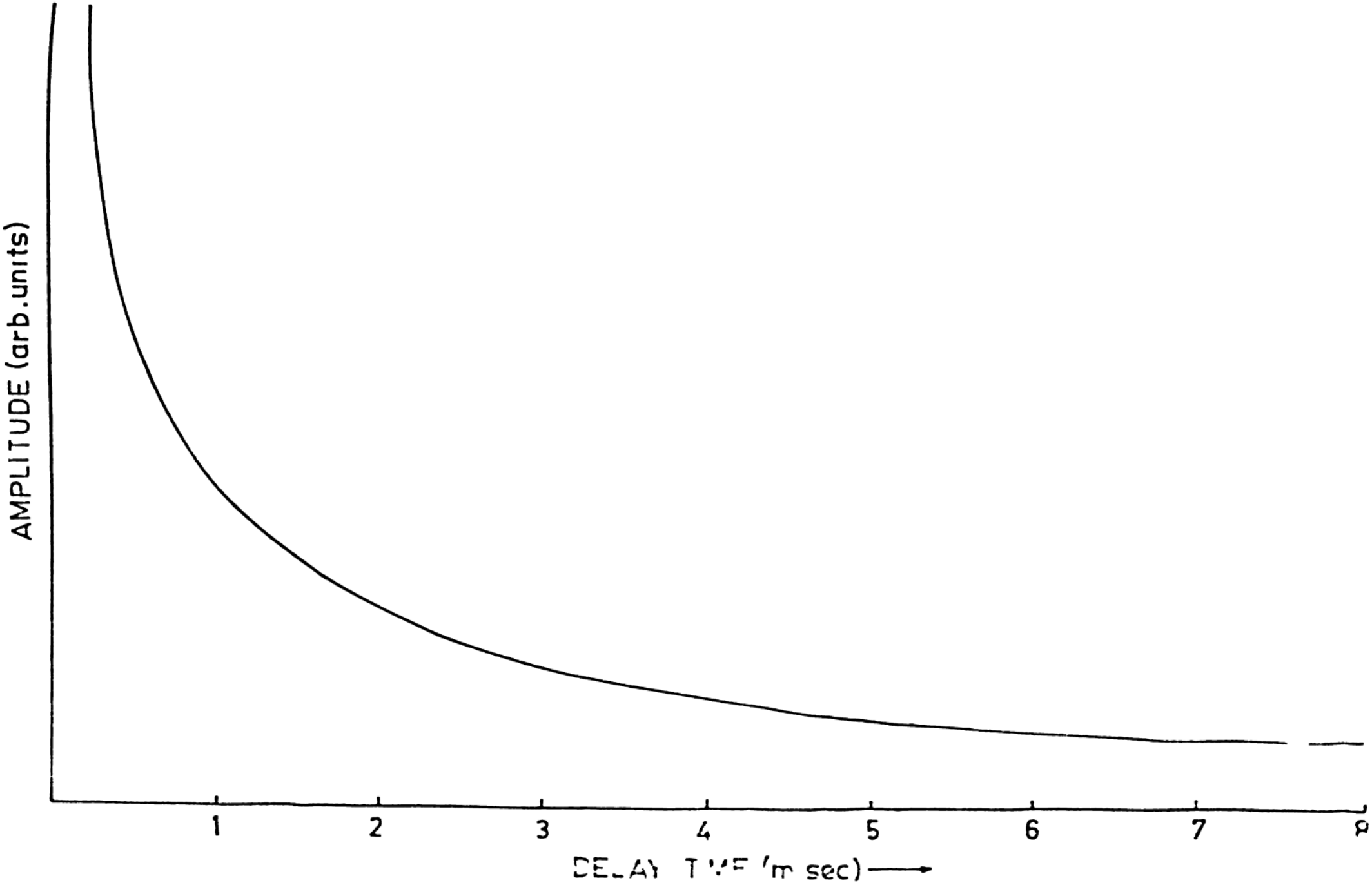
AMPLITUDE (arb.units)
1
2
3
4
5
6
7
DELAY TIME (m sec)

Fig. III.6

Luminescence decay observed for "pure" $(NH_4)_2ZnBr_4$ at 167 K (filled circles) and 303 K (open circles), following excitation by a 10-nano second pulse from nitrogen laser.

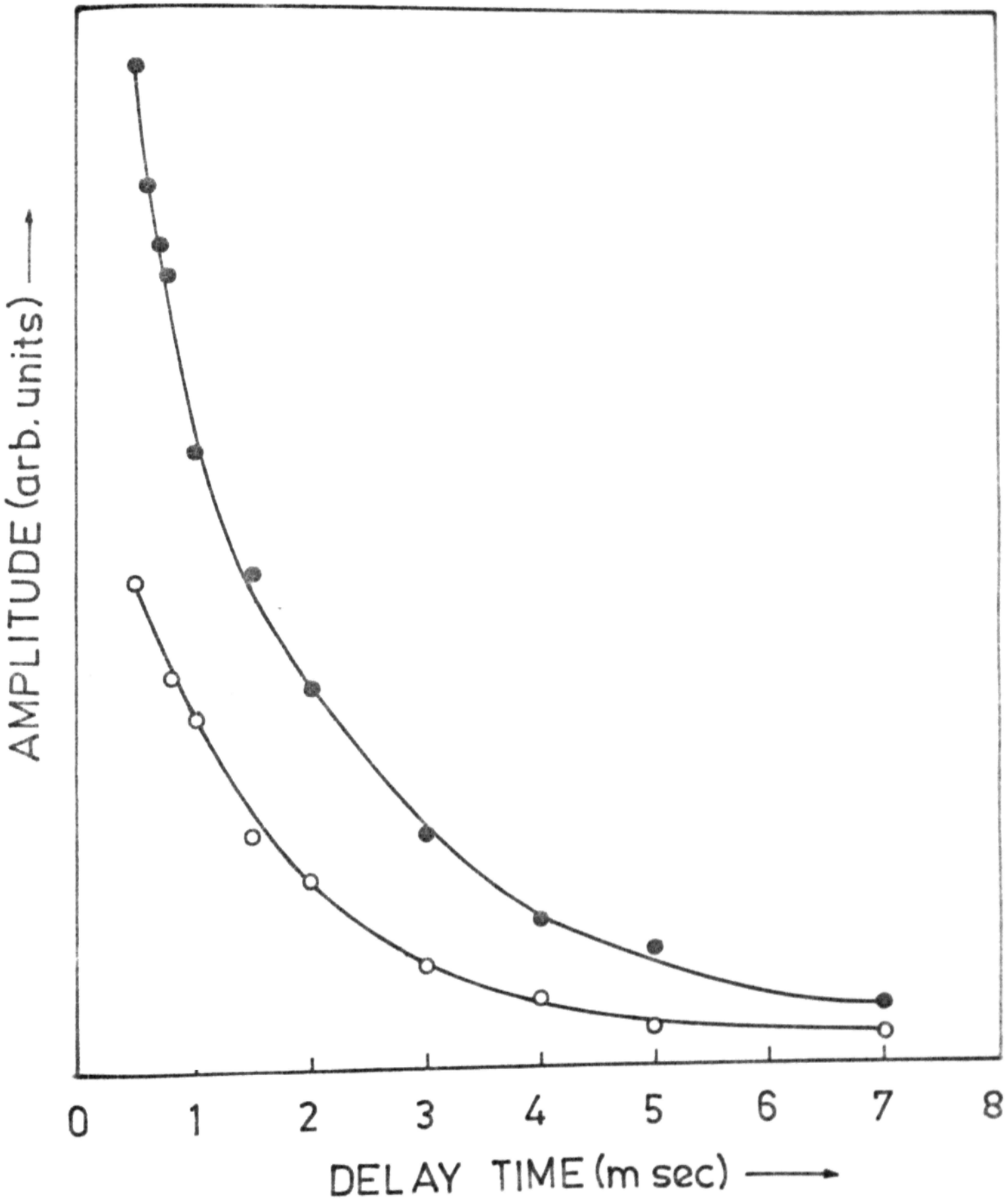
AMPLITUDE (arb. units) ⟶
0
1
2
3
4
5
6
7
8
DELAY TIME (m sec) ⟶

paper was fixed onto the copper strip. In the reference compartment, a black paper with similar hole was used. The scan was interrupted at 400 nm to change the source, and the required balancing was automatically taken care of. All the measurements were made only at RT, since the facility for low temperature measurements is not available with the instrument used.

The optical absorption spectrum recorded using an as-grown "pure" crystal and covering the range 200-600 nm is given in Fig. III.7. The spectrum shows strong absorption in the near U.V. region with a prominent absorption band at 294 nm and a composite of overlapping absorption bands in the region 200-270 nm. Since radiation damage could occur in crystalline solids, the "pure" crystals were X-irradiated for 20 minutes. The crystals have acquired orange colour upon X-irradiation, indicating the formation of radiation damage centres. The optical absorption spectrum of the X-irradiated crystal is given in Fig. III.8. As expected from the orange colour of the irradiated crystal, an intense new absorption band is seen in the visible region, which peaks at 460 nm. Also, there are changes in the absorption in the near U.V. region, bands now appearing around 206, 232 and 272 nm. To test whether the irradiation-

Fig. III.7

Optical absorption spectrum of an as-grown, "pure" $(NH_4)_2ZnBr_4$ crystal at RT.

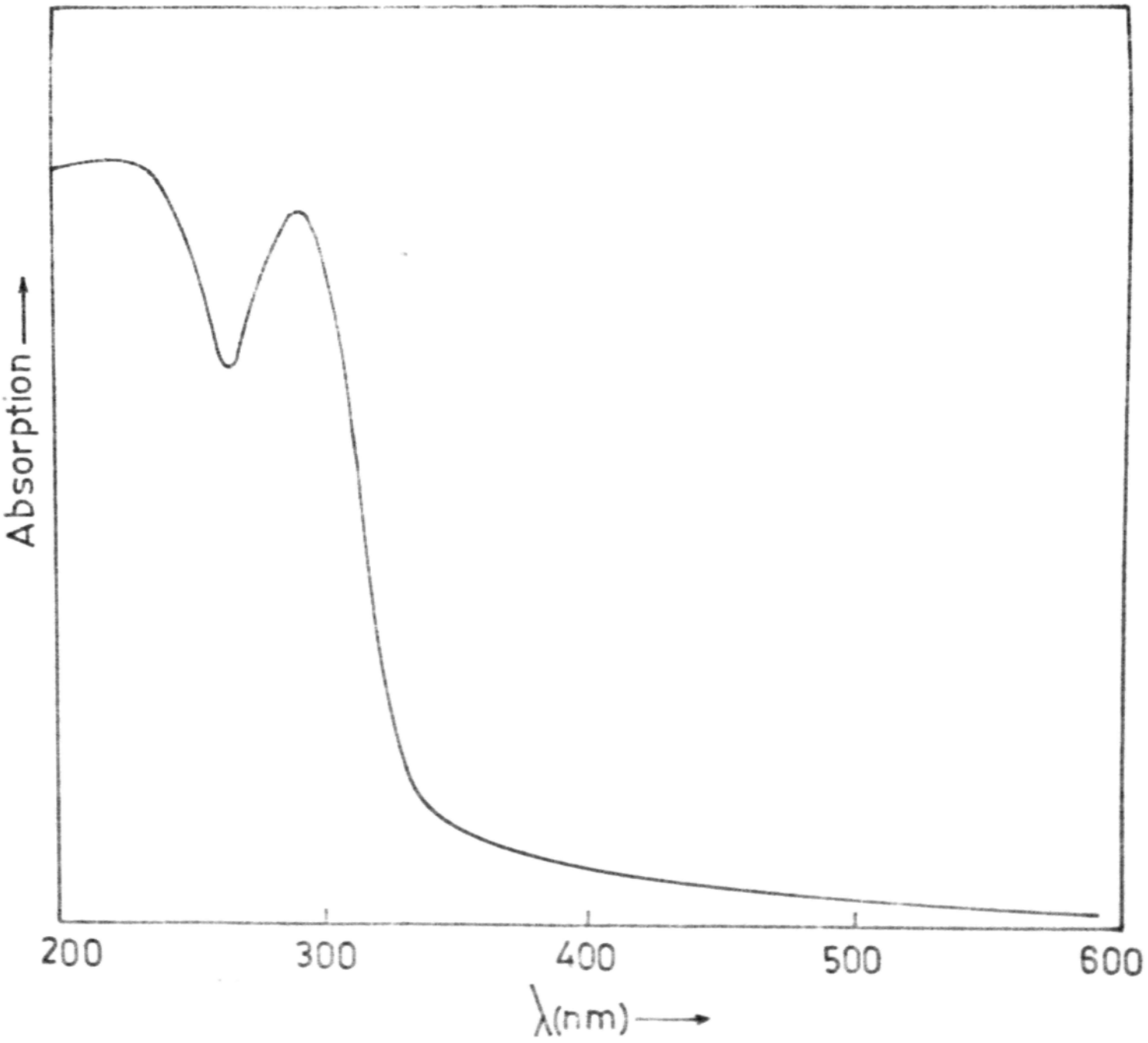
Absorption
200
300
400
500
600
λ(nm)

Fig. III.8

Optical absorption spectrum of an X-irradiated, "pure" $(NH_4)_2ZnBr_4$ crystal at RT.

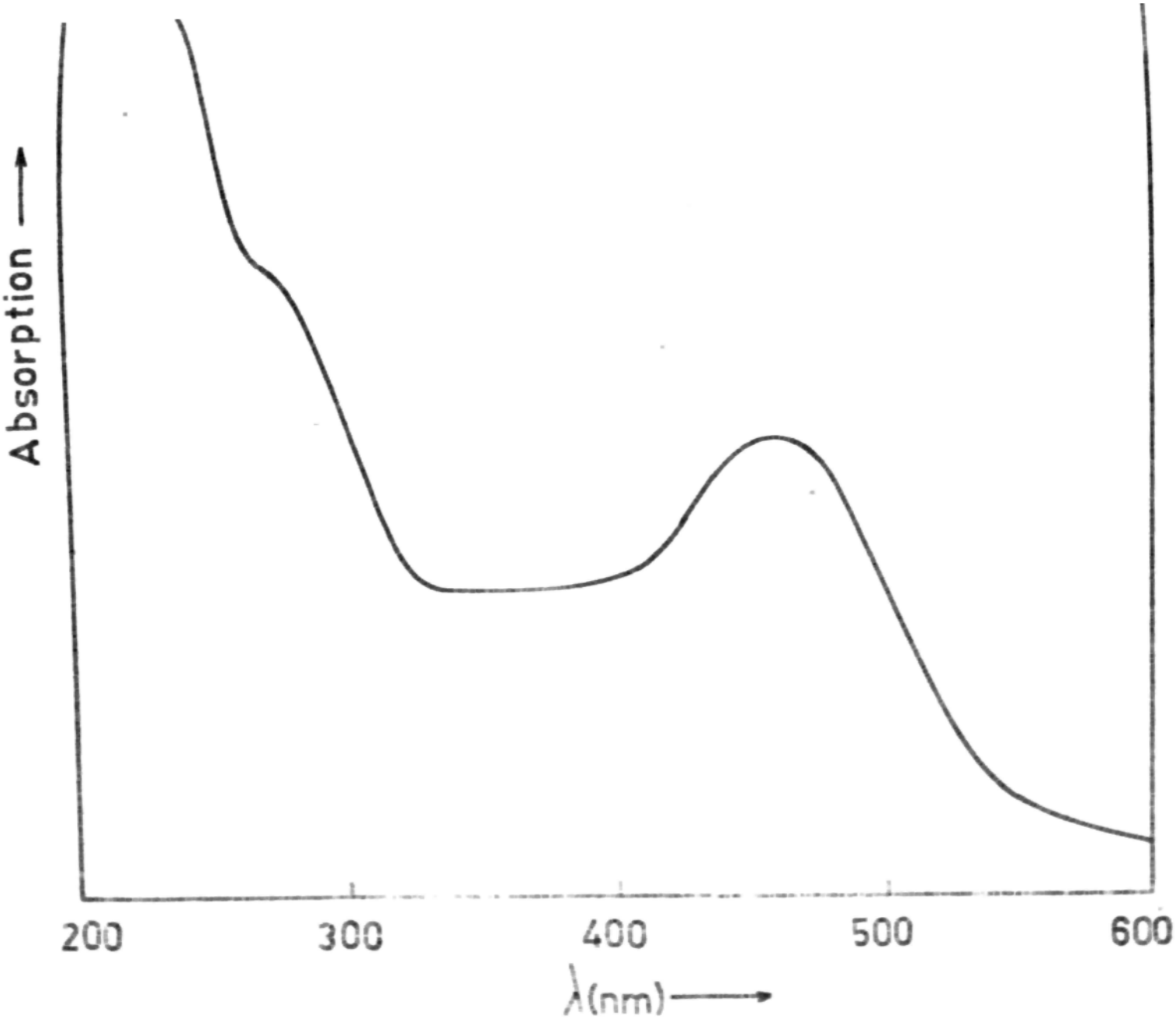
Absorption
200
300
400
500
600
λ(nm)

produced centres responsible for the 460 nm band could be bleached with the corresponding light, the irradiated crystal was exposed to 460 nm light for 1 hour. The 460 nm light was obtained from a combination of a xenon lamp and a monochromator, and was focussed onto the irradiated sample. The irradiated crystal was found to lose the orange colour completely.

4. Results and Discussion

The EPR results to be described in chapter V show that Mn^{2+} ions are present in all the crystals as background impurities. Both the 630 and 660 nm emission bands are assigned to Mn^{2+} ions. The assignment is based on the value for the life time observed for the orange emission. The observed value of 1.5 milliseconds is typical of Mn^{2+} ions in crystalline solids. The most likely substitutional site in the $(NH_4)_2ZnBr_4$ lattice for Mn^{2+} ion is the Zn^{2+} site. If the $(ZnBr_4)^{2-}$ complex is undistorted in the lattice, the symmetry of the Zn^{2+} site would be tetrahedral. The EPR results and the microhardness results to be described in chapter VI, show that the samples used in the present investigations contain associated Mn^{2+} ions. Some of the Mn^{2+} ions may be present in the interstitial sites. The 630 nm

band is assigned to Mn^{2+} ions at the Zn^{2+} sites in the lattice and the weaker band around 660 nm should be arising from Mn^{2+} ions at sites with symmetry lower than cubic. Surely, Mn^{2+} ions at sites with different symmetries lead to different EPR spectra. Infact, clearly identifiable EPR spectra from Mn^{2+} ions in different environments have been observed in the present work (Chapter V). These spectra could only be identified in the recordings of thermally quenched crystals. Unfortunately, thermal quenching leads to such a reduction in the emission intensity that it was not possible to correlate the EPR and photoluminescence observations.

Table III.2 shows the absorption and emission data of certain Mn^{2+}- doped single crystals. The absorption bands corresponding to transitions from the ground state to the low-lying excited states of Mn^{2+} in crystalline solids occur in the visible and near U.V. region. The fitting of the observed bands to the energy level diagram determined by the strength and symmetry of the crystal field to which the Mn^{2+} ions are exposed, is possible only when at least two bands are identified. The excitation wavelength of 337.1 nm falls within the absorption band peaking at 294 nm. It is probable that the 294 nm

Table III. 2

Experimentally observed positions of absorption bands and the emission band of Mn^{2+} in some insulators

System	Absorption bands nm	Emission bands nm
1. $KMgF_3$: Mn	397	340
	398	610
	399	680
2. $KZnF_3$: Mn	398	-
	400	-
3. SrF_2 : Mn	325	500
	425	-
4. NaCl : Mn^{2+}	595	-
	110	-
5. NaF : Mn^{2+}	580	-
	670 to 770 (broad band)	-
6. MgF_2:Mn^{2+}	390	-
	590	-
	670	-
	700	-
7. CaF_2:Mn^{2+}	-	310
		450

band is one of the absorption bands of Mn^{2+}, since the emission certainly arises from Mn^{2+} ions. However, the observed reduction in the intensity of the emission band after X-irradiation suggests another mechanism. The 294 nm absorption could be attributed to an imperfection in close proximity with Mn^{2+}, the emission arising from Mn^{2+} ions due to energy transfer. X-irradiation changes the charge state of the ions associated with Mn^{2+} ions. Thermoluminescence measurements to be described in Chapter IV strongly support this mechanism. In addition to the band at 272nm, the absorption spectrum (Fig.III.8) contains overlapping bands in theU.V.region. Cooling the crystal shifts the absorption bands, resulting in more efficient excitation of some other centres. This explains the reduction in intensity of the emission bands at 630 and 660 nm. The appearance of new emission band at 535 nm could be attributed to Mn^{2+} ions associated with the centres which are more efficiently excited at 100 K. The assignment of 535 nm emission band to Mn^{2+} ions is based on the luminescence life times. The luminescence decay curve at RT (Fig. III.5) represents the dynamics of centres responsible for the orange emission, whereas the curve at 168 K represents the

centres responsible for the green emission. The fact that lifetimes of 1.5 and 2.3 milliseconds were observed at the two temperature, which are typical of Mn^{2+} ions in insulators, indicates that Mn^{2+} ions are responsible for the green emission as well.

The existence of associated Mn^{2+} ions in the "pure" crystals of $(NH_4)_2ZnBr_4$ used, has been known from EPR and microhardness measurements. Additional doping of Mn^{2+} ions might be resulting in the concentration quenching of luminescence, which explains the drastic reduction in the emission intensity of Mn doped crystals.

On the basis of the effect of optical bleaching, the correlation of optical absorption and thermoluminescence results (Chapter IV) together with extensive literature available on the F-like centres in solids, the 460 nm absorption band is attributed to the formation of F-like centres in $(NH_4)_2ZnBr_4$ upon X-irradiation. F-like centres have been identified in several categories of crystalline solids. The F-centre and its aggregates like the M- and R- centres, the F^--centre and F_A-centre in alkali halides have been extensively studied. Larger aggregates of F-centres form on special treatments.

EPR, ENDOR, optical absorption, ionic-conductivity and dielectric loss are the main physical methods employed in identifying and studying the properties of these centres. In alkaline earth oxides, the F^+- and F-centres and the possible analogues of M- and R-centres in alkali halides have been identified. It is the EPR technique which played a major role in the identification of the F^+-centre in alkaline earth oxides, sulfides and selenides. The wave function of the F^+-centre is highly delocalized, and the ENDOR spectrum contained evidence of interaction with ions as far away as in the fifth shell. The identification of the absorption bands corresponding to the F^+ and F-centres in alkaline earth oxides came much later than the EPR studies. Even then, the identification was difficult because of the presence of impurity bands[23]. The conclusive identification came from a combination of several observations, including a correlation with the EPR spectrum, thermal annealing behaviour, the effects of additive colouration and optical bleaching and Faraday rotation. The emission band of F^+ centre in MgO, CaO and SrO has been identified. Vibronic structure on both the absorption and emission bands has been observed. Perturbed F^+ centres involving charged defects in the

vicinity of F^+ centres in the lattice have also been observed[24]. The formation of F^+ centres in other oxides like ZnO, BeO, Al_2O_3, TiO_2 and Bi_2O_3 has been speculated[25]. A combined study of EPR and optical absorption indicated the formation of two types of F-centres in BaFCl and SrFCl crystals[26]. X-irradiation of calcium fluorophosphate, $Ca_{10}(PO_4)_6F_2$, produced F-centres in the lattice[27]. The identification was based, again, on a correlation of EPR, ENDOR and optical absorption results. However, all the variety of careful measurements and in such details, that were required to conclusively identify the F-like centres in alkali halides and alkaline earth oxides are also required here. Since the EPR technique played a major role in identifying the F-like centres in solids, the first requirement is to grow crystals of $(NH_4)_2ZnBr_4$ without the background Mn^{2+} ions, so that the EPR spectra from centres other than Mn^{2+} could be observed. With the crystals used in the present investigations, any such spectra would be buried under the intense Mn^{2+} spectrum. Also, the absence of Mn^{2+} ions would help greatly the study of absorption and emission properties of other centres. However, we have not been successful in producing such crystals.

References

1. M. Iizumi, J.D. Axe and G. Shirane, Phys. Rev. B15, 4392 (1977).

2. I.P. Aleksandrova, A.K. Moskalev and I.A. Belobrova, J. Phys. Soc. Japan (Suppl. B) 49, 86 (1980).

3. K. Wada, A. Sawada, Y. Ishibashi and Y. Takagi, J. Phys. Soc. Japan. 42, 1229 (1977).

4. M. Takashige, T. Nakamura, M. Udagawa, S. Iojima, S. Hirotsu and S. Sawada, J. Phys. Soc. Japan 48, 150 (1980).

5. K. Gesi and M. Iizumi, J. Phys. Soc. Japan 46, 697 (1979).

6. K. Wada, A. Sawada and Y. Ishibashi, J. Phys. Soc. Japan 47, 1185 (1979).

7. K. Wada, H. Uwe, A. Sawada, Y. Ishibashi, Y. Takagi and T. Sakudo, J. Phys. Soc. Japan 43, 544 (1977).

8. K. Wada, A. Sawada and Y. Ishibashi, J. Phys. Soc. Japan 45, 1429 (1978).

9. E. Francke, F. Le Postollec, J.L. Mathieu and H. Poulet, Solid State Commun. 33, 155 (1980).

10. R. Blinc, S. Juznic, V. Rutar, J. Seliger and S. Zumer, Phys. Rev. Lett. 44, 609 (1980).

11. H. Matsunaga and E. Nakamura, J. Phys. Soc. Japan 50, 2789 (1981).

12. T. Sato, M. Endo, T. Osaka and Y. Wakita, J. Phys. Soc. Japan 51, 3411 (1982).

13. T. Ueda, S. Iida and H. Terauchi, J. Phys. Soc. Japan 51, 3953 (1982).

14. R. Blinc, D.C. Ailion, P. Prelorsek and V. Rutar, Phys. Rev. Lett. 50, 67 (1983).

15. I.P. Aleksandrova, S. Grande, Yu. N. Moskvich, A.J. Krieger and V.A. Koptsik, Phys. stat. sol. (b) 115, 603 (1983).

16. I.A. Belobrova, A.K. Moskalev, L.V. Bizukina, S.V. Milul and I.P. Aleksandrova, Solid State Commun 33, 1101 (1980).

17. S. Sawada, Y. Shiroishi, A. Yamamoto, N. Takashige and M. Matsuo, J. Phys. Soc. Japan 44, 687 (1978).

18. R. Blinc, M. Burgar, J. Slak. V. Rutar and F. Milia, Phys. stat. sol. (a) 56, K65 (1979).

19. T. Osaka, M. Komukae andY.Nakita, J. Phys. Soc. Japan 51, 3409 (1982).

20. A.K. Moskalev, L.A. Belobrova, L.I. Zherebtsova and I.P. Aleksandrova, phys. stat. sol. (a) 72, K19 (1982).

21. I.A. Belobrova, Solid State Com un. 33, 1101 (1980).

22. " Point defects in solids " Ed: J.H Crawford, Jr; and L.M. Slifkin, Plenum Press, New York - London (1972).

23. J.E Mertz, G.S. Saville, L. Hall and P. Auzins, Proc. Brit. Ceram. Soc. 1, 59 (1964).

24. J.C. Kemp, W.M. Ziniker, J.A. Blaze and J.C. Cheng Phys. Rev. 171, 1024 (1968).

25. J.M. Smith and W.E. Vense, Phys. Letts. 31A, 147 (1970).

26. M. Juste, L. Taurel, W. Rahmani and D. Lemoyne, J. Phys. Chem. Solids 37, 961 (1976).

27. W.W. Piper, L.C. Kravitz, and R.F. Swank, Phys. Rev. 138, A1802 (1965).

CHAPTER IV

THERMOLUMINESCENCE STUDY OF $(NH_4)_2ZnBr_4$

1. Introduction

2. Kinetics of TL

3. Results and Discussion

References

1. Introduction

The role of Mn^{2+} as an efficient activator in luminescence systems is well known[1]. Ionic and partially ionic crystals containing Mn^{2+} ions are ideally suitable for thermoluminescence (TL) study, since the information required for interpreting the TL results can readily be obtained for these systems by EPR, photoluminescence and optical absorption techniques. Infact, most of the ionic crystals studied by TL contained either Mn^{2+} or certain rare earth ions as impurities[2-5]. Though Mn^{2+} ions surely act as emission centres in TL process, two different mechanisms of excitation have been proposed in the literature. Conversion of Mn^{2+} to Mn^{3+} during irradiation and the formation of excited Mn^{2+} ions when the electrons are thermally released from the traps is onemode of excitation. Alternatively, Mn^{2+} ions in close proximity to primary emission centres can be excited by energy transfer. F-centres, which are readily formed in alkali halides on irradiation, have been found to play a role in the TL process[6]. Infact in SrFCl and BaFBr, which are mixed crystals, two types of F-centres corresponding to F^- and Cl^- or Br^- vacancies have been involved[7,8]. F-centres can easily be bleached out by

F-light, and the effect of optical bleaching on TL was studied by Bhan and Rao[6]. Since imperfections are directly involved in TL process thermal treatments like annealing, also effect the glow curves[9].

No TL work has been reported till now on any of the systems belonging to the β-K_2SO_4 family. The present study is aimed at investigating the thermoluminescence due to the imperfections which are evident from the optical absorption and photoluminescence studies, as well as to correlate the changes occuring on optical bleaching.

2. Kinetics of TL

In the study of the phenomenon of TL, a knowledge of kinetic order is essential to determine accurately the trap depth. This information is also helpful in forming the basis for a model to explain the TL process. However in many TL investigations, the main interest is in the trap depth rather than the determination of kinetic order "Per Se". The occurance of multiple glow curves and multiple spectral responses complicates the investigation of the kinetics for TL process. The widely used method for determining the order of kinetics

is based on the glow curve. Since the glow curves can be easily recorded, this method has experimental convenience. The kinetic order could also be determined by observing the isothermal decay of emission.

The first quantitative analysis of the glow curves was worked out by Randall and Wilkins[10]. The probability of an electron escaping from a trap is given by

$$P = P_0 \, e^{-E/kT} \qquad (1)$$

where P_0 is the " attempt - to - escape " frequency (frequency factor) and E is the trap depth. Equation (1) requires the assumption that retrapping does not occur, that P_0 and E are temperature indo endent and that freed carriers undergo radiative transitions.

If the kinetics involved are of first order, then several approximate methods of analysis of glow curves based on either the leading edge, or the trailing edge or the half width of a glow peak are available. The parameters involved in the analysis are shown in Fig. IV.1. If T_g is chosen then equation (1) leads to the following expression for the trap depth:

$$E = 25 \, kT_g \qquad (2)$$

Fig. IV.1

The parameters occuring in the analysis of glow curves ; the glow peak shown in, typical for first order kinetics and a linear heating rate.

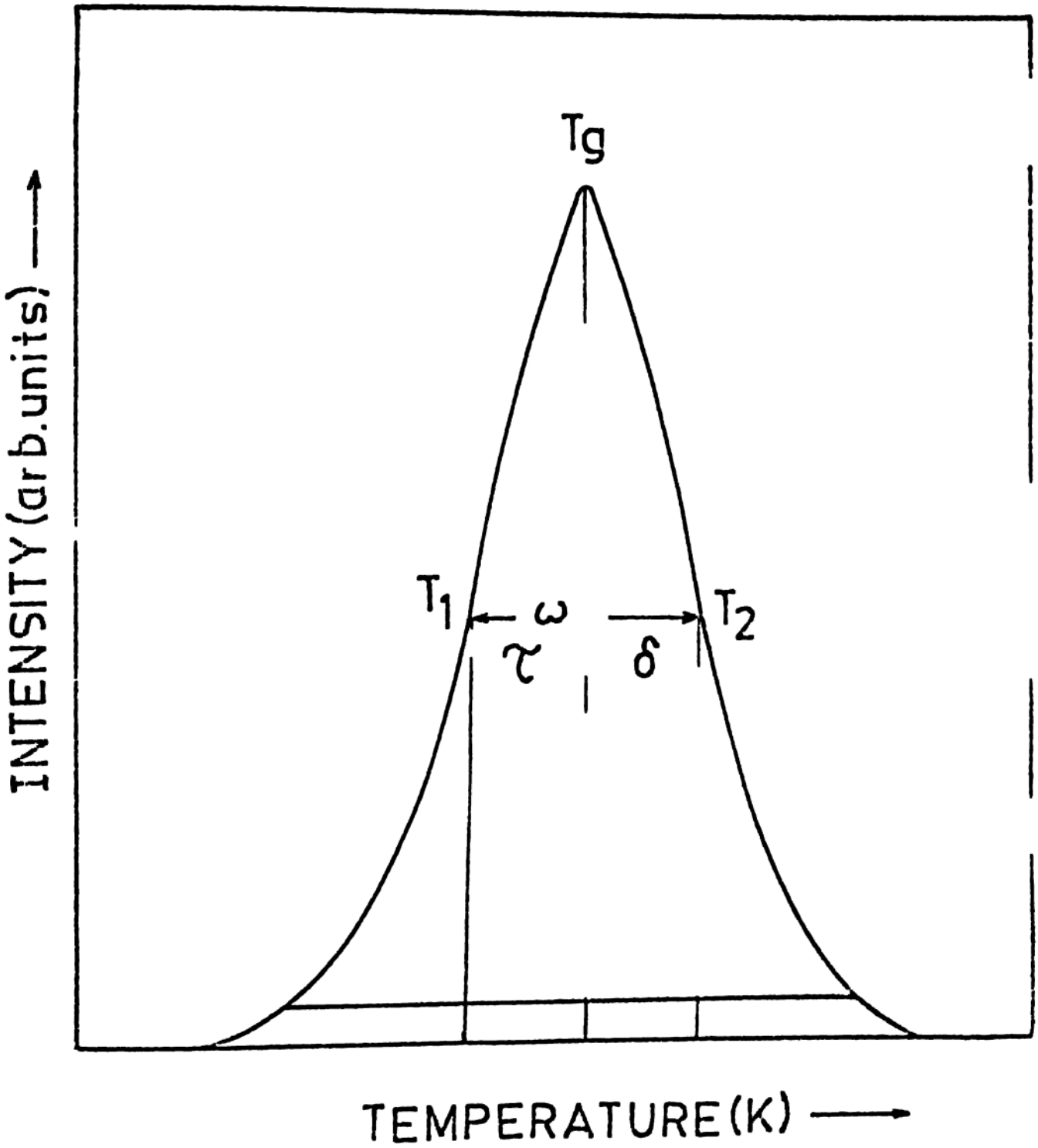
Tg
T1
ω
T2
τ
δ
INTENSITY (arb.units)
TEMPERATURE (K)

The Halperin-Branner analysis, as refined by Chen[11], gives the following expressions for E and P_o :

$$E = \frac{1.52(1 - 1.58\Delta)}{kT_g^2/\tau} - 3.16\ kT_g \qquad (3)$$

$$P_o = (E/kT_g^2)\ e^{E/kT_g} \qquad (4)$$

where $\Delta = (2\ kT_g/E)$ and β is the heating rate of the crystal.

Luschick's formula as refined by Chen reads as

$$E = 0.976\ (kT_g^2/\delta) \qquad (5)$$

Chen has proposed an analysis in terms of the total half-width ω, which leads to the expression

$$E = 2.29\ kT_g^2/\omega$$

The formulae mentioned above are all based on a very limited data corresponding to certain specific parts of the actual glow curve. For more reliable values of E and P_o more data points need to be taken. One such method is due to Garlick and Gibson[12] which involves the initial rise of the glow peak. The ideal method would, of course, involve fitting of the entire glow peak. A graphical method of curve fitting for

finding the appropriate parameters of first order thermally stimulated current peaks has been suggested by Cowell and Woods[13]. The method is also applicable to first order TL curves. Chen and his co-workers have given numerical curve fitting methods, involving the use of a computer, for glow peaks of first-order kinetics, second-order kinetics and general order kinetics[14,15]. A first-order glow peak can be described by the expression,

$$I(T) = A \exp \left\{ -E/kT - P_o/\beta \int_{T_o}^{T} \exp(-E/kT^1) dT^1 \right\} \qquad (6)$$

where A : constant

E : the activation energy

k : the Boltzman constant

T_o : the initial temperature

β : the linear heating rate

Haake[16] has given the following solution for the integral in equation (6):

$$\int_{T_o}^{T} \exp(-E/kT^1) dT^1 \cong T \exp(-E/kT) \sum_{n=1} (kT/E)^n (-1)^{n-1} \, n! \qquad (7)$$

A good approximation to equation (6) can be obtained by using two terms of the asymptotic series in equation (7) and is of the form

$$I(t) \cong A \exp \left\{ -t - B \exp(-t) t^{-2} \right\} \qquad (8)$$

where $B = P_o E/\beta k$, a constant and $t = E/kT$

For numerical curve fitting, equation (8) should ultimately contain the parameters derivable from the experiment. Accordingly, B is approximated by

$$B \cong \exp(E/kT_g)\,(E/kT_g)^3/(E/kT_g+2) \qquad (9)$$

where T_g is the temperature corresponding to the maximum of the glow peak.

The analysis starts with finding an approximate value for E from the less - detailed methods of analysis. This value, together with the experimentally obtained T_g, are used for determining the trial value for B, which enables the determination of the value of A from (8). These values of A and B are used for curve fitting. The procedure would be repeated incrementing or decrementing the value of E at small enough intervals. Temperatures in the range of 0.9 to 1.1 T_g are generally used for fitting. To determine the closeness of fit, the following procedure is adopted: From the experimental curve, the intensities I_i corresponding to 20 temperatures (T_i) covering the range 0.9 to 1.1 T_g are noted. The normalized values (I_i)are obtained by dividing each I_i by I_g. If $I(T_i)$ are the corresponding values for the computed curve, then the following expression can be used to determine the closeness of fit:

$$S = \sum_{i=1}^{N} (I'(T_1) - I_i')^2 / N$$

More reliable would be the value of E smaller the value of S.

3. Results and Discussion

As - grown crystals of $(NH_4)_2ZnBr_4$ did not show any glow peaks before X-irradiation. Fig. IV.2 shows the dependence of the intensity of glow peaks as a function of irradiation time. A time of 20 minutes is found to be optimum, and this has been used for subsequent measurements. Fig. IV.3 shows the glow curve recorded 2 minutes after X-irradiation at RT and using a heating rate of 0.5 K/sec. Glow curves with different relative intensities of the two peaks, while the peak temperatures remaining the same, were observed with crystals grown by using different dopants. The peak positions of the bands are 356 K and 407 K. Bleaching by F-light for 30 minutes after X-irradiation causes a reduction in the intensity of 356 K peak.

The glow curves were analysed by the approximate methods as well as by curve fitting, as detailed in Section 2. The varintions of A and B as a function of E obtained in the curve fitting process are shown in Tables IV.1 and IV.2. The complete set of data points

Fig. IV.2

Thermoluminescence glow curves of a " pure " $(NH_4)_2ZnBr_4$ crystal for various durations of X-irradiation (a) 20 min. (b) 60 min. (c) 30 min. (d) 10 min. and (e) 5 min.

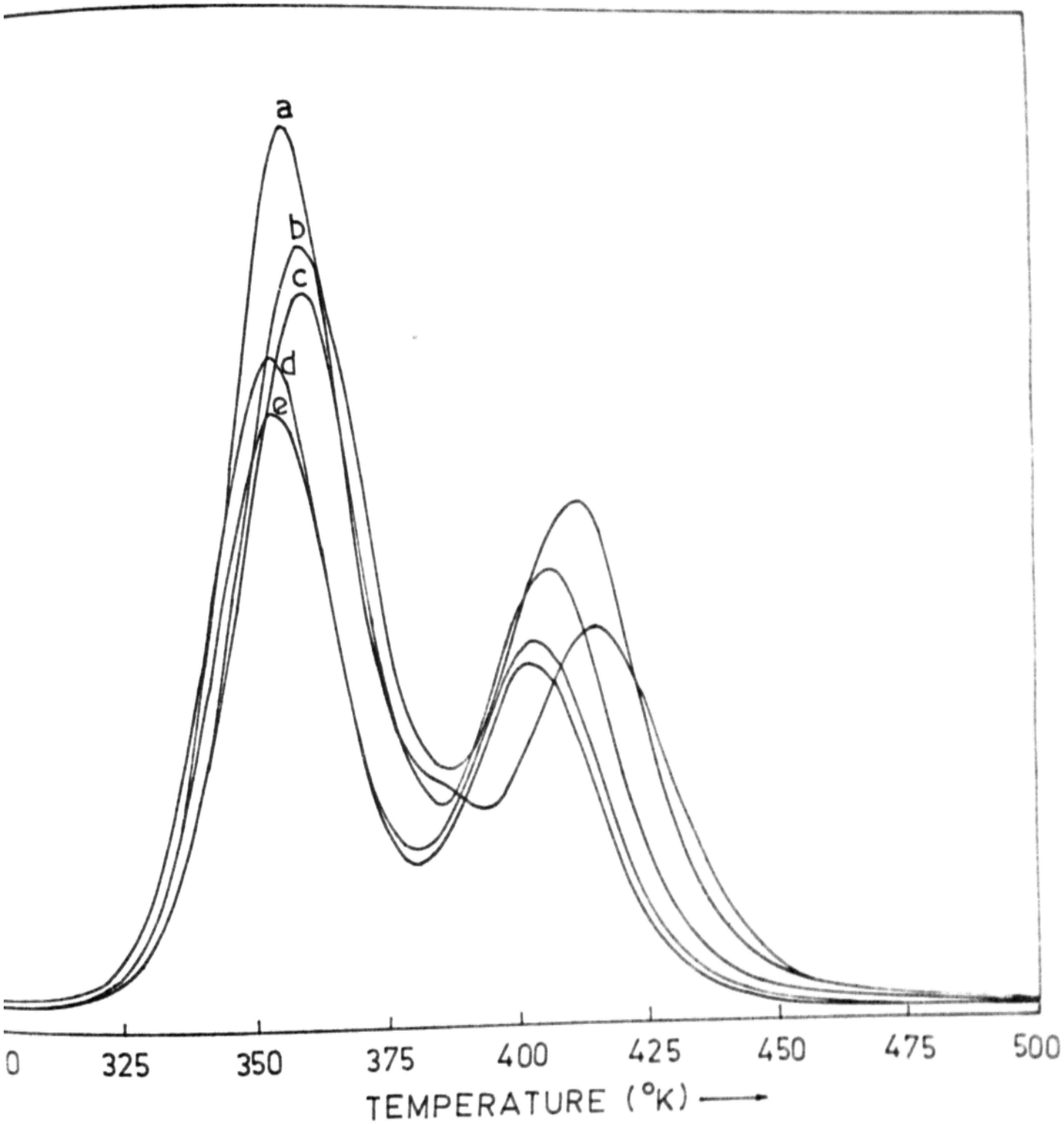
a
b
c
d
e
0
325
350
375
400
425
450
475
500
TEMPERATURE (°K) ⟶

Fig. IV.3

Thermoluminescence glow curve of a "pure" $(NH_4)_2ZnBr_4$ crystal following X-irradiation at RT for 20 minutes; a heating rate of 0.5 K/Sec. was used.

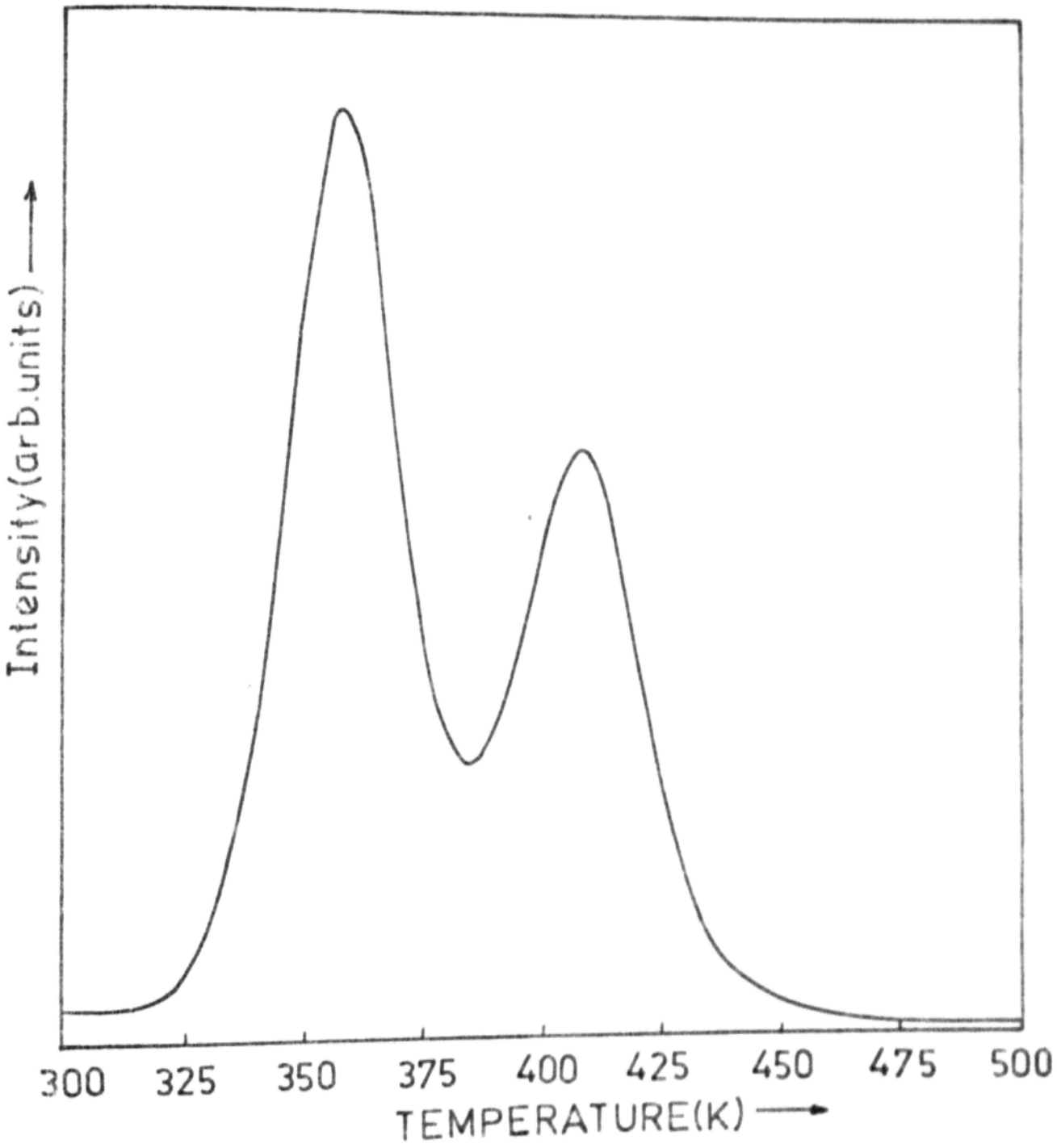
Intensity(arb.units)
300
325
350
375
400
425
450
475
500
TEMPERATURE(K)

Table IV.1

The values of A and B for different values of 'E' for Peak 1

E (ev)	A	B
0.97	2.87×10^{15}	4.85×10^{16}
0.98	3.98×10^{15}	6.86×10^{16}
0.99	5.52×10^{15}	9.69×10^{16}
1.00	7.64×10^{15}	1.37×10^{17}
1.01	1.06×10^{16}	1.94×10^{17}
1.02	1.46×10^{16}	2.74×10^{17}
1.03	2.03×10^{16}	3.87×10^{17}
1.04	2.82×10^{16}	5.46×10^{17}
1.05	3.90×10^{16}	7.71×10^{17}
1.06	5.40×10^{16}	1.08×10^{18}
1.07	7.49×10^{16}	1.54×10^{18}

Table IV.2

The values of the constants A and B for different values of 'E' (ev) for Peak 2

E (ev)	A	B
1.00	7.49×10^{13}	1.66×10^{15}
1.05	5.11×10^{14}	7.58×10^{15}
1.10	1.29×10^{15}	3.46×10^{16}
1.12	2.28×10^{15}	6.33×10^{16}
1.13	3.03×10^{15}	8.57×10^{16}
1.14	4.03×10^{15}	1.16×10^{17}
1.15	5.36×10^{15}	1.57×10^{17}
1.16	7.12×10^{15}	2.12×10^{17}
1.17	9.47×10^{15}	2.87×10^{17}
1.18	1.26×10^{16}	3.88×10^{17}

corresponding to the best fit are given in Tables IV.3 and IV.4, and a plot of these points on the experimental curves is shown in Fig. IV.4. Table IV.5 gives the values of S for the range of values of E used in the fitting process for the first peak. Table IV.6 shows similar values for the second peak. The higher value for S in the case of peak 2 could be due to larger overlap. The closeness of fit observed shows that first-order kinetics areapplicable to the system under investigation. The values obtained for the trap depth E and the frequency factor P_o by various methods are given in Table IV.7.

From the EPR measurements to be described in chapter V, it is certain that all the crystals contain Mn^{2+} ions as background impurities. The optical absorption spectra show bands at 206, 232, 272 and 460 nm of which the 272 nm band has been ascribed to an imperfection other than Mn^{2+}, and the 460 nm band to F-centres. Bleaching of X-rayed crystals with 460 nm light reduces the intensity of the 460 nm absorption band. A corresponding decrease in the intensity of the 356 K glow peak has also been observed. These observations suggest that the 356 K glow peak originates from electron-trapped

Fig. IV.4

Fitting of the glow peaks : the calculated points are denoted by •

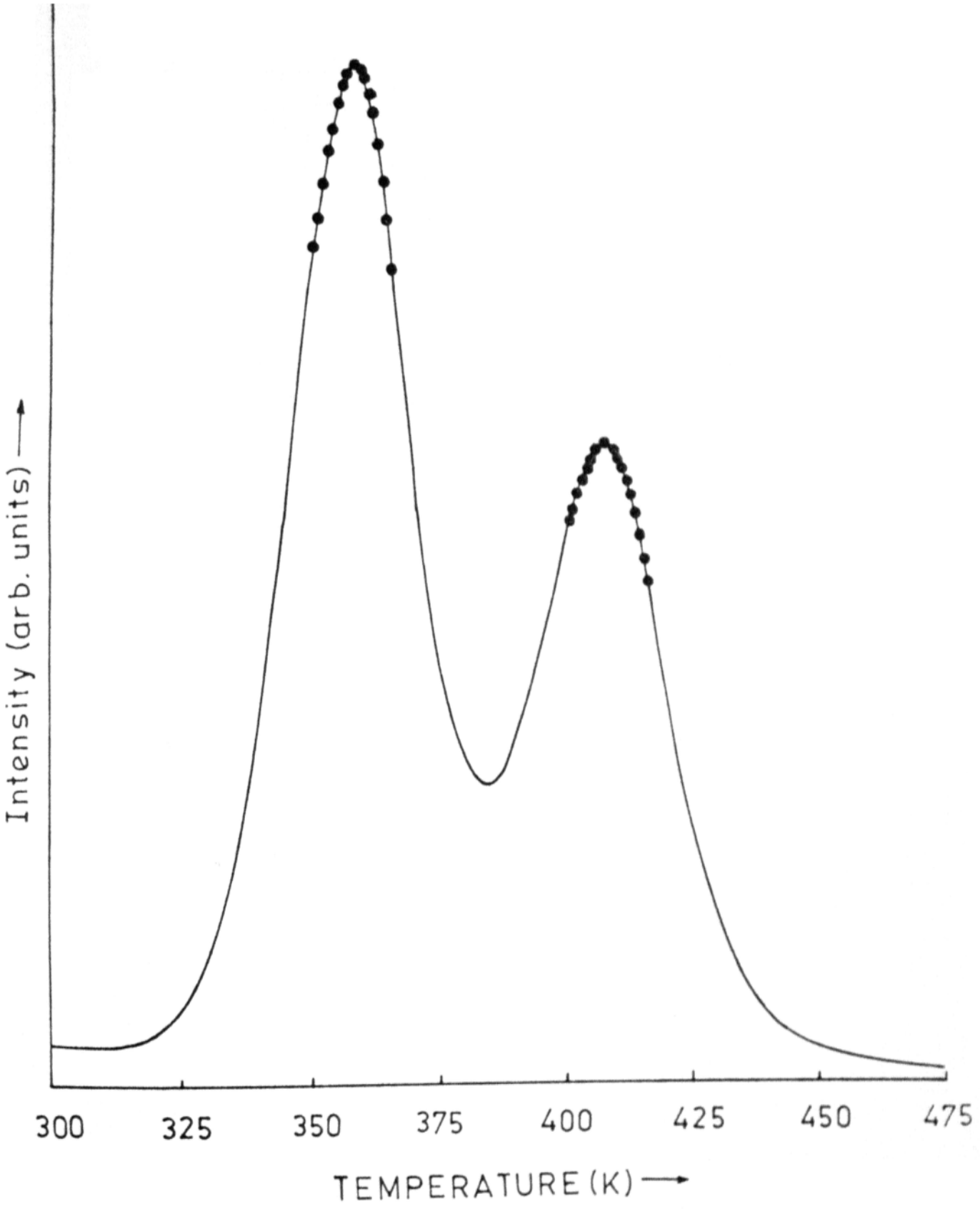
Intensity (arb. units) ⟶
300
325
350
375
400
425
450
475
TEMPERATURE (K) ⟶

Table IV.3

Temperature vs calculated values of Intensity for the activation energy E = 1.05 ev for Peak 1

Temperature (^{o}K)	Intensity (calculated)
350.0	17.6
350.8	18.4
351.6	19.0
352.4	19.7
353.2	20.2
354.0	20.7
354.8	21.2
355.6	21.5
356.0	21.7
357.2	21.65
358.0	21.6
358.8	21.4
359.6	21.0
360.4	20.6
361.2	19.9
362.0	19.1
362.8	18.2
363.6	17.1
364.4	16.0
365.2	14.7

Table IV.4

Temperature vs calculated values of intensity for the activation energy E = 1.13 eV for peak 2.

Temperature	Intensity (Calculated)
400.8	11.6
401.6	11.9
402.4	12.2
403.2	12.5
404.0	13.0
404.8	13.0
405.6	13.16
406.4	13.2
407.0	13.4
408.0	13.35
408.8	13.3
409.6	13.2
410.4	13.1
411.2	12.9
412.0	12.6
412.8	12.3
413.6	11.9
414.4	11.4
415.2	10.9
416.0	10.4

Table IV.5

Values of S representing the "goodness of fit" corresponding to the chosen values of E (Peak 1)

E (eV)	S
0.97	9.8×10^{-2}
0.98	7.8×10^{-2}
0.99	3.3×10^{-2}
1.00	2.3×10^{-2}
1.01	2.1×10^{-2}
1.02	1.4×10^{-2}
1.03	1.2×10^{-2}
1.04	1.2×10^{-2}
1.05	1.1×10^{-2}
1.06	1.4×10^{-2}
1.07	2.0×10^{-2}

Table IV.6

Values of S representing the"goodness of fit", corresponding to the chosen values of E (Peak 2)

E (eV)	S
1.00	5.8×10^{-2}
1.05	3.8×10^{-2}
1.10	2.2×10^{-2}
1.12	2.1×10^{-2}
1.13	1.8×10^{-2}
1.14	1.9×10^{-2}
1.15	2.0×10^{-2}
1.16	2.2×10^{-2}
1.17	2.8×10^{-2}
1.18	3.2×10^{-2}

Table IV.7

Calculated values of E and P_0 by several methods for glow peaks in $(NH_4)_2ZnBr_4$

Equation	Values of E (eV)		Values of P_0 (S^{-1})	
	Peak 1	Peak 2	Peak 1	Peak 2
1. $E = 1.52\ (kT_g^2/\ )\ (1-1.58\ ) - 3.16\ kT_g$ $P_0 = (E/kT_g^2)\ \exp\ (E/kT_g)$	0.97	1.20	24.30×10^{11}	30.78×10^{12}
2. $E = 0.976\ (kT_g^2/\ )$	0.71	0.93	3.68×10^{8}	10.75×10^{9}
3. $E = 2.29\ (kT_g^2/\ )$	0.86	0.96	58.97×10^{9}	26.12×10^{9}
4. $E = 25\ kT_g$	0.77	0.97	28.10×10^{8}	17.94×10^{8}
5. Numerical curve fitting	1.05	1.13	3.8×10^{13}	4.1×10^{12}

anion vacancies. Bhan and Rao[6] have attributed two glow peaks observed in NaF:Mn^{2+} to thermal decay of F-centres, since these peaks diminished on optical bleaching. The glow peak at 407 K arises from detrapping of electrons from imperfection other than Mn^{2+} ions.

Information concerning the luminescence centres is usually obtained from the TL emission spectrum. Our efforts to record the TL emission spectrum were not fruitful. However, in dark a faint orange light was observed with naked eye as the irradiated crystal was gradually heated, suggesting that Mn^{2+} ions act as luminescence centres. Since stable Mn^{3+} centres are unlikely to form in ionic crystals doped with Mn^{2+} ions[6], the possibility of a change in the valence state of Mn ions during irradiation and TL process is ruled out. However, energy tranfer to Mn^{2+} ions as activators from primary emission centres is possible. The emission arises from Mn^{2+} ions presumably when electrons freed in the heating process recombine with holes on the primary emission centres, and the liberated energy transferred to Mn^{2+} ions acting as activators. The first order kinetics observed for both the glow peaks indicate that the primary emission centres and the Mn^{2+} ions are close

enough to behave as a coupled pair, which is also an essential requirement for energy transfer. Such a mechanism has been proposed earlier by Laitano and Martinelli[17] to explain TL results in the case of $CaSO_4:Mn^{2+}$ and $Li_2B_4O_7:Mn^{2+}$, and by de Murcia et al[5] in CdF_2:Eu. It is interesting to note the proposition of de Murcia et al that in CdF_2, the energy transferred to luminescence centres arises from interstitial F^0 ions. Mariani and Alvarez Rivas[18] also involved the inter-stitial halogens to explain the TL process in KI, KBr, NaCl and NaF. In systems like $SrCl_2$, OH^0 radicals are presumed to be involved in the TL mechanism[2]. To check this possibility, we have recorded the IR spectrum of a " pure " crystal in the range 600 - 4000 cm^{-1} which contains rather intense OH^- band.

A variety of centres involving vacancies, vacancy pairs and larger aggregates, impurities at lattice sites and at interstitial positions, associated impurity - vacancy complexes etc could form in crystalline solids. Extensive measurements using a variety of physical methods are generally required to conclusively identify the centres. The crystals used in the

present investigations obviously contain more than two types of imperfections. EPR is among the most useful techniques in the identification of such imperfections whenever they are paramagnetic, but in the present case we are handicapped by the ever present spectra from Mn^{2+} ions. Changes in the relative intensities of the glow peaks observed for crystals grown using Co^{2+}, Ni^{2+} and Cu^{2+} as dopants suggest that native defects are involved. With a hope to influence these defects in a definite way, we have grown crystals using Bi^{3+} and Na^{+} as dopants. However, what we were hoping for did not happen. Obviously Bi^{3+} and Na^{+} ions have not entered the lattice.

References

1. K. Teegarden in " Luminescence of Inorganic Solids " Ed. P. Goldberg, Academic Press, New York (1966).

2. M.D. Sastry, A.G.I. Dalvi, A.G. Page and B.D. Joshi, J.Phys. C : Solid State Phys. 8, 3232 (1975).

3. F.J. Lopez, F. Jaque and F. Agullo-Lopez, J. Phys. Chem. Solids 41, 681 (1980).

4. R.F. Laitano and M.Martinelli, phys. stat. sol.(a) 11, 343 (1972).

5. M. de Murcia, J.Yixin, P. Braunlich, J.P. Jouart and H.J. von Bardeleben, J. Phys. C : Solid State Phys. 15, 2069 (1982).

6. S. Bhan and S.M.D. Rao, J. Phys. C : Solid State Phys. 15 , 6641 (1982).

7. M. Mutha Reddy, K. Somaiah and V. Hari Babu, J. Phys. C : Solid State Phys. 13, 1817 (1980).

8. M.Mutha Reddy, K. Somaiah and V. Hari Babu, phys. stat. sol. (a) 54, 245 (1979).

9. A. Tomita, N. Hirai and K. Tsutsumi, Japan J. appl. Phys. 15, 1899 (1976).

10. J.T. Randall and M.F.H. Wilkins, Proc.Roy. Soc. A184, 366 (1945).

11. R. Chen, J. Appl. Phys. 40, 570 (1969).

12. G.F.J. Garlick and A.F. Gibson, Proc. Phys. Soc. 60, 574 (1948).

13. T.A.T. Cowell and J. Woods, Brit. J. Appl. Phys. 18, 1045 (1967).

14. N.S.Mohan and R. Chen, J. Phy. D : Appl. Phys. 3, 243 (1970).

15. D.Shenker and R.Chen, J.Phys.D : Appl. Phys. 4, 287 (1971).

16. C.H. Haake, J. Opt. Soc. Am, 47, 649 (1957).

17. R.F. Laitano and M. Martinelli, phys. stat. sol. (a) 11, 343 (1972).

18. D.F. Mariani and J.L. Alvarez Rivas, J. Phys. C : Solid State Phys. 11, 3499 (1978).

CHAPTER V

EPR AND PULSED NMR STUDY OF $(NH_4)_2ZnBr_4$

1. Introduction

Electron paramagnetic resonance has been extensively used as a tool to study the structural phase transitions in crystals. EPR of Fe^{3+} doped as a probe into perovskites like $SrTi_1O_3$ provided considerable information about phase transitions, including the observation of deviation from mean field theory for an SPT in a solid[1]. The EPR of Fe^{3+} doped into KH_2PO_4(KDP) enabled a detailed investigation of the ferroelectric phase transition in KDP[2]. In the EPR spectrum of Cr^{3+} in triglycine sulfate, which is a hydrogen bonded ferroelectric, the splittings of the lines were observed to follow a $(T_c - T)^{1/2}$ dependence near T_c indicating that the local geometry followed the mean field theory and is perhaps related to the displacive order parameter[3]. Cr^{3+} has been used as an EPR probe to study phase transitions in many alums[4].

EPR technique is also useful in the investigation of incommensurate phases in solids. Since incommensurate systems do not possess the translational lattice periodicity, there is an essentially infinite number of paramagnetic sites which contribute to the magnetic

resonance spectrum. One thus expects to see a quasi-continuous distribution of resonance frequencies instead of sharp lines as in commensurate crystals. Bhat et al[5] have recently studied the phase changes in $(N(CH_3)_4)_2ZnCl_4$ by EPR using Mn^{2+} ions as probes. The observations covered the paraelectric (P), incommensurate (I), and ferroelectric (F) phases. A single EPR line in the P phase broadened, split and shifted progressively as the crystal was cooled into and through the I phase.

In solids involving a molecular group like NH_4^+, CH_4 or SiH_4, hindred rotations of the group take place and hence there exists a possibility for an order - disorder transition. At low temperatures in the ordered phase, the molecular groups have fixed average orientations, experiencing random reorientations. As the temperature is increased, the extent of reorientations and the fraction of ions reorienting at a given instant increase, and at T_c the tendency to return to an average fixed orientation is compensated by the thermal energy, leading to the onset of the cooperative order - disorder process. Since such a process directly affects the spin lattice

relaxation time of protons in the molecular group, the order - disorder transitions in solids have been extensively studied by pulsed N M R[6-8]. In Ammonium compounds the NH_4^+ ion could rotate from one equilibrium configuration to another, either around a 3-fold or a 2-fold axis[9]. The potential barrier tobe surmounted is different in the two cases, which should be reflected in the plot of spin lattice relaxation time T_1 Vs T. If the compound consists of crystallographically in-equivalent NH_4^+ ions, then the plot of T_1 vs T would contain more than one minima[10]. The phase transitions are reflected as changes in the potential barriers for the reorientations which in turn are observable in an NMR experiment as discernable slope changes in the relaxation rates as a function of temperature.

The $(NH_4)_2ZnBr_4$ crystals grown by us inherently contain Mn^{2+} impurities. It was felt worthwhile to study the paramagnetic centres in this system, and to use the Mn^{2+} EPR spectra to confirm the phase transitions and to identify the phases if possible. The results of such a study together with the results obtained from pulsed NMR experiments are presented in this chapter.

2. Results and Discussion

2.1 EPR

Fig. V.1 shows the EPR spectrum (spectrum I) of an as-grown, 'pure' sample for H parallel to one of the edges of the crystal. It consists of a broad line (ΔH = 450 gauss) around g = 2, showing that Mn^{2+} ions are present in the lattice as clusters. No new lines were observed after X-irradiation. Fig. V.2 shows the EPR recording for the pure sample after quenching from 523 K. It consists of spectrum I and two new spectra (spectra II and III). The details of the spectra unambiguously show that Mn^{2+} ions are responsible for the observed resonances. Spectra II and III show identical angular variation patterns for rotations in the ab, bc and ac planes. Within each plane, both spectra II and III were observed to repeat after 90^0, and the spectra obtained for angles from 45 to 90^0 were inverse of those obtained from 0 to 45^0. The angular dependence of the spectral details indicates that spectrum II is cubic where as spectrum III has axial symmetry. However, the movement of the lines as a function of the angle could not be followed

Fig. V.1

X-band EPR spectrum of an as-grown, " pure " $(NH_4)_2\ ZnBr_4$ crystal.

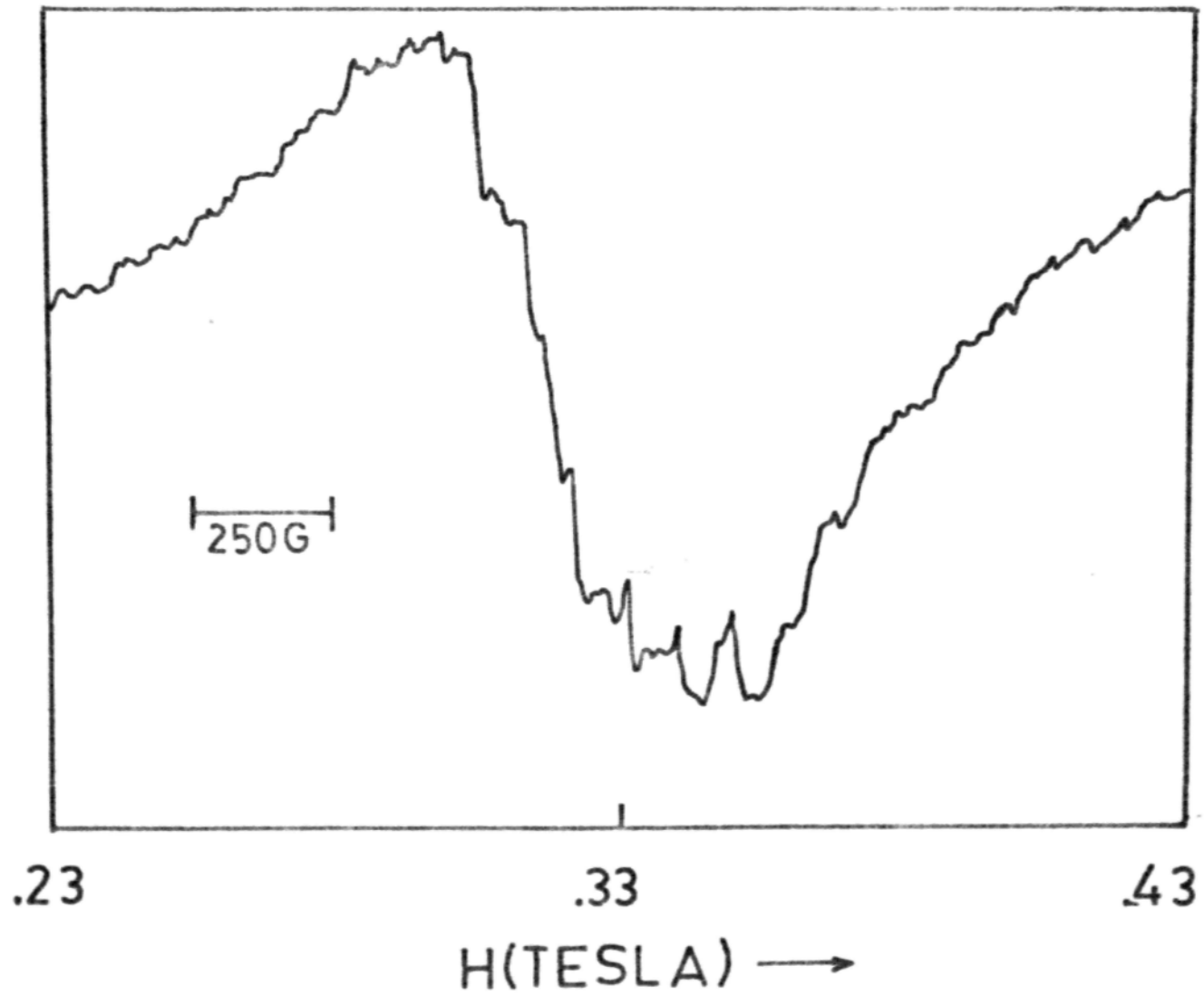
250G
.23
.33
.43
H(TESLA) ⟶

Fig. V.2

X-band EPI spectrum of a " pure " $(NH_4)_2ZnBr_4$ crystal thermally quenched from 523 K; H parallel to one of the edges of the crystal; recorded at F1

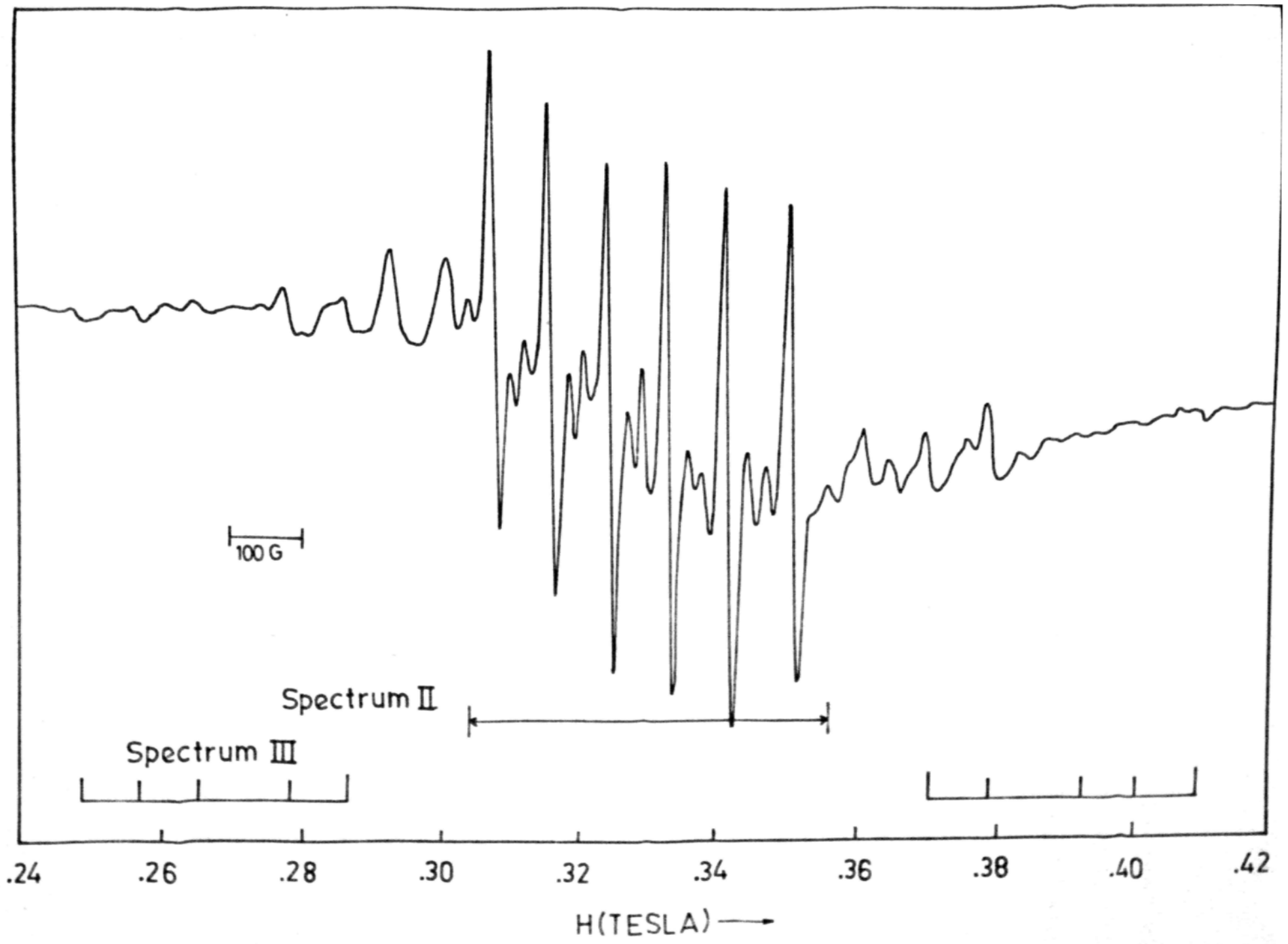
100 G
Spectrum II
Spectrum III
.24
.26
.28
.30
.32
.34
.36
.38
.40
.42
H(TESLA) ⟶

Precisely, as the resolution in spectrum II is poor with considerable overlap whereas spectrum III is weak. The following are the spin Hamiltonian parameters evaluated from the spectra :

Spectrum	II	$g = 2.02 \pm 0.01$
		$A = 85 \pm 30$
Spectrum	III	$g = 2.00 \pm 0.01$
		$A = 85 \pm 30$
		$D = 400 \pm 30$

It has not been possible to estimate the cubic field splitting parameter 'a' for spectrum II, and g, B and D_1 for spectrum III.

Detailed EPR measurements were carried out on the quenched sample over the temperature range 110 - 473 K. Interesting changes in the relative intensities of lines in spectrum II were observed around 430 K. Fig. V.3 shows the EPR spectra obtained at 403 and 443 K. Fig. V.4 shows the EPR spectra recorded at 218, 223 and 228 K and Fig. V.5 shows a part of the EPR spectrum recorded in

Fig. V.3

X-band EPR spectra of a " pure " $(NH_4)_2ZnBr_4$ crystal thermally quenched from 523 K; H parallel to one of the edges of the crystal; recorded at (a) 403 K and (b) 443 K.

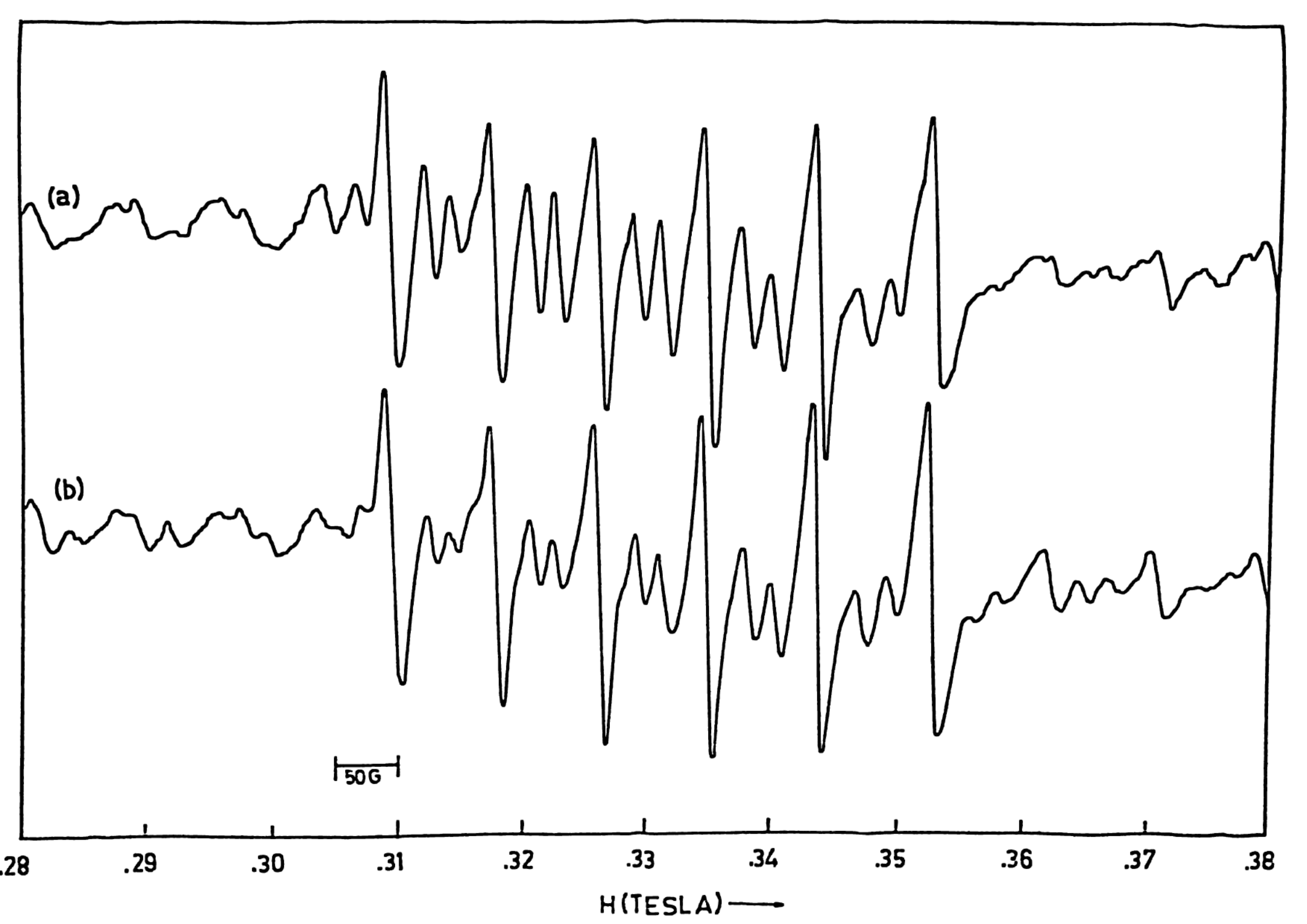
(a)
(b)
50G
.28
.29
.30
.31
.32
.33
.34
.35
.36
.37
.38
H(TESLA)

Fig. V.4

X-band EPR spectra of a " pure " $(NH_4)_2ZnBr_4$ crystal thermally quenched from 573 K; H parallel to one of the edges of the crystal; recorded at (a) 228 K (b) 223 K and (c) 218 K.

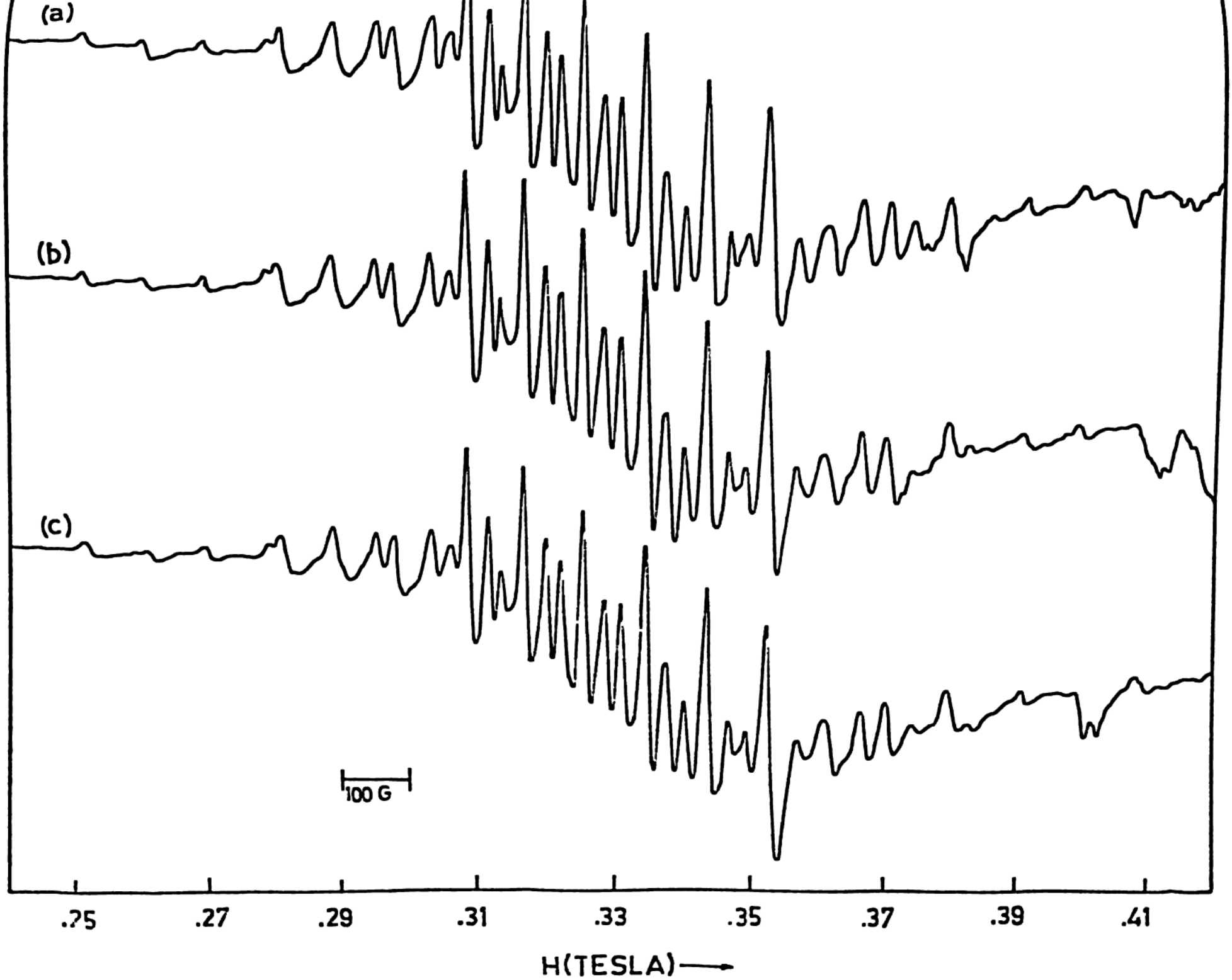
(a)
(b)
(c)
100 G
.25
.27
.29
.31
.33
.35
.37
.39
.41
H(TESLA)

Fig. V.5

A part of the EPR spectrum of quenched $(NH_4)_2ZnBr_4$ in expanded form; at (a) 223 K (b) 218 K and (c) 213 K.

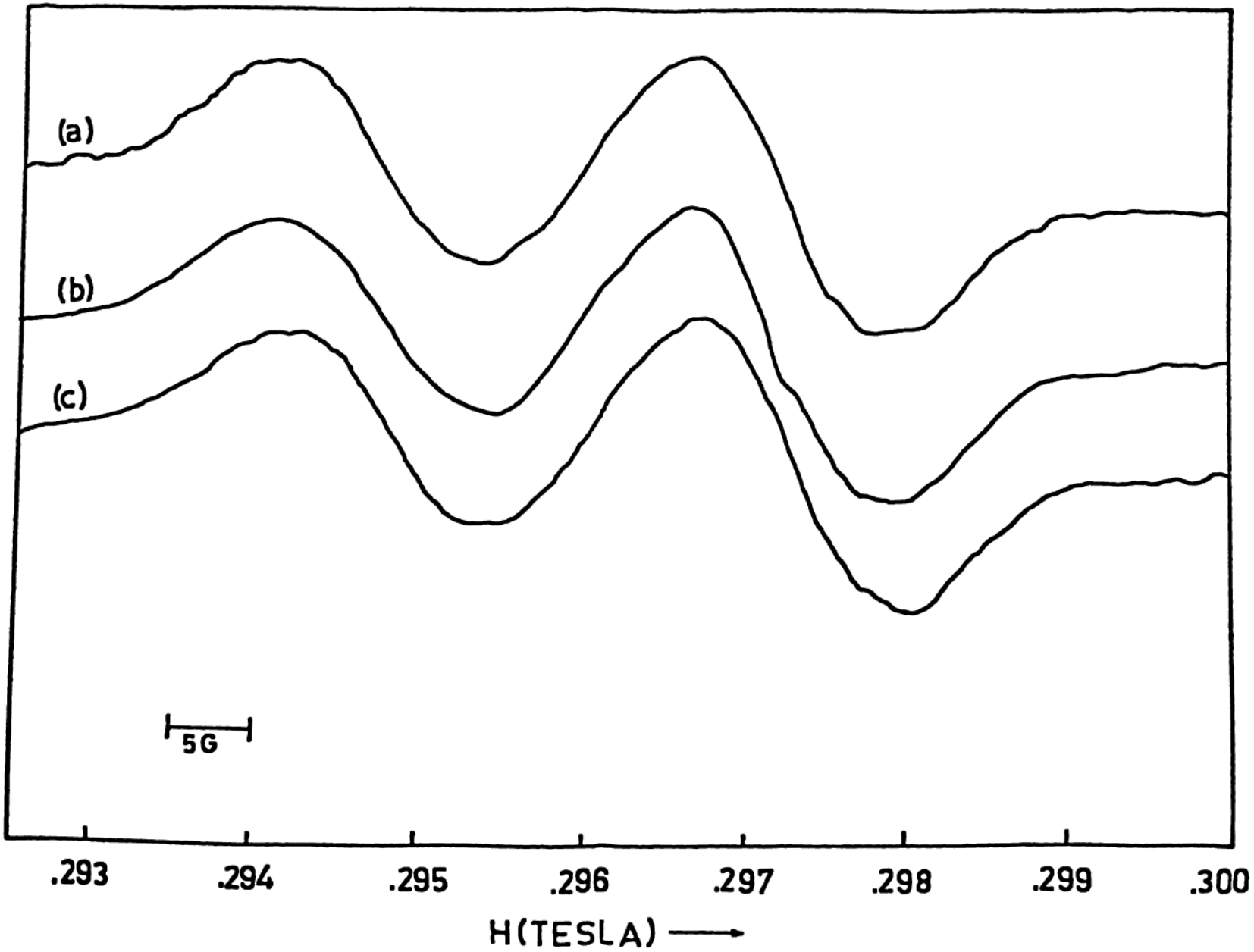
(a)
(b)
(c)
5G
.293
.294
.295
.296
.297
.298
.299
.300
H(TESLA) ⟶

expanded form at 213, 218 and 223 K. Inspite of repeated measurements on the samples grown at different times and using different dopants in the starting solution, we have not been able to observe the phase transition reported at $\approx$ 220 K by Moskalev et al[11] and Osaka et al[12].

Spectrum I indicates the presence of Mn^{2+} clusters in as-grown samples. Quenching from 523 K disperses a small fraction of the Mn^{2+} ions. Substitutional NH_4^+ and Zn^{2+} sites as well as interstitial sites are available for the dispersed Mn^{2+} ions. Spectrum II probably arises from Mn^{2+} ions substituting for Zn^{2+} ions in tetrahedral $ZnBr_4^{2-}$ complexes. This is supported by the changes occuring in spectrum II at $\approx$ 430 K. A slight distortion involving $MnBr_4^{2-}$ complex would change the value of 'a' marginally and the accompanying shifts in line positions could be such that the new overlappings result in the observed intensity changes in the spectrum. Spectrum III could also arise from Mn^{2+} ions at the substitutional Zn^{2+} sites, but in addition associated with NH_4^+ ions or some other imperfections. It is difficult to propose definite models for the centres responsible for the observed spectra until the detailed crystal structure of $(NH_4)_2ZnBr_4$ is available.

Changes in the intensity of certain lines at ≈ 430 K observed in the EPR spectrum shown in Fig. V.3 indicate the occurrence of a phase transition. The intensity of an EPR spectrum depends, apart from the number of paramagnetic ions, on the spin-lattice relaxation time associated with the transfer of energy from the excited paramagnetic ion to the lattice modes of the crystal. Also, the resonance intensity is inversely proportional to the dielectric constant of the sample. Hence a change in the dielectric constant which accompanies a ferroelectric phase transition will cause a change in the intensity of the spectrum. However, both the effects would lead to intensity changes in the entire spectrum. The observed intensity changes point out that

(a) the phase transition observed at ≈ 430 K is likely to be of displacive type and

(b) the phase below $T_c \approx 430$ K is not ferroelectric.

Also, no progressive changes in the line widths or positions were observed around T_c, which rule out the involvement of incommensurate phase. We have very carefully looked for the phase transition in the range 215 - 250 K, observed earlier by Moskalev et al[11] by

NQR and Osaka et al[12] from dielectric constant measurements, but we have neither observed changes in the spin Hamiltonian parameters nor changes in the line widths and intensities. A possible explanation for this is provided in the next section in conjunction with pulsed NMR results.

2.2 Pulsed NMR

Proton relaxation measurements were made over the temperature range 83 - 284 K. A glass sample tube of 10 mm dia filled with dried powder obtained by crushing single crystals, and sealed under vacuum, was used for measurements. T_1 measurements were made at 20 MHz by measuring the intensity of the free induction decay following the sampling pulse applied in a $(\pi - \tau - \pi/2)$ sequence. A box-car integrator was used for signal averaging. T_1 was obtained by least square fitting the data on a DCI computer. Measurements were made on two samples grown separately under different conditions. The two sets of readings compare very well within experimental error. Table V.1 gives the data obtained on one of the samples. A plot based on these data is shown in Fig. V.6. Prominent in this plot are two minima in the relaxation times at 93 and 171 K, and an indication

Fig. V.6

The temperature dependence of the proton spin-lattice relaxation time T_1 at 20 MHz for " pure " $(NH_4)_2ZnBr_4$.

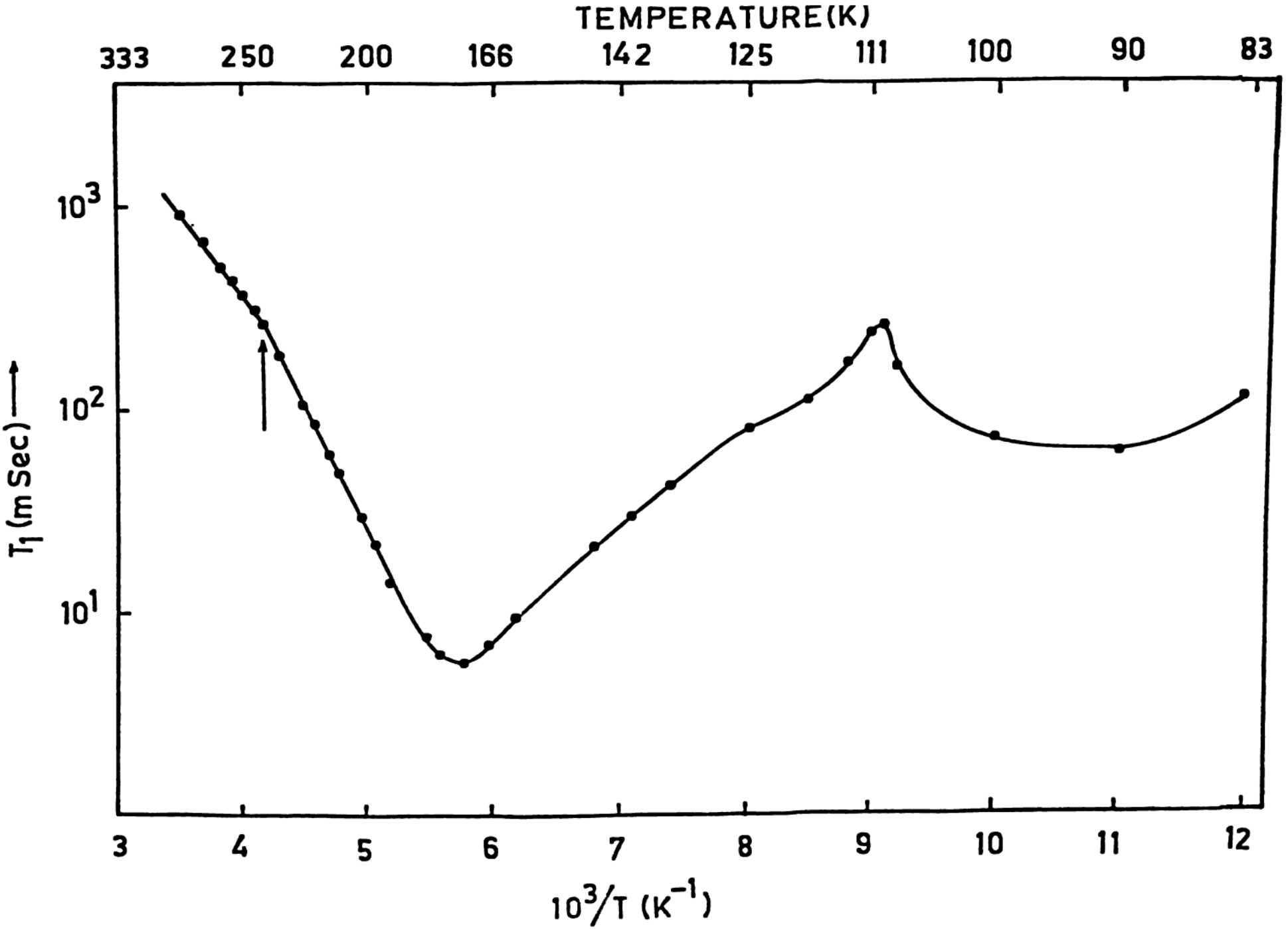
TEMPERATURE(K)
333
250
200
166
142
125
111
100
90
83
10^3
10^2
10^1
T_1 (m Sec) ⟶
3
4
5
6
7
8
9
10
11
12
$10^3/T\ (K^{-1})$

Table V.1

Temperature vs spin lattice relaxation time T_1 for $(NH_4)_2ZnBr_4$

Temperature ^oK	T_1 m.Sec.
91.0	59.4
100.5	73.9
104.2	78.3
106.4	101.4
107.3	159.4
109.0	260.9
110.1	273.4
110.6	246.4
111.7	210.1
113.1	169.5
114.6	144.9
115.6	130.4
117.5	115.9
121.0	98.55
124.9	82.60
135.7	47.80
140.3	34.70
147.7	21.70
157.0	11.60
161.2	10.14
165.3	7.24
171.0	5.79
178.4	6.66
181.8	8.26
189.6	13.91
194.9	21.74
200.8	31.88

Contd. . .

Temperature ^{o}K	T_1 m.Sec.
206.1	44.99
208.3	50.72
211.4	62.31
214.4	68.11
217.7	88.40
221.4	101.45
222.7	115.94
224.2	123.18
226.2	137.68
229.4	163.76
232.0	188.40
235.7	231.88
239.1	275.36
242.9	347.82
245.3	362.31
251.6	449.27
258.6	536.23
266.5	608.69
271.2	695.65
275.1	782.6
278.2	869.5
284.0	927.5

of a change of slope at 235 K. T_1 values are observed to be frequency dependant at lower temperatures as expected.

The T_1 measurements provide direct information on the motion of NH_4^+ ions in solids. Sudden changes in the magnitude of T_1 as a function of temperature, or change in the slope of T_1 vs 1/T curve, are interpreted to reflect a phase transition in the solid[6]. If a reorientational motion of NH_4^+ ion characterized by a correlation time τ_c is the dominant mechanism for proton relaxation, the appropriate expression for T_1 is

$$\frac{1}{T_1} = \frac{C\gamma^4\hbar^2}{b^6}\left[\frac{\tau_c}{1+\omega^2\tau_c^2} + \frac{4\tau_c}{1+4\omega^2\tau_c^2}\right] \qquad (1)$$

where γ is the magnetogyric ratio, ω is the Larmor frequency and b is the inter-proton distance in NH_4^+ ion. C is equal to 27/40 or 9/20 for motions w.r.t 3-fold or 2-fold axes; respectively[9]. In equation (1) T_1 is governed by intra-molecular dipolar interactions. The correlation times have an exponential temperature dependence governed by the Arrhenius law

$$\tau_c = \tau_c^{\circ} \exp\left(Ea/kT\right) \qquad (2)$$

where Ea is the activation energy and τ_c is the pre-exponential factor. Ea in equation (2) is a measure of the height of the potential barrier among equivalent molecular positions. Equation (1) gives a minimum in T_1 when $\omega\tau_c = 0.62$.

Todo and Tatsuzaki[7] studied $NaNH_4SO_4.2H_2O$ by pulsed NMR technique. A single minimum in the T_1 vs 1/T curve was obtained at 101 K, below which a steep increase in T_1 was observed. Using equations (1) and (2) the authors have calculated Ea to be 1.0 and 3.5 KCal/mole in paraelectric and ferroelectric phases, respectively. It is interesting to note that though dielectric anomalies were observed in $NaNH_4SO_4.2H_2O$ at 101 K and 92 K, the T_1 measurements did not exhibit any anomaly at 92 K. This was attributed to a less violent nature of the transition at 92 K. Miller et al[6] have performed T_1 measurements on $(NH_4)_2SO_4$ where in a distinct change in the slope of T_1 vs 1/T curve was observed at 223 K. The activation energies determined are 2.3 and 6.1 KCal/mole in the paraelectric and ferroelectric phase respectively. Similar measurements by the same authors on $(NH_4)_2BeF_4$ revealed only a change of slope in the T_1 vs 1/T curve

near the Curie point. Dielectric and thermal measurements on $(NH_4)_2BeF_4$ had earlier shown a ferroelectric transition of second order at 173 K. The T_1 measurements support the earlier assumption of a less violent nature of the transition. Pulsed NMR measurements by Koksal and Bahceli[8] on NH_4Br, NH_4SCN, NH_4NO_3, $(NH_4)_2S_2O_8$, $(NH_4)_2Cr_2O_7$ and $(NH_4)_2Ce(NO_3)_6$ have shown that spin rotational interaction contributes to T_1 at high temperatures. Accordingly, the measured values of T_1 were fitted by adding a term representing the spin-rotational interaction, to equation (1).

The following general conclusions could be made from the results of pulsed NMR experiments on ammonium compounds:

1) The barrier for the isotropic tumbling of NH_4^+ ion is generally higher in the ferroelectric than in the paraelectric phase. Hence the change to a ferroelectric phase could be interpreted as generally involving a change in the lattice structure.

2) In ammonium compounds containing protons other than those in NH_4^+ ion, phase transitions occur corresponding to ordering of protons in bonds like N-H-O and O-H-O arising from ionic shifts.

3) Spin rotational interactions of NH_4^+ ions contribute to T_1 at elevated temperatures.

4) The T_1 vs 1/T plots generally exhibit one or more minima at low temperatures.

5) The reorientation motion could be described adequntely in terms of the motions of independent NH_4^+ ions. However, cases exist where in the values of T_c^o indicate some long range co-operative behaviour between NH_4^+ ions.

NH_4 group is the only NMR sensitive probe in the present studies. Sundaram et al[10]. have studied $(NH_4)_2ZnCl_4$ by pulsed NMR. The crystal structure of $(NH_4)_2ZnCl_4$ is such that there are two types of tetrahedra NH_4^+ and $ZnCl_4^{2-}$ which are connected by a net work of hydrogen bonds. In the unit cell, there are two types of NH_4^+ ions which are chemically inequivalent. Since NH_4^- group is the only NMR sensitive probe in $(NH_4)_2ZnCl_4$ also, the T_1 vs 1/T plot of this compound is expected to contain two prominent minimacorresponding to the reorientations of the two in-equivalent NH_4^+ ions in the lattice. Sundaram et al. have observed two minima at 80 and 93.5 K which they have assigned to the

two in-equivalent NH_4^+ ions. The observed values of the two T_1 minima are reasonable as compared to the expected values. Genin and O.Reilly[9] observed two minima at 120 K and 172 K in the T_1 vs 1/T plot for $NaNH_4SO_4 \cdot 2H_2O$. Based on the comparision of the measured values of the two T_1 minima with those calculated from equation (1), the two minima have been assigned to reorientational motions of NH_4^+ ions w.r.t. the 2-fold and 3-fold axes. The values of T_1 minima obtained by Sundaram et al., Genin and O.Reilly and in the present work, scaled to 20 MHZ, are summarized in Table V.2. It is clear from the table that the T_1 minimum observed at 171 K for $(NH_4)_2ZnBr_4$ is associated with the reorientational motion of the NH_4^+ ion in the lattice. The observed T_1(min) of 6.7 m.Sec is less than the corresponding values in $(NH_4)_2ZnCl_4$ and $NaNH_4SO_4 \cdot 2H_2O$. This is due to the fact that the $(NH_4)_2ZnBr_4$ samples used by us inherently contained a high concentration of paramagnetic ions leads to faster relaxation of the protons in the NH_4 - group.

The effect of a phase transition on various physical properties of a solid is not always strong.

Table V.2

Data on T_1 minima in some ammonium compounds.

System	Temperature	T_1
$(NH_4)_2ZnCl_4$	82 K	10.8 m sec
	93 K	10.6 m sec
$NaNH_4SO_4.2H_2O$	120 K	12.4 m sec
	170 K	24 m sec
$(NH_4)_2ZnBr_4$	93 K	55 m sec
	171 K	6.7 m sec

It is not uncommon to miss a phase transition altogether because there is no detectable effect on the chosen physical property. The minute change in slope of the curve in Fig. V.6 around 235 K indicates the occurrence of a phse transition as explained earlier in this section. The transition temperature observed is higher as compared to the values reported by Moskalev et al[11] and Osaka et al[12]. Table V.3, which summarizes the transition temperatures observed by different techniques for systems similar to $(NH_4)_2ZnBr_4$, shows that such differences have been observed earlier. The fact that the transition is observed in pulsed NMR which is sensitive to molecular motions, and not in EPR enables us to remark on the nature of the phase transition at 235 K. If it were a structural phase transition involving displacements in ionic positions, we would have observed changes in the spin Hamiltonian parameters. However, reorientations of molecular groups not directly associated with paramagnetic centres are unlikely to have a measurable effect on the EPR spectrum. Since the pulsed NMR measurements carried out by us are on protons in the NH_4^+ group, any motional changes involving

physical methods

System	Raman Scattering	Neutron Scattering	X-ray	DTA	Dielectric constant	Spontaneous Polarization	Hysteresis	NMR	EPR	NQR
Rb_2ZnCl_4[a]	189 K	192 K		192 K		192 K	192 K	333 K		
	302 K	303 K		302 K				370 K		
$(NH_4)_2ZnCl_4$[b]			313 K	270 K	270 K	153 K				194 K
			406 K	406 K	319 K	270 K				266 K
Rb_2ZnBr_4[c]	187 K		80 K	187 K			187 K	355 K		
	346 K		108 K	291 K				193 K		
			200 K							
$(NH_4)_2ZnBr_4$[d]				365 K	205 K	133 K	210 K	235 K*	430 K*	233 K
				428 K	217 K	216 K				425 K
					365 K					
					439 K					
$(N(CH_3)_4)_2ZnCl_4$[e]				161 K	161 K	276 K				
				181 K	181 K	279 K				
				276 K						
				279 K						
				293 K						

(Contd.....)

(a) : S.Sawada et al. J.Phys. Soc. Japan 43, 2099 (1977); T.Nakamura et al. J.Phys.Soc.Japan 49, 1429 (1980); M.Wada et al. J.Phys.Soc.Japan 47, 1185 (1979); K.Gesi et al. J.Phys. Soc.Japan 46, 697(1979).

(b) : G.A.Smolensky et al. Ferroelectrics 36, 351 (1981); H.Matsunaga et al. J.Phys.Soc. Japan 50, 2789 (1981); T.Sato et al. J.Phys.Soc. Japan 51, 3411 (1982);

(c) : S.Sawada et al. J.Phys. Soc.Japan 43, 2101 (1977); T.Nakamura et al. J.Phys.Soc.Japan 48, 1588 (1980); K.Gesi. et. al. J.Phy.Soc. Japan 45 ,1777(1978); C.J.de pater; Phys. Stat. Solidi a 48, 503 (1978).

(d) : I.A.Belobrova et al. Solid State Commun, 32, 1101 (1980); T.Osaka et al. J.Phys.Soc. Japan 51, 3409 (1982); A.K.Moskalev et al. Phys.Stat.Sol. a 72, K 19 (1982); T.Sato et al. J.Phys.Soc. Japan 52, 3297 (1983).

(e) : K.Gesi et al. J.Phys. Soc.Japan 48, 337 (1980); S.Tanisaki et al. J.Phys.Soc.Japan 49, 1405 (1980); H.Shinizu et al. J.Phys. Soc. Japan 49 , 223 (1980);

this group would reflect in the values of T_1.

Put together, our EPR and pulsed NMR results lead to the following picture concerning phase transitions in $(NH_4)_2ZnBr_4$.

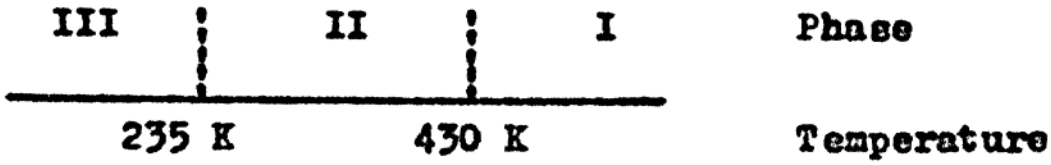

Phase II is neither ferroelectric nor incommensurate. The transition at 235 K is unlikely to be of displacive or distortive type, where as the transition at 430 K is of displacive or distortive type.

References

1. K.A.Muller, in "Phase Transitions and Soft Modes" edited by E.J. Samuelsen, E. Andersen and J. Feder, Univ. Forlaget, Oslo (1971).

2. K. Tsuchida and R. Abe, J. Phys. Soc. Japan 40, 204 (1976).

3. F.J. Owens, J. Phys. Chem. Solids 39, 291 (1978).

4. R.Navalgund and L.C. Gupta, J.Phys. Soc. Japan 39 880 (1975).

5. S.V. Bhat, J. Rangarajan and R. Srinivasan, Nuclear Physics and Solid State Physics Symposium (India), 24C, 407 (1981).

6. S.R. Miller, R.Blinc, M. Brenman and J.S. Wangh, Phys. Rev. 126, 528 (1962).

7. I.Todo and I. Tatsuzaki, Phys. Letts. 22, 22 (1966).

8. F. Koksal and S. Bahceli, J. Chem. Soc. Faraday II, 74, 1844 (1978).

9. D.J. Genin and D.E. O' Reilly, J. Chem. Phys. 50, 2842 (1969).

10. C.S. Sundaram, J. Rama Krishna, K. Chandrasekhar and V.S.S. Sastry, " Ferroelectrics ", (tobe published).

11. A.K. Moskalev, I.A. Belobrova, L.I. Zherebtsova and I.P. Aleksandrova, Phys. stat. sol. (a) 72, K 19 (1982).

12. J. Osaka, M. Komukae and Y. Makita, J. Phys. Soc. Japan 51, 3409 (1982).

CHAPTER VI

MICROHARDNESS STUDY OF $(NH_4)_2ZnBr_4$

1. Introduction

Imperfections strongly influence the microhardness of single crystals. When divalent cations are doped into an alkali halide crystal, the isolated impurity ions, the impurity aggregates and the cation vacancies act as obstacles to dislocation motion and thus lead to an increase in microhardness. However, an increase in the doping concentration results in impurity precipitation and a reduction in microhardness. Lakshmipathi Rao and Hari Babu[1] have shown that the microhardness is independent of the size, shape and orientation of precipitates.

The microhardness of alkali halide crystals containing precipitates increases on thermal quenching. However, as to be expected, it remains constant beyond the temperature at which the precipitates are completely dispersed. Etching studies on as - grown and quenched KCl:Ba, Sr[2] have indicated that dislocations act as nucleation sites for the formation and growth of such precipitates.

For mixed crystals of alkali halides, the microhardness is found to vary nonlinearly with relative composition. Subba Rao and Hari Babu[3] investigated the nature

of defects in such systems using etching, ionic conductivity and dielectric loss techniques and concluded that the mixed crystals contain a higher concentration of dislocations, low-angle grain boundaries and vacancies than the end crystals. The differences in the size of the ions in the mixed lattice lead to local strains which ultimately influence the microhardness.

Though considerable work has been done on alkali halides, microhardness measurements on crystals of inorganic salts containing ammonium ion have been rare[4]. As in the case of alkali halides, doping by divalent metal ions appears to lead to an increase in microhardness. The information obtained on such systems is too limited to permit any generalization. We have carried out systematic measurements on $(NH_4)_2ZnBr_4$ crystals with a variety of dopings, doping concentrations and thermal quenching, and the results are presented here.

2. Results and Discussion

Fig. VI.1 shows the dependence of microhardness (H_μ) on the applied load for a "pure" crystal. Microhardness decreases as the load increases upto about 60 gms beyond which it remains constant. Fig. VI.2

Fig. VI.1

The load dependence of microhardness for a "pure" $(NH_4)_2ZnBr_4$ crystal.

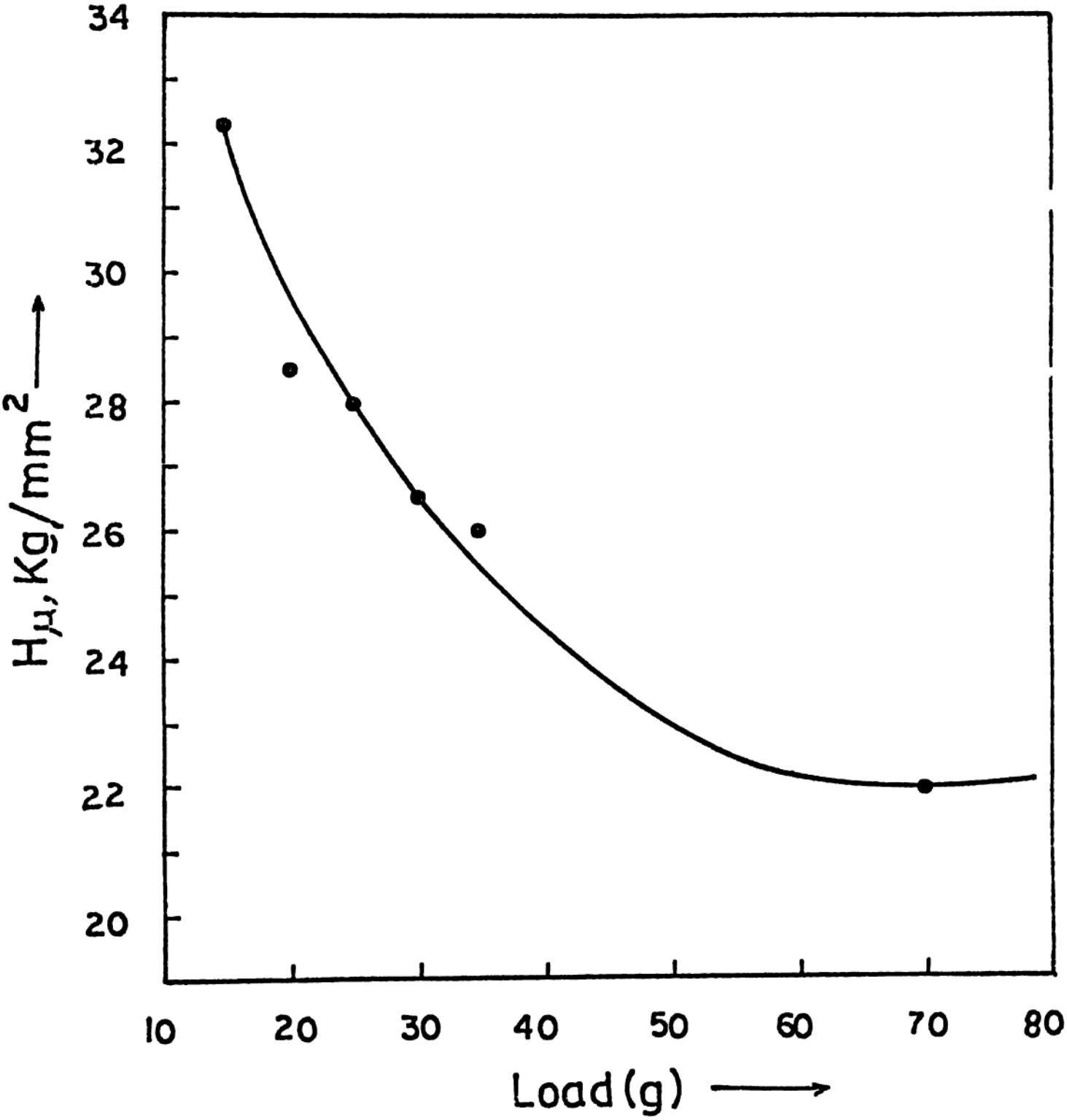
34
32
30
28
26
24
22
20
H_μ, Kg/mm^2
10
20
30
40
50
60
70
80
Load (g)

Fig. VI.2

The dependence of microhardness on Mn^{2+} concentration for $(NH_4)_2ZnBr_4$ crystals doped with Mn^{2+} ions.

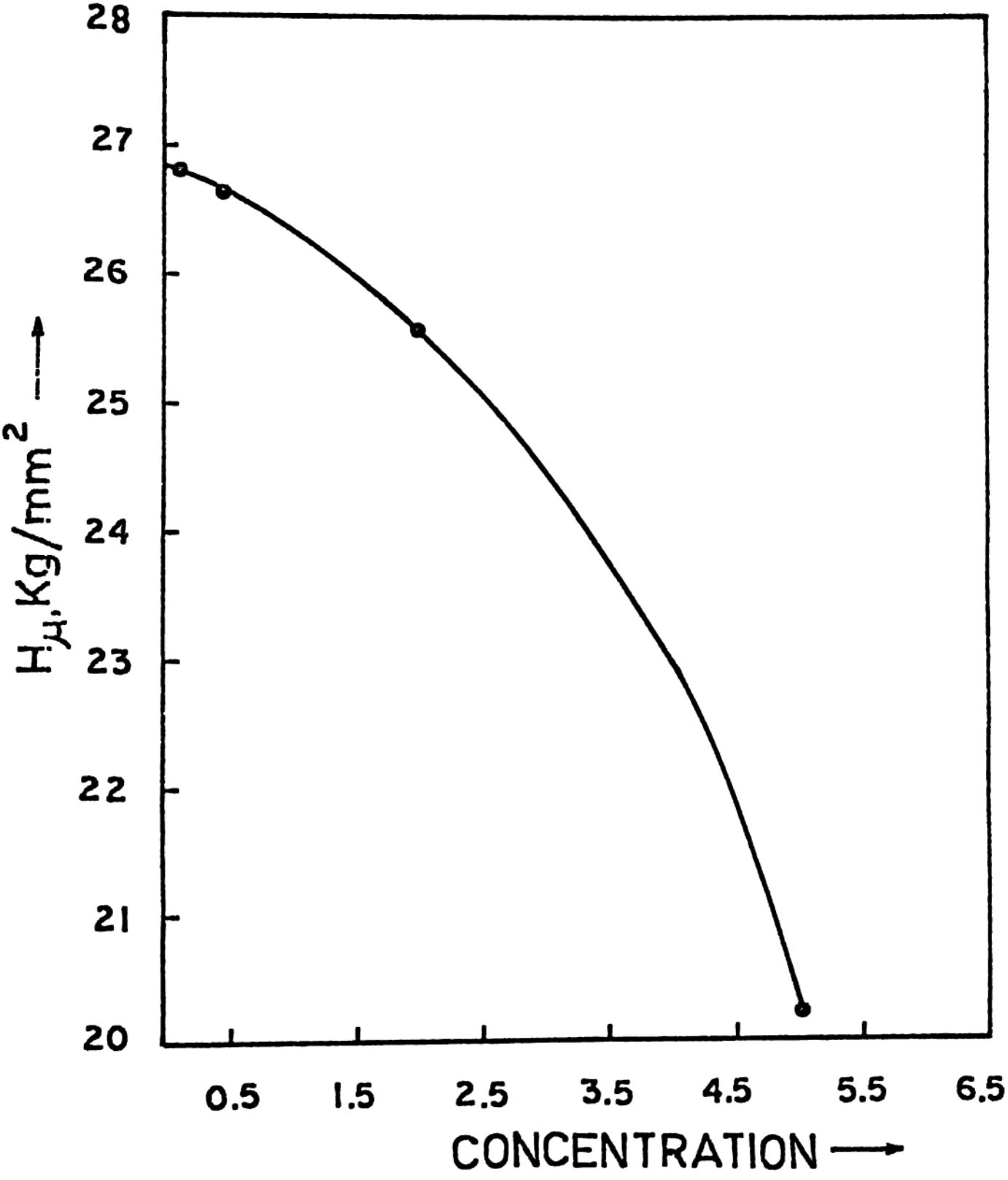
28
27
26
25
24
23
22
21
20
H_μ, Kg/mm^2 ⟶
0.5
1.5
2.5
3.5
4.5
5.5
6.5
CONCENTRATION ⟶

shows the dependence of microhardness on Mn^{2+} concentration and Fig. VI.3 shows the dependence on the quenching temperature. Fig. VI.4 shows the EPR spectrum before and after quenching from 523 K, of a sample similar to the one used for measurements shown in Fig.VI.3.

The dependence of microhardness on load shown in Fig. VI.1 is similar to the trend observed in alkali halides. The observation of identical curves for the " pure " crystals as well as for crystals grown using Na^{+} and Bi^{3+} as dopants leads to the conclusion that Na^{+} and Bi^{3+} ions have not gone into the lattice. Since the charge compensation requirements are different for Na^{+}, Mn^{2+} and Bi^{3+} ions, the incorporation of these ions would have influenced the load dependence. In Fig. VI.2, the microhardness has the highest value for the least concentration (0.5%) used. This shows that precipitation is already taking place at 0.5% concentration, and that this trend increases as the concentration increases to 5%. This is confirmed by the observations shown in Figs. VI.3 and VI.4. The presence of most of the Mn^{2+} ions as precipitates in the as-grown crystal leads to the broad EPR signal as in Fig. VI.4(a). Quenching disperses the Mn^{2+} ions resulting

Fig. VI.3

The dependence of microhardness on the quenching temperature for $(NH_4)_2ZnBr_4$ crystals.

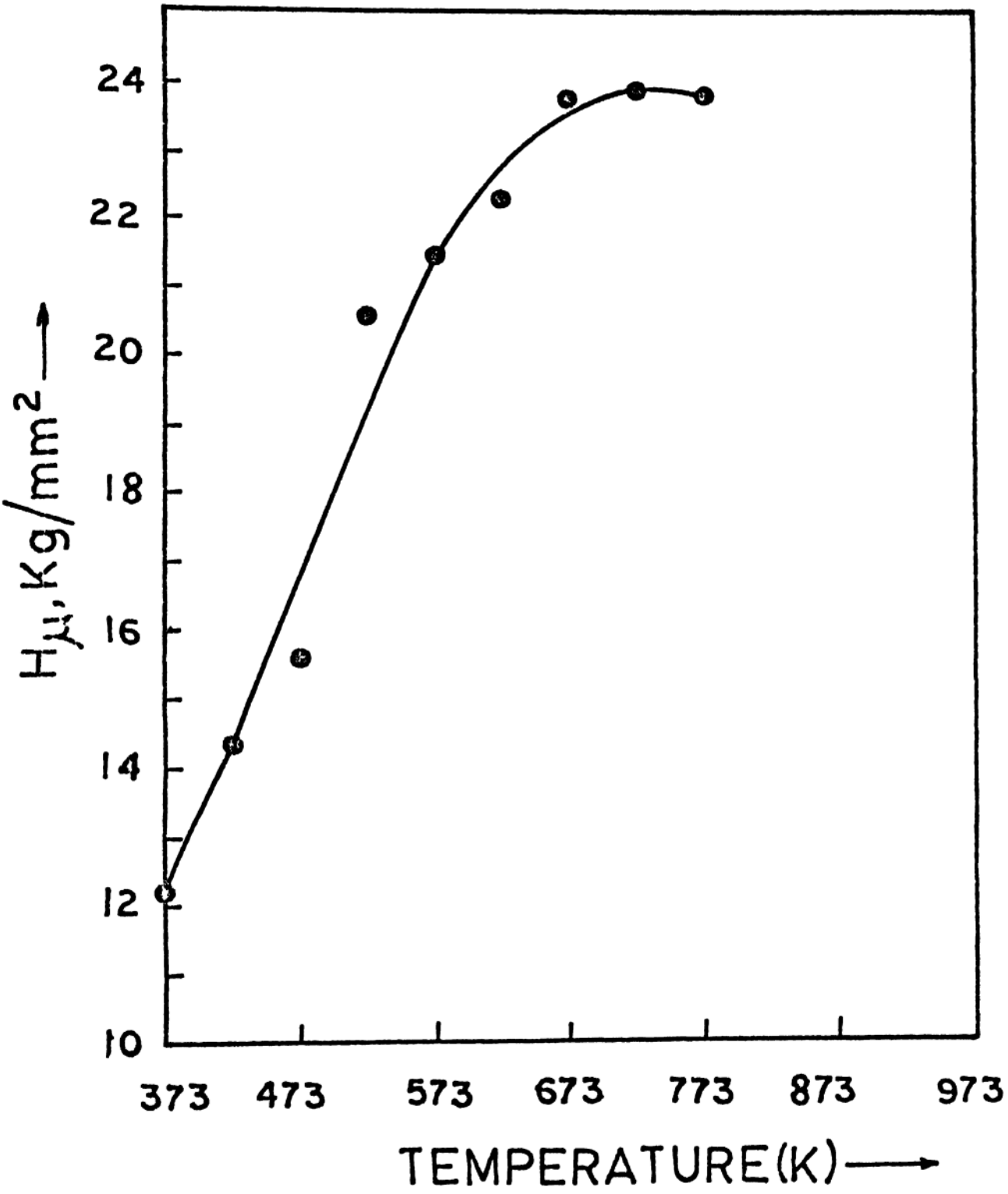
24
22
20
18
16
14
12
10
H_μ, Kg/mm^2
373
473
573
673
773
873
973
TEMPERATURE(K)

Fig. VI.4

EPR spectra of a " pure " $(NH_4)_2ZnBr_4$ crystal before (a) and after (b) quenching from 523 K.

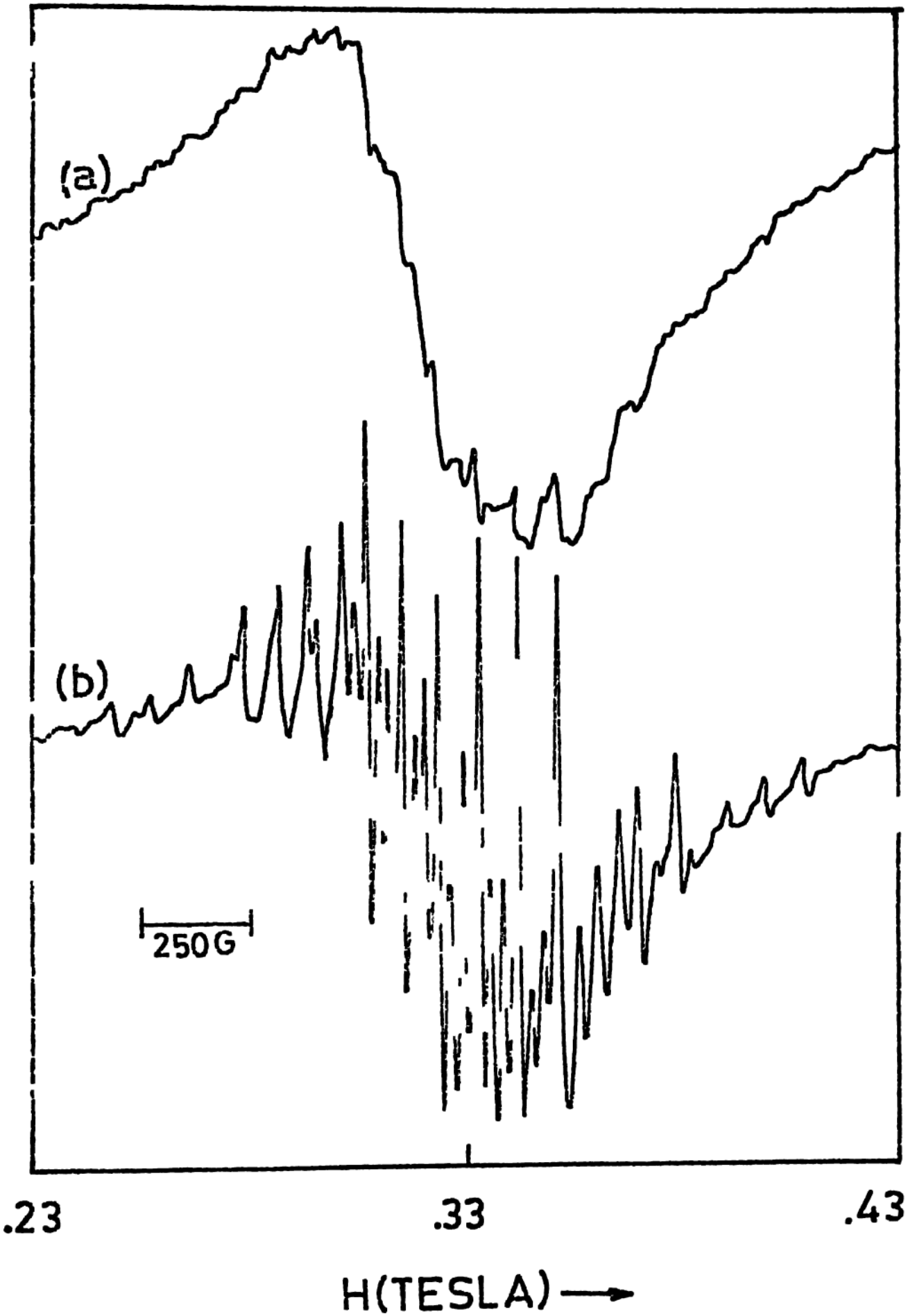
(a)
(b)
250G
.23
.33
.43
H(TESLA) ⟶

in the resolved spectrum as in Fig. VI.4(b), and increased microhardness in Fig. VI.3. It is obvious that the trends observed for $(NH_4)_2ZnBr_4$ are similar to those observed for alkali halides. In comparison with observations on KCl:Ba,Sr^2, it is concluded that Mn^{2+} ions in $(NH_4)_2ZnBr_4$ precipitate near the dislocations during crystal growth from solution.

References

1. M. Lakshmipathi Rao and V. Hari Babu, Indian J. pure appl. Phys. 16, 821 (1978).

2. M. Lakshmipathi Rao and V. Hari Babu, Indian J. pure appl. Phys. 14, 769 (1976).

3. U.V. Subba Rao and V. Hari Babu, Pramāna 11, 149 (1978).

4. K.J. Pratap and V. Hari Babu, Bull. Mater. Sci. 2, 43 (1980).